

SPACE VEHICLE GUIDANCE, NAVIGATION, CONTROL, AND ESTIMATION OPERATIONS TECHNOLOGIES

Brett Newman

**Old Dominion University
Research Foundation ODURF
4111 Monarch Way, Ste 204
Norfolk, VA 23508-2561**

29 Mar 2018

Final Report

APPROVED FOR PUBLIC RELEASE; DISTRIBUTION IS UNLIMITED.



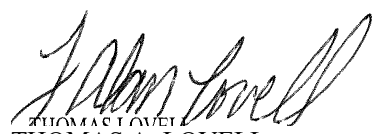
**AIR FORCE RESEARCH LABORATORY
Space Vehicles Directorate
3550 Aberdeen Ave SE
AIR FORCE MATERIEL COMMAND
KIRTLAND AIR FORCE BASE, NM 87117-5776**

NOTICE AND SIGNATURE PAGE

Using Government drawings, specifications, or other data included in this document for any purpose other than Government procurement does not in any way obligate the U.S. Government. The fact that the Government formulated or supplied the drawings, specifications, or other data does not license the holder or any other person or corporation; or convey any rights or permission to manufacture, use, or sell any patented invention that may relate to them.

This report is the result of contracted fundamental research which is exempt from public affairs security and policy review in accordance with AFI 61-201, paragraph 2.3.5.1. This report is available to the general public, including foreign nationals. Copies may be obtained from the Defense Technical Information Center (DTIC) (<http://www.dtic.mil>).

AFRL-RV-PS-TR-2018-0023 HAS BEEN REVIEWED AND IS APPROVED FOR PUBLICATION IN ACCORDANCE WITH ASSIGNED DISTRIBUTION STATEMENT.



THOMAS A. LOVELL
Program Manager



PAUL HAUSGEN, Ph.D.
Technical Advisor, Spacecraft Component Technology



JOHN BEAUCHEMIN
Chief Engineer, Spacecraft Technology Division
Space Vehicles Directorate

This report is published in the interest of scientific and technical information exchange, and its publication does not constitute the Government's approval or disapproval of its ideas or findings.

Approved for public release; distribution is unlimited.

REPORT DOCUMENTATION PAGE				Form Approved OMB No. 0704-0188	
Public reporting burden for this collection of information is estimated to average 1 hour per response, including the time for reviewing instructions, searching existing data sources, gathering and maintaining the data needed, and completing and reviewing this collection of information. Send comments regarding this burden estimate or any other aspect of this collection of information, including suggestions for reducing this burden to Department of Defense, Washington Headquarters Services, Directorate for Information Operations and Reports (0704-0188), 1215 Jefferson Davis Highway, Suite 1204, Arlington, VA 22202-4302. Respondents should be aware that notwithstanding any other provision of law, no person shall be subject to any penalty for failing to comply with a collection of information if it does not display a currently valid OMB control number. PLEASE DO NOT RETURN YOUR FORM TO THE ABOVE ADDRESS.					
1. REPORT DATE (DD-MM-YY) 29-03-2018		2. REPORT TYPE Final Report		3. DATES COVERED (From - To) 28 Aug 2015 – 24 Mar 2018	
4. TITLE AND SUBTITLE Space Vehicle Guidance, Navigation, Control, and Estimation Operations Technologies		5a. CONTRACT NUMBER FA9453-15-1-0307			
		5b. GRANT NUMBER			
		5c. PROGRAM ELEMENT NUMBER 62601F			
6. AUTHOR(S) Brett Newman		5d. PROJECT NUMBER 8809			
		5e. TASK NUMBER PPM00004135			
		5f. WORK UNIT NUMBER EF126403			
7. PERFORMING ORGANIZATION NAME(S) AND ADDRESS(ES) Old Dominion University Research Foundation ODURF 4111 Monarch Way, Ste 204 Norfolk, VA 23508-2561		8. PERFORMING ORGANIZATION REPORT NUMBER			
9. SPONSORING / MONITORING AGENCY NAME(S) AND ADDRESS(ES) Air Force Research Laboratory Space Vehicles Directorate 3550 Aberdeen Ave., SE Kirtland AFB, NM 87117-5776		10. SPONSOR/MONITOR'S ACRONYM(S) AFRL/RVSV			
		11. SPONSOR/MONITOR'S REPORT NUMBER(S) AFRL-RV-PS-TR-2018-0023			
12. DISTRIBUTION / AVAILABILITY STATEMENT Approved for public release; distribution is unlimited.					
13. SUPPLEMENTARY NOTES					
14. ABSTRACT Relative orbital elements provide a geometric description of satellite motion referenced to another satellite in close formation flight under two-body circular reference conditions. When the relative motion is adequately characterized by first order theory, the six relative orbital elements describe the location and size of the instantaneous in-the-plane ellipse, the angular position around the ellipse, and the out-of-plane amplitude and angular position. These elements are explicitly relatable to the six rectangular position and velocity coordinates. Second order theories become necessary when the close-proximity assumption is violated. Two distinct theories for (quasi) second order relative orbital elements are explored. One theory uses the expanded solution form and introduces several instantaneous ellipses with corresponding element sets totaling twenty-one individual elements. Overall motion is described by a linear combination of the ellipses. Another theory uses the compacted solution form and introduces a single instantaneous ellipse with corresponding element set totaling nine individual elements. In each case, the theory quantifies distortion of the first order relative orbital elements when including second order effects. The new variables are described as quasi elements because they form a non-minimal set of coordinates. Several examples are presented, both analytically and numerically. New periodic conditions, geometric interpretations, and relations to fixed and variable Lissajous curves are also explored.					
15. SUBJECT TERMS Relative Motion, Close-Proximity Operation, Formation Flight, Relative Orbital Elements, Geometric Coordinates, Clohessy-Wiltshire, Quadratic Volterra, Lissajous Curve, Periodic Condition, Local-Vertical Local-Horizontal					
16. SECURITY CLASSIFICATION OF:			17. LIMITATION OF ABSTRACT	18. NUMBER OF PAGES	19a. NAME OF RESPONSIBLE PERSON
a. REPORT	b. ABSTRACT	c. THIS PAGE			Thomas Alan Lowell
Unclassified	Unclassified	Unclassified	Unlimited	68	19b. TELEPHONE NUMBER (include area code)

(This page intentionally left blank)

TABLE OF CONTENTS

Section	Page
LIST OF FIGURES	ii
LIST OF TABLES	iii
ACKNOWLEDGMENTS	iv
DISCLAIMER.....	iv
1.0 SUMMARY	1
2.0 INTRODUCTION	2
3.0 METHODS, ASSUMPTIONS, AND PROCEDURES.....	4
3.1 FIRST ORDER RELATIVE ORBITAL ELEMENTS	4
3.2 FIXED AND VARIABLE LISSAJOUS CURVES	6
4.0 RESULTS AND DISCUSSION	18
4.1 SECOND ORDER RELATIVE ORBITAL ELEMENTS - EXPANDED FORM.....	18
4.2 SECOND ORDER RELATIVE ORBITAL ELEMENTS - COMPACTED FORM.....	29
4.3 LISSAJOUS CURVES - REVISITED	36
4.4 SECOND ORDER PERIODICITY	47
5.0 CONCLUSIONS.....	52
6.0 RECOMMENDATIONS.....	53
REFERENCES	54
LIST OF SYMBOLS, ABBREVIATIONS, AND ACRONYMS.....	58

LIST OF FIGURES

Figure	Page
1 Relative Motion Geometry	4
2 "Orbiting" Particle on Fixed Lissajous Curve (In-Plane View).....	7
3 Harmonograph with Generated Curve	8
4 "Orbiting" Particle on Variable Lissajous Curve.....	9
5 Variable Phase Lissajous Curve	10
6 Variable Amplitude Lissajous Curve	11
7 Variable Phase-Amplitude Lissajous Curve	12
8 Space Curve Classification	13
9 "Orbiting" Particle on Fixed Lissajous Curve (Out-Plane View).....	13
10 "Orbiting" Particle on Fixed Lissajous Curve (Perspective View).....	15
11 "Orbiting" Particle on Variable Lissajous Space Curve	15
12 Variable Phase-Amplitude Lissajous Space Curve.....	17
13 QV vs. NLS for 2.5T.....	25
14 QV for 8T - Expanded Formulation	25
15 Component Motions - Expanded Formulation	25
16 Overlaid Elliptic Component Motions - Expanded Formulation	27
17 Second Order Relative Orbital Element Responses - Expanded Formulation	28
18 QV for 8T - Compacted Formulation	33
19 Component Motions - Compacted Formulation	33
20 Second Order Relative Orbital Element Responses - Compacted Formulation	35
21 Variable Polynomial Frequency Repeating Lissajous Curve	38
22 Variable Polynomial Frequency Non-Repeating Lissajous Curve	38
23 Variable Sinusoid Frequency Repeating Lissajous Curve.....	40
24 Variable Sinusoid Frequency Spatial Non-Repeating Lissajous Curve	40
25 Variable Polynomial Amplitude Repeating Lissajous Curve	44
26 Variable Polynomial Amplitude Non-Repeating Lissajous Curve.....	44
27 Variable Sinusoid Amplitude Repeating Lissajous Curve.....	46
28 Variable Sinusoid Amplitude Spatial Non-Repeating Lissajous Curve	46

LIST OF TABLES

Table	Page
1 ROE Initial and Final Values - Expanded Formulation.....	24
2 ROE Initial and Final Values - Compacted Formulation.....	33

ACKNOWLEDGMENTS

This material is based on research sponsored by the Air Force Research Laboratory under agreement number FA9453-15-1-0307. The U.S. Government is authorized to reproduce and distribute reprints for Governmental purposes notwithstanding any copyright notation thereon.

DISCLAIMER

The views and conclusions contained herein are those of the authors and should not be interpreted as necessarily representing the official policies or endorsements, either expressed or implied, of the Air Force Research Laboratory or the U.S. Government.

1.0 SUMMARY

Relative orbital elements provide a geometric description of satellite motion referenced to another satellite in close formation flight under two-body circular reference conditions. When the relative motion is adequately characterized by first order theory such as the linear Clohessy-Wiltshire model and analytic solution, the six relative orbital elements describe the location and size of the instantaneous in-the-plane ellipse, the angular position around the ellipse, and the out-of-plane amplitude and angular position. These elements are explicitly relatable to the six rectangular position and velocity coordinates. Second order theories, such as the Quadratic Volterra model and analytic solution, become necessary when the close-proximity assumption is violated. Two distinct theories for (quasi) second order relative orbital element sets are explored. One theory uses the expanded solution form and introduces several instantaneous ellipses with corresponding element sets totaling twenty-one individual elements. Overall motion is described by a linear combination of the ellipses. Another theory uses the compacted solution form and introduces a single instantaneous ellipse with corresponding element set totaling nine individual elements. In each case, the theory quantifies distortion of the first order relative orbital elements when including second order effects. The new variables are described as *quasi* elements because they form a non-minimal set of coordinates, and hence cannot be constructed as output from a general transformation having a six-dimensional state epoch input, without knowledge of the approximate analytic solution. Several examples are presented, both analytically and numerically. New periodic conditions, geometric interpretations, and relations to fixed and variable Lissajous curves and the double-pendulum harmonograph are also explored.

2.0 INTRODUCTION

Although a mathematical representation of a physical system can exhibit certain invariant behaviors, many commonly encountered properties are dependent on the coordinates used to represent the system. Such properties include stability, nonlinearity, symmetry, diagonality, singularity, and others. Typical engineering analysis efforts involve establishing such properties using a given set of coordinates, followed almost involuntarily (and incorrectly) by replacing the notion of coordinate-dependent properties with a notion of system-dependent properties. Refs. [1,2] give a deep, enlightening discussion of this topic, particularly for orbital mechanics and space attitude dynamics. To further complicate matters, an infinite number of coordinate sets for the engineer to choose from exist. Ref. [2] develops a quantifiable measure to identify optimum coordinate selection regarding the specific property of nonlinearity, or the minimization thereof. An astrodynamics example investigated a coordinate comparison of Classical Cartesian, Burdet Regularization, Kustaanheimo-Stiefel Regularization, and Quaternion Regularization sets; while a rotational motion example compared various attitude descriptions using Euler Angle, Classical Rodrigues, Modified Rodrigues, and Euler Parameter sets. For the specific propagated cases, Kustaanheimo-Stiefel Regularization (without the temporal equation) vs. Classical Cartesian (with the temporal equation) and Euler Parameter coordinate sets exhibited the most linear behavior. When performing coordinate selections, further difficulties arise when emphasis is given to the important property of geometry, or the facilitation of insight thereof. An analyst will intuitively recognize when one set of coordinates, through some visualization or mechanism, offers qualitative advantages over other coordinate sets, yet a suitable procedure for making choices based on this property does not appear to exist. This work focuses on retaining this type of geometric property for a specific set of coordinates when increasing analytic solution fidelity for relative orbital motion between two satellites. Throughout this discussion, the reference satellite, or reference point in space-time, is denoted "chief", while the perturbed satellite is called "deputy".

For absolute motion, a large number of coordinate sets have been developed with varying attributes, mostly defined with respect to an inertial reference frame with origin coinciding with the primary attracting body. Ref. [3] provides a thorough survey of at least twenty-two of these sets. Some of these coordinates include classical, rectangular (Cartesian), geographic, spherical, Delaunay, Poincaré, Kustaanheimo-Stiefel, equinoctial, quaternion, and many others arising from modifications-combinations of Euler angles, Euler parameters, and functions of classical elements. Refs. [4-6] provide other sets when concepts like universal coordinates and fundamental invariants are considered. Driving motivations for the creation of this plethora of coordinate sets include singularity elimination, dynamical theory heritage, conic curve unification, and computational performance. Adoption of such coordinates often comes at the expense of losing transparent geometry, insight, and/or simplicity. For relative motion, a smaller but still large library of coordinate sets exists, which are typically defined with respect to the local-vertical local-horizontal reference frame with origin coinciding with the chief satellite. A thorough survey of coordinates, models, and solutions for relative motion is given in Ref. [7]. Rectangular, cylindrical, and spherical coordinate sets have been considered at least as far back as 1959-1960, 1961, 1963, [8-11] with lunar-geo relative motion in a Cartesian description going back to Hill [12]. Non-standard cylindrical and spherical coordinate definitions are commonly used and based on differences of absolute deputy and chief variables [13]. These three sets facilitate strong connection to the underlying geometry. Cylindrical and spherical coordinates

possess the extra advantage of not requiring small azimuth angle assumptions when deriving simplified governing differential equations [14,15]. Orbital element differences (OED) are a popular coordinate choice and were originally suggested by Hill [12]. These coordinates are based on differencing absolute classical elements of the deputy and chief, but any set of elements can also be employed. Refs. [16,17] first seriously considered this approach using Lagrange coefficients or F and G functions. Ref. [18] used this approach to analyze relative motion along highly elliptic orbits. Refs. [19,20] use OED based on classical elements to generate higher order Cartesian solutions for elliptic orbits. Ref. [21] formulates relative orbit geometry and relationships between Cartesian coordinates and classic OED for first order dynamics. Refs. [22,23] use OED based on Deprit-Rom like elements [24] to remove singularities associated with circular orbits, and on equinoctial elements to remove singularities associated with both circular orbits and equatorial orbits. This formulation is known as the geometric method. Ref. [25] uses OED based on generalized relative eccentricity and inclination vector separation coordinates to quantify deputy relative motion, which was used heavily in the PRISMA mission. Ref. [26] uses quaternion-based elements to describe deputy motion that is singularity free, at the expense of increased complexity and indirect ties to the geometry. One of the most intuitive coordinate sets for relative motion is relative orbital elements (ROE), defined in Refs. [27-30]. These coordinates were conceived from the first order circular chief analytic solution (Clohessy-Wiltshire or CW solution) expressions for relative motion, and are closely aligned with classical orbital elements in absolute motion, in that the elements are explicitly tied to the solution path geometry. The six relative orbital elements describe the location and size of the instantaneous in-the-plane ellipse, the angular position around the ellipse, and the out-of-plane harmonic amplitude and angular position, and are explicitly relatable to the six rectangular position and velocity coordinates. Finally, Ref. [31] investigated how these relative orbital elements can be extended under the second order circular chief analytic solution (Quadratic Volterra or QV solution) expressions from Ref. [32].

The objective of this work is to further investigate extensions of relative orbital elements under the QV solution framework. Two distinct theories for second order relative orbital element sets are explored. One theory uses the expanded solution form and introduces several instantaneous ellipses with corresponding element sets totaling twenty-one individual elements. Overall motion is described by a linear combination of the ellipses. This theory is similar to Ref. [31] with further development. Another theory uses the compacted solution form and introduces a single instantaneous ellipse with corresponding element set totaling nine individual elements. In each case, the theory quantifies distortion of the first order relative orbital elements when including second order effects. Several examples are presented, both analytically and numerically. New periodic conditions, geometric interpretations, and relations to fixed and variable Lissajous curves and the double-pendulum harmonograph are also explored.

3.0 METHODS, ASSUMPTIONS, AND PROCEDURES

3.1 FIRST ORDER RELATIVE ORBITAL ELEMENTS

Fig. 1 describes the relative motion of a deputy satellite with respect to a chief satellite. Two reference frames are shown. The first frame is the standard XYZ Earth-centered inertial (ECI) frame. The second frame is the xyz local-vertical local-horizontal (LVLH) frame with origin located on the chief, x axis in the radial direction, y axis in the transverse (along-track) direction, and z axis in the normal (cross-track) direction. Chief and deputy absolute position vectors in algebraic form are denoted by \mathbf{R}_c and \mathbf{R}_d while the relative position vector of deputy with respect to chief is \mathbf{r} . Position vector components expressed in the LVLH frame are

$$\begin{aligned}\mathbf{R}_c &= [\mathbf{R}_c \ 00]^T \\ \mathbf{R}_d &= \mathbf{R}_c + \mathbf{r} = [(\mathbf{R}_c + x) \ y \ z]^T\end{aligned}\tag{1}$$

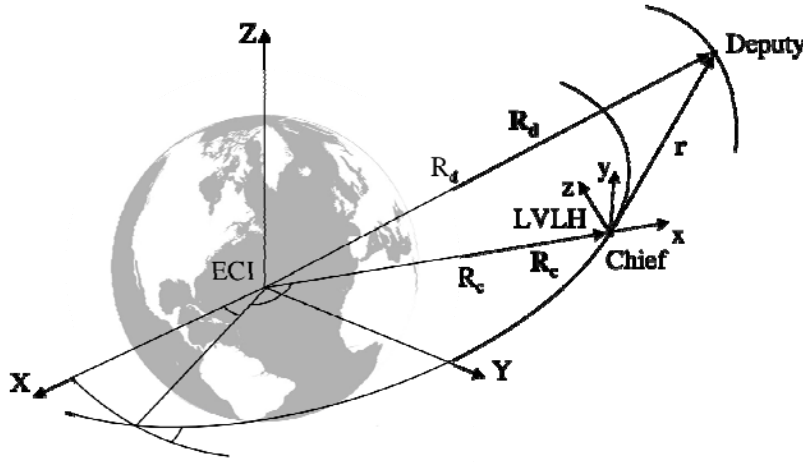


Figure 1. Relative Motion Geometry

The linear closed-form CW relative trajectory expressions for positions $x(t)$, $y(t)$, and $z(t)$, which are accurate to first order, are given in Eq. (2) [9]. In these equations, subscript "0" denotes the value of a quantity at the initial time t_0 , and elapsed time from the reference is $\tau = t - t_0$. Additional variables in Eq. (2) include chief mean motion n_0 , and $S = \sin(\cdot)$, $C = \cos(\cdot)$.

$$\begin{aligned}x(t) &= \{4-3C_{n_0\tau}\}x_0 + \{\frac{1}{n_0}S_{n_0\tau}\}\dot{x}_0 + \{\frac{2}{n_0}(1-C_{n_0\tau})\}\dot{y}_0 \\ y(t) &= \{6(S_{n_0\tau}-n_0\tau)\}x_0 + \{1\}y_0 + \{\frac{2}{n_0}(-1+C_{n_0\tau})\}\dot{x}_0 + \{\frac{1}{n_0}(4S_{n_0\tau}-3n_0\tau)\}\dot{y}_0 \\ z(t) &= \{C_{n_0\tau}\}z_0 + \{\frac{1}{n_0}S_{n_0\tau}\}\dot{z}_0\end{aligned}\tag{2}$$

Using trigonometric identities, expressions in Eq. (2) can be converted to the form in Eq. (3)

$$\begin{aligned}
x(t) &= x_c(\tau) + a_x C_{\theta_x(\tau)} &= x_e - a_e C_{\alpha(\tau)} \\
y(t) &= y_c(\tau) + a_y S_{\theta_y(\tau)} &= y_e(\tau) + 2a_e S_{\alpha(\tau)} \\
z(t) &= z_c(\tau) + a_z S_{\theta_z(\tau)} &= b_e S_{\beta(\tau)} \\
\hline
\dot{x}(t) &= \dot{x}_c(\tau) - a_x \dot{\theta}_x(\tau) S_{\theta_x(\tau)} &= a_e n_o S_{\alpha(\tau)} \\
\dot{y}(t) &= \dot{y}_c(\tau) + a_y \dot{\theta}_y(\tau) C_{\theta_y(\tau)} &= \dot{y}_e(\tau) + 2a_e n_o C_{\alpha(\tau)} \\
\dot{z}(t) &= \dot{z}_c(\tau) + a_z \dot{\theta}_z(\tau) C_{\theta_z(\tau)} &= b_e n_o C_{\beta(\tau)}
\end{aligned} \tag{3}$$

where

$$\begin{aligned}
x_e &= 4x_0 + \frac{2}{n_o} \dot{y}_0, & y_e(\tau) &= (y_0 - \frac{2}{n_o} \dot{x}_0) - (6x_0 + \frac{3}{n_o} \dot{y}_0) n_o \tau \\
a_e^2 &= (3x_0 + \frac{2}{n_o} \dot{y}_0)^2 + (\frac{1}{n_o} \dot{x}_0)^2, & \alpha(\tau) &= n_o \tau + \tan^{-1} \{ (\frac{1}{n_o} \dot{x}_0) / (3x_0 + \frac{2}{n_o} \dot{y}_0) \} \\
b_e^2 &= (z_0)^2 + (\frac{1}{n_o} \dot{z}_0)^2, & \beta(\tau) &= n_o \tau + \tan^{-1} \{ (z_0) / (\frac{1}{n_o} \dot{z}_0) \}
\end{aligned}$$

where it becomes transparent that deputy motion is described by the sum of an in-the-plane $y \times x = 2 \times 1$ ellipse that drifts along the y axis and a harmonic out-of-plane motion. Following Ref. [29], six ROE are defined directly from the solution form in Eq. (3) and include constant variables x_e , a_e , b_e and linear increasing variables y_e , α , β . Variables x_e , y_e represent the in-plane ellipse center point, a_e represents the in-plane ellipse semi-minor axis, α represents angular position around the in-plane ellipse, b_e represents the out-plane harmonic amplitude, and β represents angular position along the out-plane harmonic path. These six elements form a minimal coordinate realization of the relative motion. Eq. (3) is the transformation from ROE to rectangular states, while Eq. (4) is the reverse transformation [29].

$$\begin{aligned}
x_e &= 4x(t) + \frac{2}{n_o} \dot{y}(t), & y_e(\tau) &= y(t) - \frac{2}{n_o} \dot{x}(t) \\
a_e^2 &= [3x(t) + \frac{2}{n_o} \dot{y}(t)]^2 + [\frac{1}{n_o} \dot{x}(t)]^2, & \alpha(\tau) &= \tan^{-1} \{ [\frac{1}{n_o} \dot{x}(t)] / [3x(t) + \frac{2}{n_o} \dot{y}(t)] \} \\
b_e^2 &= [z(t)]^2 + [\frac{1}{n_o} \dot{z}(t)]^2, & \beta(\tau) &= \tan^{-1} \{ [z(t)] / [\frac{1}{n_o} \dot{z}(t)] \}
\end{aligned} \tag{4}$$

3.2 FIXED AND VARIABLE LISSAJOUS CURVES

Before introducing second order ROE, a discussion of Lissajous curve theory and the double-pendulum harmonograph is presented. These topics are closely related to the concept of second order ROE. A two-dimensional Lissajous curve is generated by the parametric equations below [33-35].

$$\begin{aligned}x(t) &= a_x \cos(\omega_x \tau - \phi_x) \\ y(t) &= a_y \sin(\omega_y \tau + \phi_y)\end{aligned}\tag{5}$$

These curves were first studied by Bowditch in 1815 and later by Lissajous in 1857. Eq. (5) can represent a wide variety of coupled harmonic responses to initial excitation or harmonic forcing in physical systems, and the $x(t)$ vs. $y(t)$ Lissajous curves they produce are commonly encountered during experimental signal analysis with modern instrumentation. Elementary curves can be generated by certain combinations of parameters: $\omega_x = \omega_y$ and $\phi_x + \phi_y = \pm\pi/2$ produces a line; $\omega_x = 2\omega_y$ and $\phi_x + 2\phi_y = 0, \pm\pi$, or $2\omega_x = \omega_y$ and $2\phi_x + \phi_y = \pm\pi/2$, produces a parabola; $\omega_x = \omega_y$, $\phi_x + \phi_y = 0, \pm\pi$ and $a_x = \pm a_y$ produces a circle; $\omega_x = \omega_y$, $\phi_x + \phi_y = 0, \pm\pi$ and $a_x \neq \pm a_y$ produces an unrotated ellipse; and $\omega_x = \omega_y$, $\phi_x + \phi_y \neq 0, \pm\pi/2, \pm\pi$ and $a_x \neq \pm a_y$ or $a_x = \pm a_y$ produces a rotated ellipse. Although these simple cases are examples of Lissajous curves, the implied meaning of Lissajous curves is often reserved for more complex shapes. Multi-lobe curves, or equivalently multiple extrema points, are generated when frequency ratio ω_x/ω_y consists of higher integer values, such as 3/1 or 3/2. Finally, closed Lissajous curves occur when ω_x/ω_y is rational (commensurate), and when irrational (non-commensurate), the curves are open.

Suppose a particle is "orbiting" the center point of a rotated elliptic Lissajous path as indicated in Fig. 2 for the specific set of parameter values. In general, four state variables are needed to define the planar particle motion. Along this programmed path, four suitable states or "orbital" elements are a_x , a_y , $\theta_x(\tau) = \omega_x \tau - \phi_x$, $\theta_y(\tau) = \omega_y \tau + \phi_y$; the first two elements describe the path size-shape, the last two elements describe the particle position. Note this situation is more involved than the first order CW curvilinear motion component around the instantaneous ellipse since no *single* underlying parameter exists to determine the motion amplitudes and also there is no *common* angle for the harmonic function arguments. To further underscore how a_x , a_y , $\theta_x(\tau)$, $\theta_y(\tau)$ can be used for motion interpretation, these elements are shown in Fig. 2 along with two auxiliary circles of radius a_x and a_y . Fixed elements a_x and a_y describe dimensions of a rectangular area that encloses the orbit path. Note the path is tangent to the boundary of the rectangular area at four points, not generally coincident with the principal axis points of the rotated ellipse. The particle initial position at time $t = t_0$ or $\tau = 0$, and a general position at time t or τ , are highlighted in Fig. 2. The actual particle on the Lissajous path projects to shadow particles moving along the auxiliary circles, also indicated in Fig. 2. Linearly increasing elements $\theta_x(\tau)$ and $\theta_y(\tau)$ describe the angular position, measured from the x axis, of the shadow particles around the auxiliary circles of constant radii equal to elements a_x and a_y , which in turn locates the actual particle on the Lissajous path. Another but equivalent viewpoint is where angles $\omega_x \tau$ and $\omega_y \tau$ locate the shadow particles from the reference marks determined by phase angles ϕ_x , ϕ_y , which correspond to the initial position at $t = t_0$ or $\tau = 0$. The four elements and the auxiliary circles through Eq. (5) provide a clear depiction of the particle motion. With this geometry and Eq. (5), a clear representation of the motion is captured. Given a_x and $\theta_x(\tau)$ (shadow particle on

the x auxiliary circle), the actual particle and its x coordinate can always be generated and interpreted by a cosine projection. Likewise, given a_y and $\theta_y(\tau)$ (shadow particle on y auxiliary circle), the actual particle and its y coordinate can always be generated and interpreted by a sine projection.

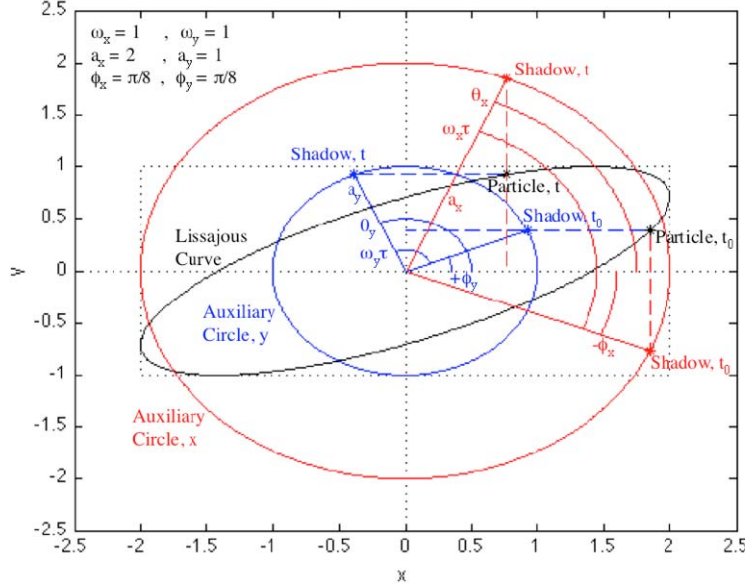


Figure 2. "Orbiting" Particle on Fixed Lissajous Curve (In-Plane View)

The two-dimensional Lissajous curve considered thus far can be classified as *fixed*, meaning a_x , a_y , ω_x , ω_y , ϕ_x , ϕ_y are constant. A *variable* Lissajous curve is now defined where these parameters are time dependent. A two-dimensional variable Lissajous curve is thus generated by the parametric equations below.

$$\begin{aligned} x(t) &= a_x(\tau) \cos\{\omega_x(\tau)\tau - \phi_x(\tau)\} \\ y(t) &= a_y(\tau) \sin\{\omega_y(\tau)\tau + \phi_y(\tau)\} \end{aligned} \quad (6)$$

Variable Lissajous curves provide a considerably more diverse framework that is well-suited for characterizing higher order approximations of relative orbital motion. The concept of a variable Lissajous curve is not necessarily new. Fig. 3 shows the double-pendulum harmonograph, a mechanical apparatus consisting of two separated pendulums swinging about orthogonal axes, with an attached marker that records on paper a complex curve [36]. This device could be considered an analog propagator for physical systems that exhibit multi-axis complex harmonic motion, including relative satellite motion. The concept can also be mechanized by harmonic signals driving a gimbal mounted laser to trace out the curve. The harmonograph is quite popular in mathematical description of tones, music, and sound, along with generating modern artistic drawings or visual entertainment [37,38]. Under ideal assumptions with no pivot friction or air resistance, small-amplitude pendulum motion, and a stiff pivot support, the harmonograph generated figure is a fixed Lissajous curve governed by Eq. (5). An example of a variable Lissajous curve is generated when non-ideal assumptions are considered: frictional damping leading to variable amplitude, large-angle swinging leading to variable frequency, and soft supporting leading to variable phase. Various sources describe the case where $a_x(\tau)$ and $a_y(\tau)$ are

exponential decaying functions reflecting system damping. With servo driven pendulums, the harmonograph could be made to generate tailored multi-axis complex harmonic motions.

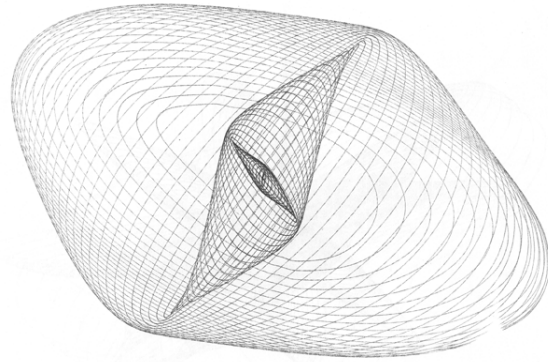


Figure 3. Harmonograph with Generated Curve

(Figure courtesy of Paul Bourke, <http://paulbourke.net/geometry/harmonograph/>)

Now suppose the particle is "orbiting" the center point of the variable Lissajous path, a continuously varying and distorting rotated planar ellipse. In general, four state variables are again necessary and sufficient to define the planar particle motion. Four suitable "orbital" elements are $a_x(\tau)$, $a_y(\tau)$, $\theta_x(\tau) = \omega_x(\tau)\tau - \phi_x(\tau)$, $\theta_y(\tau) = \omega_y(\tau)\tau + \phi_y(\tau)$; which have the same geometric meaning as before, except that amplitude, frequency, and phase are varying with time. Fig. 4 illustrates this geometry. The actual particle on the variable Lissajous path projects to shadow particles moving along the variable radii instantaneous auxiliary circles ($a_x(\tau), a_y(\tau)$) with variable rates ($\omega_x(\tau), \omega_y(\tau)$) measured from variable reference marks ($\phi_x(\tau), \phi_y(\tau)$). This concept is similar to the concept already employed with first order ROE where the relative orbital path is described by a continuously moving or instantaneous ellipse. Here, the conceptual elements are instantaneous auxiliary circles and the instantaneous "fixed" Lissajous curve. Given $a_x(\tau)$ and $\theta_x(\tau)$ (shadow particle on the x auxiliary "circle"), the actual particle and its x coordinate can always be generated and interpreted by a cosine projection. Likewise, given $a_y(\tau)$ and $\theta_y(\tau)$ (shadow particle on y auxiliary "circle"), the actual particle and its y coordinate can always be generated and interpreted by a sine projection. With the Fig. 4 geometry and Eq. (6), a clear, but more intellectually involved, representation of the motion is captured. All four time varying elements are physical variables that can be indicated on a drawing of the motion, and hence are geometrically meaningful. This framework is also very similar to the idea of osculating orbital elements in absolute satellite motion used to preserve the geometric usefulness of the coordinates when higher fidelity modeling is incorporated, i.e., perturbations.



Again using the parameter values from Fig. 2 as a baseline, Fig. 6 shows an example variable amplitude Lissajous curve with a linearly time varying amplitude function $a_x(\tau)$. Amplitude $a_x(\tau)$ starts at 2 and decreases by 0.2 for every cycle of motion. Four cases are shown with final times of $1(2\pi)$, $2(2\pi)$, $4(2\pi)$, $8(2\pi)$. For a final time of $1(2\pi)$, the particle closely approaches but does not reach the initial position forming an open curve. Openness occurs because $2\cos(-\pi/8) = x(0) \neq x(1(2\pi)) = 1.8\cos(-\pi/8)$. For a final time of $2(2\pi)$, note how the continuously varying ellipse is shrinking in width as $a_x(\tau)$ decreases. Referring back to Fig. 4, the auxiliary circle radius related

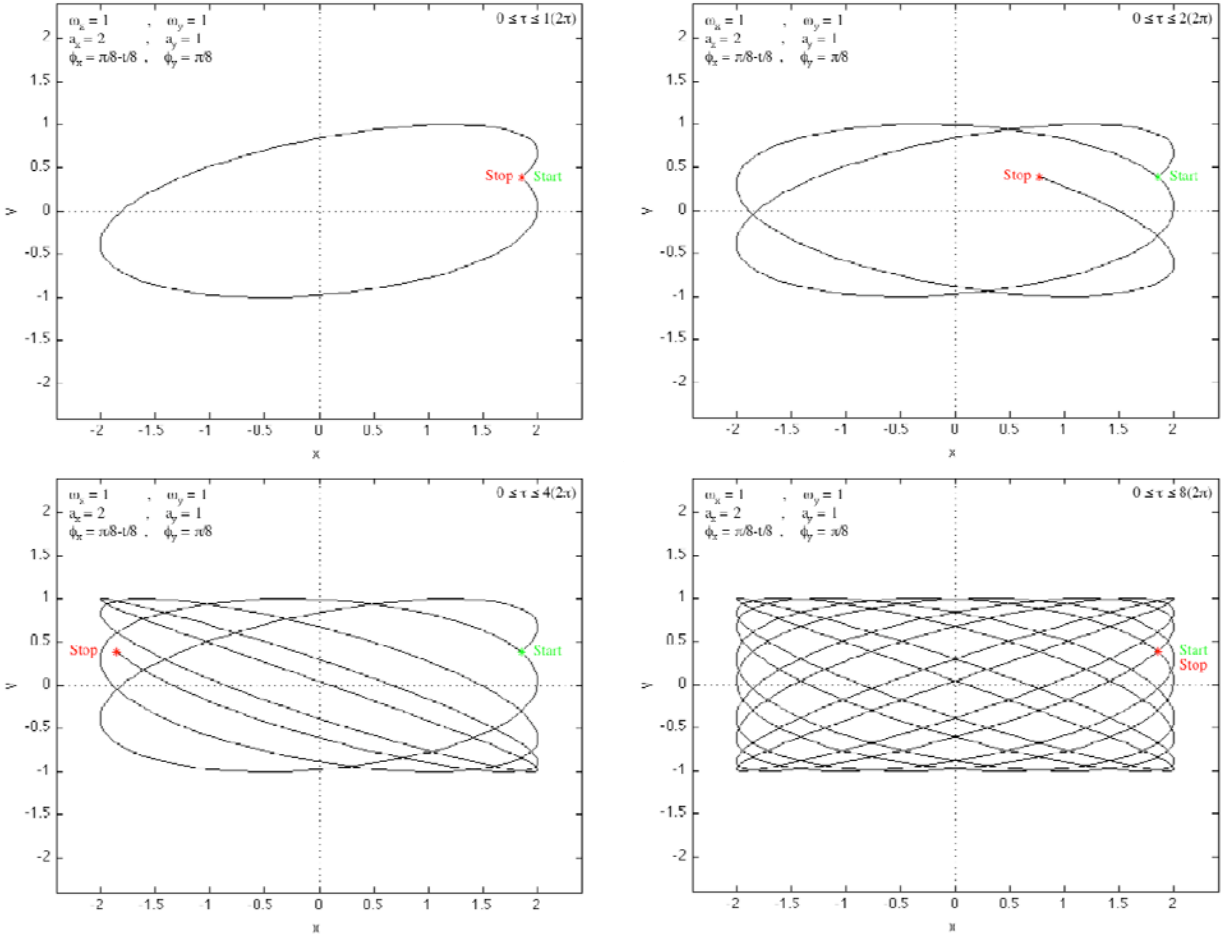


Figure 5. Variable Phase Lissajous Curve

to $a_x(\tau)$ is decreasing, causing the x harmonic to diminish over each cycle that occurs, which has the effect of initially circularizing the variable ellipse (final time of $4(2\pi)$) and then leading to a reversal of the semi-major and semi-minor axes (final time of $8(2\pi)$). If an auxiliary circle was introduced, the shadow particle would be located for this changing radius through element $a_x(\tau)$, and the x coordinate of the actual particle could be easily determined. In this variable amplitude case, the Lissajous curve never becomes a closed curve.

As a final two-dimensional example, Fig. 7 shows an example variable phase and variable amplitude Lissajous curve with a linearly time varying phase function $\phi_x(\tau)$ and linearly time varying amplitude functions $a_x(\tau)$ and $a_y(\tau)$. Phase angle $\phi_x(\tau)$ starts at $+\pi/8$ and decreases by $\pi/16$ for every cycle of motion. Amplitude $a_x(t)$ starts at 2 and increases by 0.2 for every cycle of motion, while amplitude $a_y(\tau)$ starts at 1 and increases by 0.1 for every cycle of motion. Four cases are shown with final times of $1(2\pi)$, $2(2\pi)$, $4(2\pi)$, $8(2\pi)$. For a final time of $1(2\pi)$, the particle approaches but does not reach the initial position forming an opened curve. Openness occurs because $2\cos(-\pi/8) = x(0) \neq x(1(2\pi)) = 2.2\cos(-\pi/16)$ and $1\sin(+\pi/8) = y(0) \neq y(1(2\pi)) = 1.1\sin(+\pi/8)$. For a final time of $2(2\pi)$, note how the continuously varying ellipse is rotating clockwise as $\phi_x(\tau)$ decreases, or $-\phi_x(\tau)$ increases. In the context of Fig. 4, the reference line corresponding to $-\phi_x(\tau)$ is again advancing, causing the x harmonic to peak at an earlier time for each cycle, which has the effect of rotating the variable ellipse in a retrograde sense. Also note

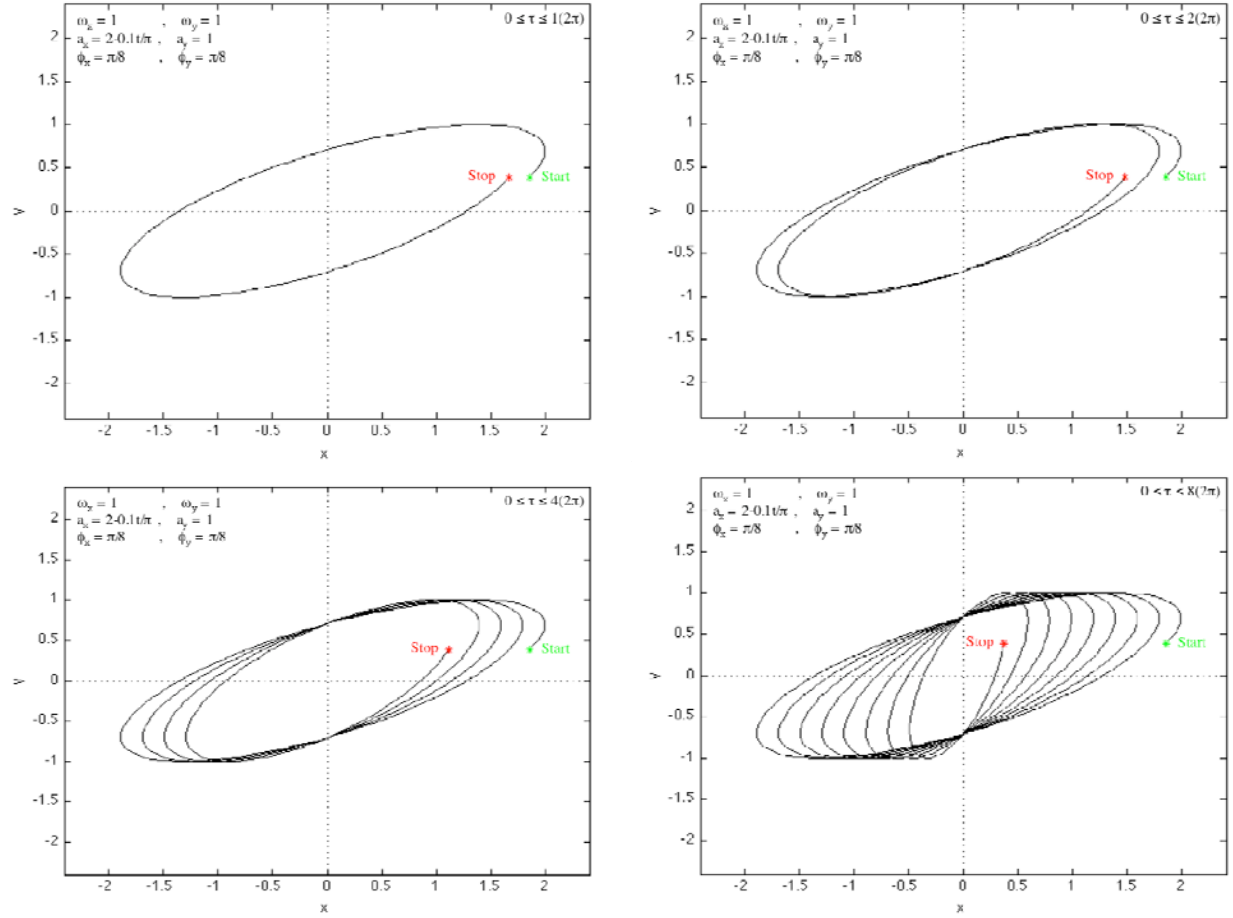


Figure 6. Variable Amplitude Lissajous Curve

the continuously varying ellipse is expanding as $a_x(\tau)$ and $a_y(\tau)$ increase in a 2-to-1 fashion. In the context of Fig. 4, the auxiliary circle radii corresponding to $a_x(\tau)$ and $a_y(\tau)$ are increasing, causing the x and y harmonics to swell over each cycle that occurs, which has the effect of preserving the 2×1 aspect ratio as the variable ellipse rotates (final times of $4(2\pi)$ and $8(2\pi)$). If an auxiliary circle was introduced, the shadow particles would be located for these changing distances and angles through elements $a_x(\tau)$, $a_y(\tau)$, $\theta_x(\tau) = \omega_x\tau - \phi_x(\tau)$, $\theta_y(\tau) = \omega_y\tau + \phi_y$, and the x,y coordinates of the actual particle could be easily determined. In this example, the variable Lissajous curve is open and never repeats a periodic path.

A three-dimensional fixed Lissajous space curve is generated by the parametric equations below [33,39-41].

$$\begin{aligned} x(t) &= a_x \cos(\omega_x \tau - \phi_x) \\ y(t) &= a_y \sin(\omega_y \tau + \phi_y) \\ z(t) &= a_z \sin(\omega_z \tau + \phi_z) \end{aligned} \quad (7)$$

General space curves can be classified according to whether they are closed vs. open (periodic vs. non-periodic) and self-intersecting vs. non-self-intersecting (conjunctive vs. non-conjunctive). Fig. 8 illustrates the four possibilities and indicates required conditions for each case.

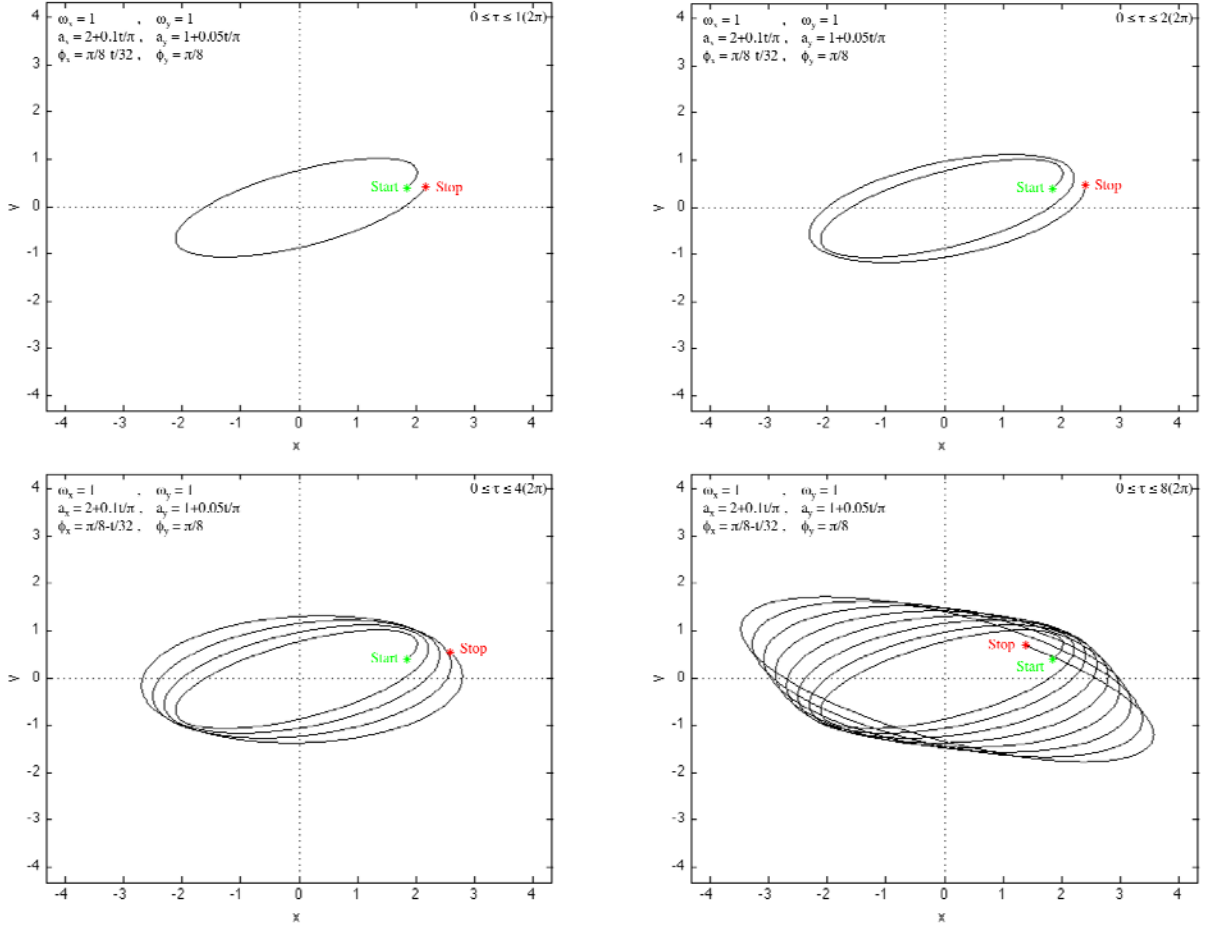


Figure 7. Variable Phase-Amplitude Lissajous Curve

From these conditions, closed Lissajous space curves occur when ω_x/ω_y , ω_y/ω_z , ω_z/ω_x are all rational, and when at least one of the frequency ratios is irrational, the curves are open. Further, several statements can be proved regarding Eq. (7) Lissajous space curve intersections, all of which require ω_x , ω_y , ω_z to be pairwise relative prime (greatest common denominator is 1). First, if $\phi_y/\omega_y + \phi_x/\omega_x \neq \pi\{(2n_y+1)/\omega_y - n_x/\omega_x\}$, $\phi_z/\omega_z - \phi_y/\omega_y \neq \pi\{(2n_z+1)/\omega_z - (2n_y+1)/\omega_y\}$, $-\phi_x/\omega_x - \phi_z/\omega_z \neq \pi\{n_x/\omega_x - (2n_z+1)/\omega_z\}$ for integer n_x , n_y , n_z , then the curve is non-self-intersecting. Second, if no more than two of the previous phase-frequency conditions are equalities rather than inequalities, then the curve is self-intersecting with a finite number of crossings. Note this statement excludes the exceptional case where two of the three frequencies are equal to 1 (which still satisfies the relative prime condition). Third, if all three of the previous phase-frequency conditions are equalities rather than inequalities, then the curve is self-intersecting with an infinite number of crossings. Note this case corresponds to a singular curve where the curve backtracks along the same path causing every point to be a crossing point, although when plotted the curve gives the "appearance" of a non-self-intersecting curve. A non-conjunctive periodic Lissajous curve is called a Lissajous knot in mathematical knot theory [41]. A three-dimensional periodic orbit in the restricted three-body problem, although not specifically generated by Eq. (7), is similar to a Lissajous knot and is commonly referred to as a halo orbit [42-44]. Further, a three-dimensional quasi-periodic (nearly periodic) orbit solving the restricted three-body problem is referred to as a Lissajous orbit [42-44].

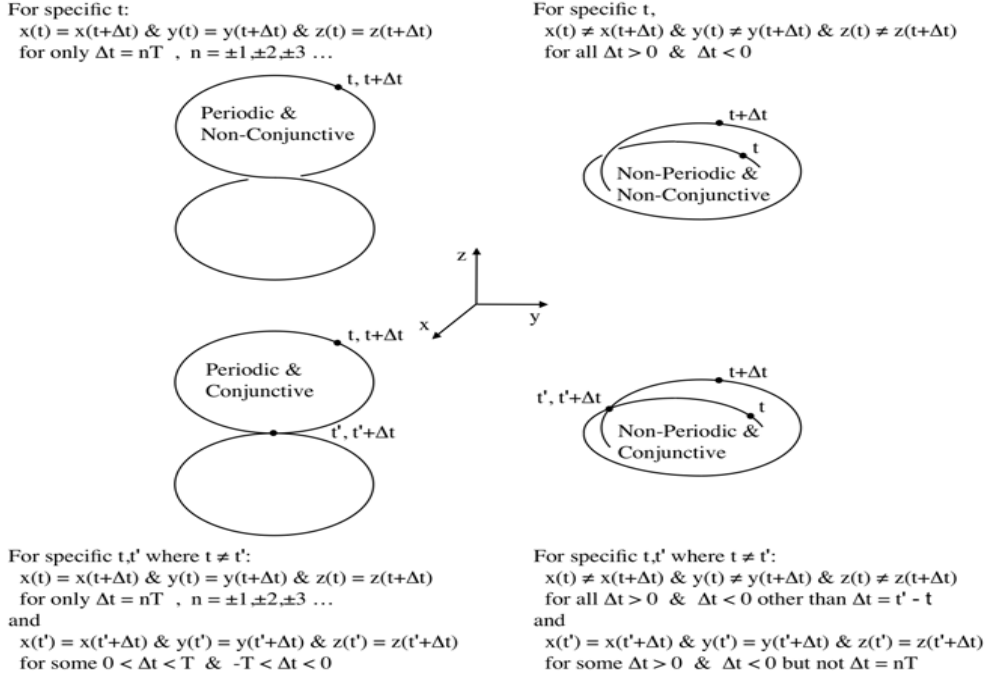


Figure 8. Space Curve Classification

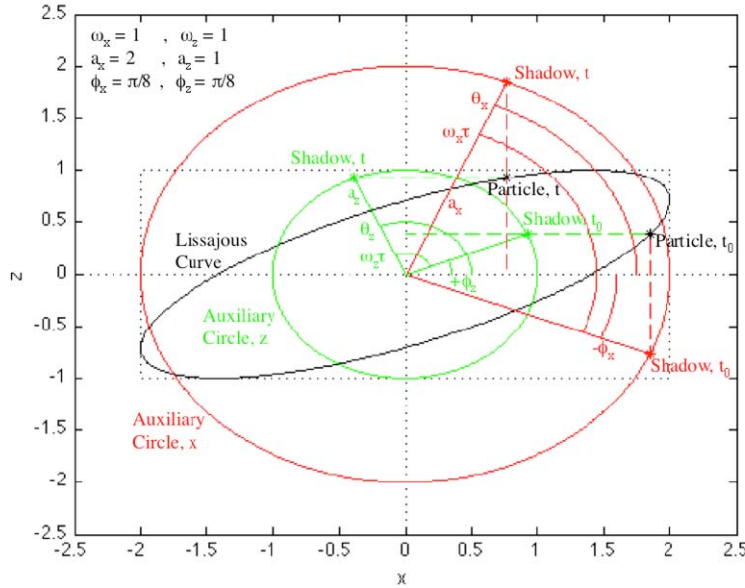


Figure 9. "Orbiting" Particle on Fixed Lissajous Curve (Out-Plane View)

Suppose a particle is "orbiting" the center point of a rotated elliptic Lissajous space path. The projected in-plane x, y motion appears as in Fig. 2, and simultaneously the projected out-plane x, z motion is indicated in Fig. 9 for the specific set of parameter values. In general, six state variables are needed to define the space particle motion. Along this programmed path, six suitable states or "orbital" elements are $a_x, a_y, a_z, \theta_x(\tau) = \omega_x \tau - \phi_x, \theta_y(\tau) = \omega_y \tau + \phi_y, \theta_z(\tau) = \omega_z \tau + \phi_z$; the first three elements describe the path size-shape, the last three elements describe the particle position. The x and y related orbital elements can be used for in-plane motion tracking as

previously discussed, and the x and z related orbital elements can be used in the same way to describe the out-plane motion. Fig. 9 shows the projected Lissajous planar curve and auxiliary circles for the xz plane. Fixed elements a_x and a_z describe dimensions of a rectangular area that encloses the orbit path. The particle initial and general positions on the Lissajous path are highlighted in Fig. 9, and the corresponding shadow particles appear on the auxiliary circles. Linearly increasing elements $\theta_x(\tau)$ and $\theta_z(\tau)$ describe the angular position of the shadow particles around the auxiliary circles, which in turn locates via projections the actual particle on the Lissajous path. The six elements and the auxiliary circles in Figs. 2 and 9 along with Eq. (7) provide a clear depiction of the particle motion. With this geometry and Eq. (7), a clear representation of the motion is captured. Rather than interpreting the motion geometry in two separate planar images, a three-dimensional image can be constructed where all three projections are processed in one view. However, for purposes of clarity, two separate three-dimensional images, one containing only the in-plane element geometry and the other containing only the out-plane geometry, are shown in Fig. 10. To further reduce clutter in Fig. 10, only the particle general position is shown but the auxiliary circles are retained. Computer generated three-dimensional color images can facilitate the practical use of the six "orbital" elements and the geometrical information they depict. In Fig. 10, θ_a denotes azimuth view angle measured from -y axis with a right-hand rotation sense and θ_e denotes elevation view angle positive above xy plane.

The final topic needed before returning to second order ROE for deputy-chief satellite motion, is variable Lissajous space curves. A three-dimensional variable Lissajous curve with time dependent amplitude, frequency, and phase parameters is generated by the equation set below.

$$\begin{aligned} x(t) &= a_x(\tau)\cos\{\omega_x(\tau)\tau - \phi_x(\tau)\} \\ y(t) &= a_y(\tau)\sin\{\omega_y(\tau)\tau + \phi_y(\tau)\} \\ z(t) &= a_z(\tau)\sin\{\omega_z(\tau)\tau + \phi_z(\tau)\} \end{aligned} \quad (8)$$

Suppose the particle is "orbiting" the center point of a variable Lissajous space path, a continuously varying and distorting rotated space ellipse. In general, six state variables are again necessary and sufficient to define the space particle motion. Six suitable "orbital" elements are $a_x(\tau)$, $a_y(\tau)$, $a_z(\tau)$, $\theta_x(\tau) = \omega_x(\tau)\tau - \phi_x(\tau)$, $\theta_y(\tau) = \omega_y(\tau)\tau + \phi_y(\tau)$, $\theta_z(\tau) = \omega_z(\tau)\tau + \phi_z(\tau)$; which have the same geometric meaning as before, except that amplitude, frequency, and phase are varying with time. Fig. 11 illustrates this geometry. The actual particle on the variable Lissajous path projects to shadow particles moving along the variable radius auxiliary circles ($a_x(\tau), a_y(\tau)$ and $a_x(\tau), a_z(\tau)$) with variable rates ($\omega_x(\tau), \omega_y(\tau)$ and $\omega_x(\tau), \omega_z(\tau)$) measured from variable reference marks ($\phi_x(\tau), \phi_y(\tau)$ and $\phi_x(\tau), \phi_z(\tau)$) in the xy and xz planes. Given $a_x(\tau)$ and $\theta_x(\tau)$ (shadow particle on the instantaneous x auxiliary circle), the actual particle and its x coordinate can always be generated and interpreted by a cosine projection. Likewise, given $a_y(\tau)$ and $\theta_y(\tau)$ (shadow particle on instantaneous y auxiliary circle), and $a_z(\tau)$ and $\theta_z(\tau)$ (shadow particle on the instantaneous z auxiliary circle), the actual particle and its y and z coordinates can always be generated and interpreted by sine projections. In Fig. 11, the instantaneous "fixed" Lissajous curve is a planar curve while the varying Lissajous curve is a non-planar twisted curve [45]. With the Fig. 11 geometry and Eq. (8), a systematic and geometric characterization of the motion is captured.

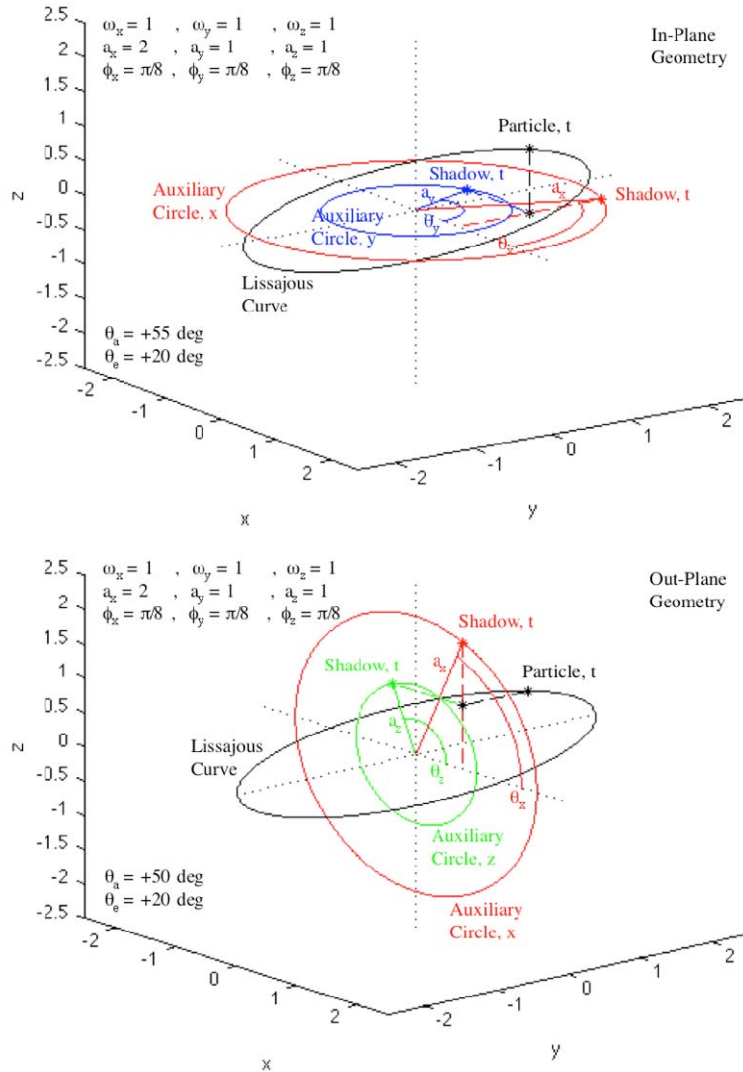


Figure 10. "Orbiting" Particle on Fixed Lissajous Curve (Perspective View)

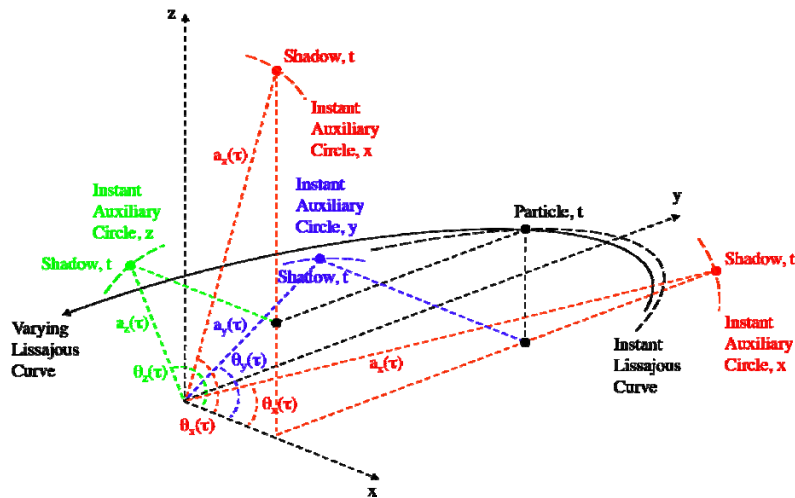


Figure 11. "Orbiting" Particle on Variable Lissajous Space Curve

Only one example of a variable phase and variable amplitude Lissajous space curve is considered here. The planar example in Fig. 7 serves as the baseline, and is extended with the z dimension motion. Fig. 12 shows the example curve with a linearly time varying phase function $\phi_x(\tau)$ and linearly time varying amplitude functions $a_x(\tau)$, $a_y(\tau)$, and $a_z(\tau)$. As in the previous example, phase angle $\phi_x(\tau)$ starts at $+\pi/8$ and decreases by $\pi/16$ for every cycle of motion, and amplitude $a_x(\tau)$ starts at 2 and increases by 0.2 for every cycle of motion, while amplitude $a_y(\tau)$ starts at 1 and increases by 0.1 for every cycle of motion. New amplitude $a_z(\tau)$ starts at 1 and increases by 0.1 for every cycle of motion, which is identical to $a_y(\tau)$. Also the new z axis frequency and phase are constant and relate to corresponding y axis values as $\omega_z = \omega_y$ and $\phi_z = -\phi_y$. Only one curve with a final time of $8(2\pi)$ is examined, but four different perspective views are shown in Fig. 12. First, if the amplitudes $a_x(\tau)$, $a_y(\tau)$, $a_z(\tau)$ and phase $\phi_x(\tau)$ were maintained at their initial values, the Lissajous curve would be a closed curve (an ellipse) lying in a fixed plane skewed from the horizontal, similar to the curve shown in Fig. 10. Second, if the amplitudes $a_x(\tau)$, $a_y(\tau)$, $a_z(\tau)$ varied as functionally indicated but phase $\phi_x(\tau)$ was still maintained at the initial value, the Lissajous curve would be an open curve but still lying in the fixed skewed plane. The curve would appear as an expanding spiral preserving the initial $x \times y \times z = 2 \times 1 \times 1$ elliptic shape. Finally, when the amplitudes $a_x(\tau)$, $a_y(\tau)$, $a_z(\tau)$ and phase $\phi_x(\tau)$ vary as functionally indicated, the Lissajous curve becomes an open, non-self-intersecting, space curve, as shown in Fig. 12. In this example, the twisted path characteristic is due to the decreasing phase $\phi_x(\tau)$. Expanding and twisting signatures are observed in Fig. 12. In the $\theta_a = 30$ deg view, note the growing positive z and negative x motions in the upper left and the growing negative z and positive x motions in the lower right. With this azimuth angle, growth in the y motion is obscured. Simultaneously, note how the peak x motions occur earlier for each cycle of motion as the curve is twisted in a retrograde sense. Although each image is of the same curve, individual azimuth perspectives give different characteristic "shapes": $\theta_a = 30$ deg produces a conchiglie pasta or seashell shape, $\theta_a = +120$ deg produces a deformable membrane shape, $\theta_a = -60$ deg produces a cornucopia shape, and $\theta_a = -100$ deg produces a multi-coil spring shape. The shape of the Lissajous curve is really none of these, and perhaps oversimplifying, the Lissajous curve is simply a complex three-dimensional curve. However, the concept of a continuously varying and distorting elliptic Lissajous curve is naturally "visualized" when examining Fig. 12. Further, the geometry of this osculating construct is precisely described by the methods previously discussed.

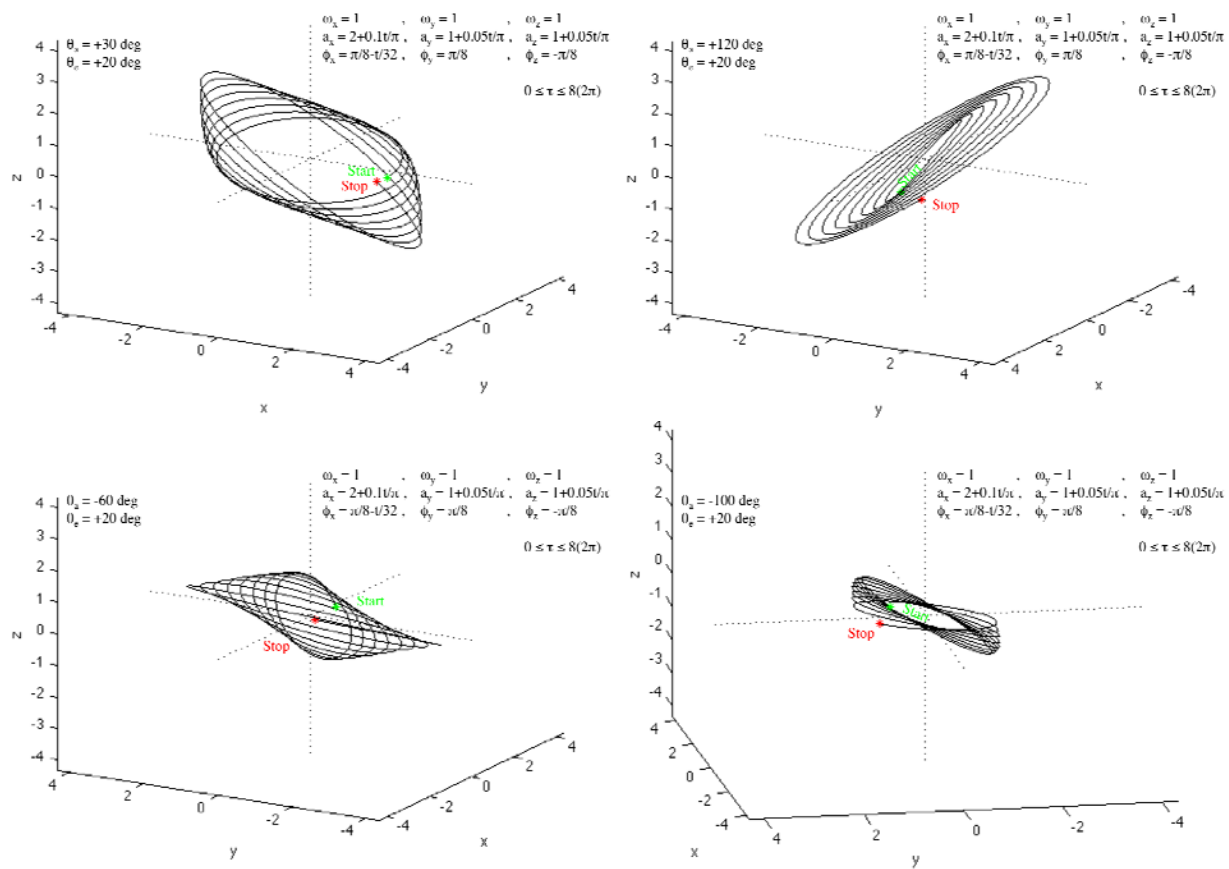


Figure 12. Variable Phase-Amplitude Lissajous Space Curve

4.0 RESULTS AND DISCUSSION

4.1 SECOND ORDER RELATIVE ORBITAL ELEMENTS - EXPANDED FORM

Return to the topic of second order ROE for deputy-chief motion. The nonlinear closed-form QV relative trajectory expressions for $x(t)$, $y(t)$, and $z(t)$, which are accurate to second order, are given in Eq. (9) [32]. In these equations, subscript "0" again denotes the value of a quantity at the initial time t_0 , and elapsed time from the reference is $\tau = t - t_0$. Additional variables in Eq. (9) include chief mean motion n_0 , chief mean radius $\bar{R}_0 = R_c$, and $S = \sin()$, $C = \cos()$. By grouping terms according to individual expansion functions: 1, $n_0\tau$, $(n_0\tau)^2$, $\cos(n_0\tau)$, $\sin(n_0\tau)$, $n_0\tau\cos(n_0\tau)$, $n_0\tau\sin(n_0\tau)$, $\cos(2n_0\tau)$, $\sin(2n_0\tau)$, and using trigonometric identities, expressions in Eq. (9) can be converted to the form in Eq. (10), where Eq. (11) provides lower level coefficient definitions. Eq. (10) indicates trajectory expressions contain three sets of three-dimensional parametric Lissajous functions: one for harmonic $n_0\tau$ indicated by subscript "h1", one for the product of secular $n_0\tau$ with harmonic $n_0\tau$ indicated by subscript "sh1", and one for harmonic $2n_0\tau$ indicated by subscript "h2", in addition to a set of polynomial functions of $n_0\tau$ indicated by subscript "c". The Lissajous functions produce three elliptical space curves and correspondingly three sets of xy and xz planar ellipses, and the polynomial functions produce a secular quadratic space curve. Following Sections 3-4 and Ref. [31], a set of twenty-one ROE are defined directly from the expanded solution form in Eq. (10) and include: $\{x_c, y_c, z_c\}$, $\{a_{x,h1}, a_{y,h1}, a_{z,h1}, \theta_{x,h1}, \theta_{y,h1}, \theta_{z,h1}\}$, $\{a_{x,sh1}, a_{y,sh1}, a_{z,sh1}, \theta_{x,sh1}, \theta_{y,sh1}, \theta_{z,sh1}\}$, $\{a_{x,h2}, a_{y,h2}, a_{z,h2}, \theta_{x,h2}, \theta_{y,h2}, \theta_{z,h2}\}$. Elements $\{x_c, y_c, z_c\}$ represent the in-plane and out-plane center point coordinates for the two-dimensional ellipses. Elements $\{a_{x,h1}, a_{y,h1}, a_{z,h1}, \theta_{x,h1}, \theta_{y,h1}, \theta_{z,h1}\}$ characterize the size-shape of, and angular position along, the two-dimensional ellipses corresponding to harmonic $n_0\tau$. Recall each ellipse will have two associated auxiliary circles that are explicitly described by the elements, which in turn implicitly describe the actual geometry of the motion along the ellipse in a meaningful way. Elements $\{a_{x,sh1}, a_{y,sh1}, a_{z,sh1}, \theta_{x,sh1}, \theta_{y,sh1}, \theta_{z,sh1}\}$ and $\{a_{x,h2}, a_{y,h2}, a_{z,h2}, \theta_{x,h2}, \theta_{y,h2}, \theta_{z,h2}\}$ play similar roles for the (secular) \times (harmonic) $n_0\tau$ and harmonic $2n_0\tau$ ellipses. Note the pure harmonic ellipses correspond to fixed Lissajous curves, but the mixed secular-harmonic ellipses are linearly expanding variable Lissajous curves.

A comparison of second order and first order ROE expressions is considered next. The center point coordinate x_e is constant in the first order theory (Eq. (3)) but x_c is time dependent in the second order theory (Eq. (10)). This time dependency involves secular terms of powers 0,1,2 indicated by subscripts "s0", "s1", "s2" in Eq. (10). Observe the first two terms in coefficient $b_{x,s0}$, which are linear functions of initial conditions x_0 and \dot{y}_0 (Eq. (11)), are precisely the first order x_e expression terms. Other second order initial condition terms in $b_{x,s0}$ represent a constant distortion to the first order ROE x_e . Other distortions that vary with time are represented by the $b_{x,s1}$ and $b_{x,s2}$ coefficients in Eq. (10). In a similar fashion, the center point coordinate y_e involves static and linearly increasing terms in the first order theory (Eq. (3)), and this behavior for y_c is preserved in the second order theory but with distortion of the relevant parameters. The first two terms in coefficient $b_{y,s0}$ involve initial conditions y_0 and \dot{x}_0 , and the first two terms in coefficient $b_{y,s1}$ are a linear combination of x_0 and \dot{y}_0 (Eq. (11)). These terms match the terms in Eq. (3) for y_e . The many extra terms in $b_{y,s0}$ and $b_{y,s1}$ are distortions on the first order ROE from second order gravitational effects. Center point z_e equals zero in the first order framework but z_c is non-zero in the second order framework. Consequently, all three terms of coefficient $b_{z,s0}$ are the

distortion on the first order ROE z_c . A summary of these center point distortions on the first order ROE is given in Eq. (12) where the new terms are not explicitly written out but have obvious definitions from the given data.

$$\begin{aligned}
 \begin{array}{l}
 x(t) \\
 = \{4-3C_{n_o\tau}\}x_0 \\
 + \{\frac{1}{n_o}S_{n_o\tau}\}x_0 + \{\frac{2}{n_o}(1-C_{n_o\tau})\}y_0 \\
 + \{\frac{3}{2}\frac{1}{R_o}(7-10C_{n_o\tau}+3C_{2n_o\tau}+12n_o\tau S_{n_o\tau}-12n_o^2\tau^2)\}x_0^2 \\
 + \{\frac{3}{2}\frac{1}{R_o}(1-C_{n_o\tau})\}y_0^2 \\
 + \{\frac{1}{4}\frac{1}{R_o}(3-2C_{n_o\tau}-C_{2n_o\tau})\}z_0^2 \\
 + \{\frac{1}{2}\frac{1}{n_o^2R_o}(-3+4C_{n_o\tau}-C_{2n_o\tau})\}x_0^2 \\
 + \{\frac{1}{2}\frac{1}{n_o^2R_o}(6-10C_{n_o\tau}+4C_{2n_o\tau}+12n_o\tau S_{n_o\tau}-9n_o^2\tau^2)\}y_0^2 \\
 + \{\frac{1}{4}\frac{1}{n_o^2R_o}(3-4C_{n_o\tau}+C_{2n_o\tau})\}z_0^2 \\
 + 2\{\frac{3}{2}\frac{1}{R_o}(-S_{n_o\tau}+n_o\tau)\}x_0y_0 \\
 + 2\{\frac{3}{2}\frac{1}{n_oR_o}(4S_{n_o\tau}-S_{2n_o\tau}-4n_o\tau+2n_o\tau C_{n_o\tau})\}x_0x_0 \\
 + 2\{\frac{3}{2}\frac{1}{n_oR_o}(4-6C_{n_o\tau}+2C_{2n_o\tau}+7n_o\tau S_{n_o\tau}-6n_o^2\tau^2)\}x_0y_0 \\
 + 2\{\frac{3}{2}\frac{1}{n_oR_o}(-S_{n_o\tau}+n_o\tau)\}y_0y_0 \\
 + 2\{\frac{1}{4}\frac{1}{n_oR_o}(2S_{n_o\tau}-S_{2n_o\tau})\}z_0z_0 \\
 + 2\{\frac{1}{2}\frac{1}{n_o^2R_o}(7S_{n_o\tau}-2S_{2n_o\tau}-6n_o\tau+3n_o\tau C_{n_o\tau})\}x_0y_0
 \end{array}
 &
 \begin{array}{l}
 y(t) \\
 = \{6(S_{n_o\tau}-n_o\tau)\}x_0 + \{1\}y_0 \\
 + \{\frac{2}{n_o}(-1+C_{n_o\tau})\}x_0 + \{\frac{1}{n_o}(4S_{n_o\tau}-3n_o\tau)\}y_0 \\
 + \{\frac{3}{4}\frac{1}{R_o}(40S_{n_o\tau}+3S_{2n_o\tau}-22n_o\tau-24n_o\tau C_{n_o\tau})\}x_0^2 \\
 + \{\frac{3}{4}\frac{1}{R_o}(S_{n_o\tau}-n_o\tau)\}y_0^2 \\
 + \{\frac{1}{4}\frac{1}{R_o}(4S_{n_o\tau}+S_{2n_o\tau}-6n_o\tau)\}z_0^2 \\
 + \{\frac{1}{4}\frac{1}{n_o^2R_o}(8S_{n_o\tau}-S_{2n_o\tau}-6n_o\tau)\}x_0^2 \\
 + \{\frac{1}{n_o^2R_o}(10S_{n_o\tau}+S_{2n_o\tau}-6n_o\tau-6n_o\tau C_{n_o\tau})\}y_0^2 \\
 + \{\frac{1}{4}\frac{1}{n_o^2R_o}(8S_{n_o\tau}-S_{2n_o\tau}-6n_o\tau)\}z_0^2 \\
 + 2\{\frac{3}{2}\frac{1}{R_o}(1-C_{n_o\tau})\}x_0y_0 \\
 + 2\{\frac{3}{4}\frac{1}{n_oR_o}(-5+4C_{n_o\tau}+C_{2n_o\tau}+4n_o\tau S_{n_o\tau})\}x_0x_0 \\
 + 2\{\frac{3}{2}\frac{1}{n_oR_o}(12S_{n_o\tau}+S_{2n_o\tau}-7n_o\tau-7n_o\tau C_{n_o\tau})\}x_0y_0 \\
 + 2\{\frac{3}{2}\frac{1}{n_oR_o}(-S_{n_o\tau}+n_o\tau)\}y_0x_0 \\
 + 2\{\frac{1}{4}\frac{1}{n_oR_o}(-3+4C_{n_o\tau}-C_{2n_o\tau})\}z_0z_0 \\
 + 2\{\frac{1}{2}\frac{1}{n_o^2R_o}(-3+2C_{n_o\tau}+C_{2n_o\tau}+3n_o\tau S_{n_o\tau})\}x_0y_0
 \end{array}
 \end{array}
 \quad (9)$$

$$\begin{aligned}
 z(t) \\
 = \{C_{n_o\tau}\}z_0 + \{\frac{1}{n_o}S_{n_o\tau}\}z_0 \\
 + 2\{\frac{3}{4}\frac{1}{R_o}(-3+2C_{n_o\tau}+C_{2n_o\tau}+4n_o\tau S_{n_o\tau})\}x_0z_0 \\
 + 2\{\frac{3}{4}\frac{1}{n_oR_o}(2S_{n_o\tau}+S_{2n_o\tau}-4n_o\tau C_{n_o\tau})\}x_0z_0 \\
 + 2\{\frac{1}{4}\frac{1}{n_oR_o}(2S_{n_o\tau}-S_{2n_o\tau})\}z_0x_0 \\
 + 2\{\frac{1}{2}\frac{1}{n_oR_o}(-3+2C_{n_o\tau}+C_{2n_o\tau}+3n_o\tau S_{n_o\tau})\}z_0y_0 \\
 + 2\{\frac{1}{4}\frac{1}{n_o^2R_o}(3-4C_{n_o\tau}+C_{2n_o\tau})\}x_0z_0 \\
 + 2\{\frac{1}{2}\frac{1}{n_o^2R_o}(S_{n_o\tau}+S_{2n_o\tau}-3n_o\tau C_{n_o\tau})\}y_0z_0
 \end{aligned}$$

$$\begin{aligned}
x(t) &= x_c(\tau) + x_{h1}(\tau) + x_{sh1}(\tau) + x_{h2}(\tau) \\
y(t) &= y_c(\tau) + y_{h1}(\tau) + y_{sh1}(\tau) + y_{h2}(\tau) \\
z(t) &= z_c + z_{h1}(\tau) + z_{sh1}(\tau) + z_{h2}(\tau)
\end{aligned} \tag{10}$$

where

$$\begin{aligned}
x_c(\tau) &= b_{x,s0}(1) + b_{x,s1}(n_o\tau) + b_{x,s2}(n_o\tau)^2 \\
y_c(\tau) &= b_{y,s0}(1) + b_{y,s1}(n_o\tau) \\
z_c &= b_{z,s0}(1)
\end{aligned}$$

$$\begin{aligned}
x_{h1}(\tau) &= a_{x,h1}\cos\{\theta_{x,h1}(\tau)\} , \quad x_{sh1}(\tau) = a_{x,sh1}(\tau)\cos\{\theta_{x,sh1}(\tau)\} , \quad x_{h2}(\tau) = a_{x,h2}\cos\{\theta_{x,h2}(\tau)\} \\
y_{h1}(\tau) &= a_{y,h1}\sin\{\theta_{y,h1}(\tau)\} , \quad y_{sh1}(\tau) = a_{y,sh1}(\tau)\sin\{\theta_{y,sh1}(\tau)\} , \quad y_{h2}(\tau) = a_{y,h2}\sin\{\theta_{y,h2}(\tau)\} \\
z_{h1}(\tau) &= a_{z,h1}\sin\{\theta_{z,h1}(\tau)\} , \quad z_{sh1}(\tau) = a_{z,sh1}(\tau)\sin\{\theta_{z,sh1}(\tau)\} , \quad z_{h2}(\tau) = a_{z,h2}\sin\{\theta_{z,h2}(\tau)\}
\end{aligned}$$

$$\theta_{x,h1}(\tau) = n_o\tau - \phi_{x,h1} , \quad \theta_{x,sh1}(\tau) = n_o\tau - \phi_{x,sh1} , \quad \theta_{x,h2}(\tau) = 2n_o\tau - \phi_{x,h2}$$

$$\theta_{y,h1}(\tau) = n_o\tau + \phi_{y,h1} , \quad \theta_{y,sh1}(\tau) = n_o\tau + \phi_{y,sh1} , \quad \theta_{y,h2}(\tau) = 2n_o\tau + \phi_{y,h2}$$

$$\theta_{z,h1}(\tau) = n_o\tau + \phi_{z,h1} , \quad \theta_{z,sh1}(\tau) = n_o\tau + \phi_{z,sh1} , \quad \theta_{z,h2}(\tau) = 2n_o\tau + \phi_{z,h2}$$

$$a_{x,h1}^2 = b_{x,h1}^2 + c_{x,h1}^2 , \quad a_{x,sh1}^2(\tau) = \{b_{x,sh1}^2 + c_{x,sh1}^2\}(n_o\tau)^2 , \quad a_{x,h2}^2 = b_{x,h2}^2 + c_{x,h2}^2$$

$$a_{y,h1}^2 = b_{y,h1}^2 + c_{y,h1}^2 , \quad a_{y,sh1}^2(\tau) = \{b_{y,sh1}^2 + c_{y,sh1}^2\}(n_o\tau)^2 , \quad a_{y,h2}^2 = b_{y,h2}^2 + c_{y,h2}^2$$

$$a_{z,h1}^2 = b_{z,h1}^2 + c_{z,h1}^2 , \quad a_{z,sh1}^2(\tau) = \{b_{z,sh1}^2 + c_{z,sh1}^2\}(n_o\tau)^2 , \quad a_{z,h2}^2 = b_{z,h2}^2 + c_{z,h2}^2$$

$$\tan(\phi_{x,h1}) = c_{x,h1} / b_{x,h1} , \quad \tan(\phi_{x,sh1}) = c_{x,sh1} / b_{x,sh1} , \quad \tan(\phi_{x,h2}) = c_{x,h2} / b_{x,h2}$$

$$\tan(\phi_{y,h1}) = b_{y,h1} / c_{y,h1} , \quad \tan(\phi_{y,sh1}) = b_{y,sh1} / c_{y,sh1} , \quad \tan(\phi_{y,h2}) = b_{y,h2} / c_{y,h2}$$

$$\tan(\phi_{z,h1}) = b_{z,h1} / c_{z,h1} , \quad \tan(\phi_{z,sh1}) = b_{z,sh1} / c_{z,sh1} , \quad \tan(\phi_{z,h2}) = b_{z,h2} / c_{z,h2}$$

$$\begin{aligned}
b_{x,s0} &= 4x_0 + \frac{2}{n_0} \dot{y}_0 + \frac{21}{2} \frac{1}{R_0} x_0^2 + \frac{3}{2} \frac{1}{R_0} y_0^2 + \frac{3}{4} \frac{1}{R_0} z_0^2 - \frac{3}{2} \frac{1}{n_0^2 R_0} \dot{x}_0^2 + 3 \frac{1}{n_0^2 R_0} \dot{y}_0^2 + \frac{3}{4} \frac{1}{n_0^2 R_0} \dot{z}_0^2 + 12 \frac{1}{n_0 R_0} x_0 \dot{y}_0 \\
b_{x,s1} &= 6 \frac{1}{R_0} x_0 \dot{y}_0 - 12 \frac{1}{n_0 R_0} x_0 \dot{x}_0 + 3 \frac{1}{n_0 R_0} y_0 \dot{y}_0 - 6 \frac{1}{n_0^2 R_0} \dot{x}_0 \dot{y}_0 \\
b_{x,s2} &= -18 \frac{1}{R_0} x_0^2 - \frac{9}{2} \frac{1}{n_0^2 R_0} \dot{y}_0^2 - 18 \frac{1}{n_0 R_0} x_0 \dot{y}_0 \\
b_{y,s0} &= y_0 - \frac{2}{n_0} \dot{x}_0 + 3 \frac{1}{R_0} x_0 \dot{y}_0 - \frac{15}{2} \frac{1}{n_0 R_0} x_0 \dot{x}_0 - \frac{3}{2} \frac{1}{n_0 R_0} z_0 \dot{z}_0 - 3 \frac{1}{n_0^2 R_0} \dot{x}_0 \dot{y}_0 \\
b_{y,s1} &= -6x_0 - \frac{3}{n_0} \dot{y}_0 - \frac{33}{2} \frac{1}{R_0} x_0^2 - 3 \frac{1}{R_0} y_0^2 - \frac{3}{2} \frac{1}{R_0} z_0^2 - \frac{3}{2} \frac{1}{n_0^2 R_0} \dot{x}_0^2 - 6 \frac{1}{n_0^2 R_0} \dot{y}_0^2 - \frac{3}{2} \frac{1}{n_0^2 R_0} \dot{z}_0^2 - 21 \frac{1}{n_0 R_0} x_0 \dot{y}_0 + 3 \frac{1}{n_0 R_0} y_0 \dot{x}_0 \\
b_{z,s0} &= -\frac{9}{2} \frac{1}{R_0} x_0 z_0 - 3 \frac{1}{n_0 R_0} z_0 \dot{y}_0 + \frac{3}{2} \frac{1}{n_0^2 R_0} \dot{x}_0 \dot{z}_0 \\
b_{x,h1} &= -3x_0 - \frac{2}{n_0} \dot{y}_0 - 15 \frac{1}{R_0} x_0^2 - \frac{3}{2} \frac{1}{R_0} y_0^2 - \frac{1}{2} \frac{1}{R_0} z_0^2 + 2 \frac{1}{n_0^2 R_0} \dot{x}_0^2 - 5 \frac{1}{n_0^2 R_0} \dot{y}_0^2 - \frac{1}{n_0^2 R_0} \dot{z}_0^2 - 18 \frac{1}{n_0 R_0} x_0 \dot{y}_0 \\
c_{x,h1} &= \frac{1}{n_0} \dot{x}_0 - 6 \frac{1}{R_0} x_0 \dot{y}_0 + 12 \frac{1}{n_0 R_0} x_0 \dot{x}_0 - 3 \frac{1}{n_0 R_0} y_0 \dot{y}_0 + \frac{1}{n_0 R_0} z_0 \dot{z}_0 + 7 \frac{1}{n_0^2 R_0} \dot{x}_0 \dot{y}_0 \\
b_{x,sh1} &= 6 \frac{1}{n_0 R_0} x_0 \dot{x}_0 + 3 \frac{1}{n_0^2 R_0} \dot{x}_0 \dot{y}_0 \\
c_{x,sh1} &= 18 \frac{1}{R_0} x_0^2 + 6 \frac{1}{n_0^2 R_0} \dot{y}_0^2 + 21 \frac{1}{n_0 R_0} x_0 \dot{y}_0 \\
b_{x,h2} &= \frac{9}{2} \frac{1}{R_0} x_0^2 - \frac{1}{4} \frac{1}{R_0} z_0^2 - \frac{1}{2} \frac{1}{n_0^2 R_0} \dot{x}_0^2 + 2 \frac{1}{n_0^2 R_0} \dot{y}_0^2 + \frac{1}{4} \frac{1}{n_0^2 R_0} \dot{z}_0^2 + 6 \frac{1}{n_0 R_0} x_0 \dot{y}_0 \\
c_{x,h2} &= -3 \frac{1}{n_0 R_0} x_0 \dot{x}_0 - \frac{1}{2} \frac{1}{n_0 R_0} z_0 \dot{z}_0 - 2 \frac{1}{n_0^2 R_0} \dot{x}_0 \dot{y}_0 \\
b_{y,h1} &= \frac{2}{n_0} \dot{x}_0 - 3 \frac{1}{R_0} x_0 \dot{y}_0 + 6 \frac{1}{n_0 R_0} x_0 \dot{x}_0 + 2 \frac{1}{n_0 R_0} z_0 \dot{z}_0 + 2 \frac{1}{n_0^2 R_0} \dot{x}_0 \dot{y}_0 \\
c_{y,h1} &= 6x_0 + \frac{4}{n_0} \dot{y}_0 + 30 \frac{1}{R_0} x_0^2 + 3 \frac{1}{R_0} y_0^2 + \frac{1}{R_0} z_0^2 + 2 \frac{1}{n_0^2 R_0} \dot{x}_0^2 + 10 \frac{1}{n_0^2 R_0} \dot{y}_0^2 + 2 \frac{1}{n_0^2 R_0} \dot{z}_0^2 + 36 \frac{1}{n_0 R_0} x_0 \dot{y}_0 - 3 \frac{1}{n_0 R_0} y_0 \dot{x}_0 \\
b_{y,sh1} &= -18 \frac{1}{R_0} x_0^2 - 6 \frac{1}{n_0^2 R_0} \dot{y}_0^2 - 21 \frac{1}{n_0 R_0} x_0 \dot{y}_0 \\
c_{y,sh1} &= 6 \frac{1}{n_0 R_0} x_0 \dot{x}_0 + 3 \frac{1}{n_0^2 R_0} \dot{x}_0 \dot{y}_0 \\
b_{y,h2} &= \frac{3}{2} \frac{1}{n_0 R_0} x_0 \dot{x}_0 - \frac{1}{2} \frac{1}{n_0 R_0} z_0 \dot{z}_0 + \frac{1}{n_0^2 R_0} \dot{x}_0 \dot{y}_0 \\
c_{y,h2} &= \frac{9}{4} \frac{1}{R_0} x_0^2 + \frac{1}{4} \frac{1}{R_0} z_0^2 - \frac{1}{4} \frac{1}{n_0^2 R_0} \dot{x}_0^2 + \frac{1}{n_0^2 R_0} \dot{y}_0^2 - \frac{1}{4} \frac{1}{n_0^2 R_0} \dot{z}_0^2 + 3 \frac{1}{n_0 R_0} x_0 \dot{y}_0 \\
b_{z,h1} &= z_0 + 3 \frac{1}{R_0} x_0 z_0 + 2 \frac{1}{n_0 R_0} z_0 \dot{y}_0 - 2 \frac{1}{n_0^2 R_0} \dot{x}_0 \dot{z}_0 \\
c_{z,h1} &= \frac{1}{n_0} \dot{z}_0 + 3 \frac{1}{n_0 R_0} x_0 \dot{z}_0 + \frac{1}{n_0 R_0} z_0 \dot{x}_0 + \frac{1}{n_0^2 R_0} \dot{y}_0 \dot{z}_0 \\
b_{z,sh1} &= -6 \frac{1}{n_0 R_0} x_0 \dot{z}_0 - 3 \frac{1}{n_0^2 R_0} \dot{y}_0 \dot{z}_0 \\
c_{z,sh1} &= 6 \frac{1}{R_0} x_0 z_0 + 3 \frac{1}{n_0 R_0} z_0 \dot{y}_0 \\
b_{z,h2} &= \frac{3}{2} \frac{1}{R_0} x_0 z_0 + \frac{1}{n_0 R_0} z_0 \dot{y}_0 + \frac{1}{2} \frac{1}{n_0^2 R_0} \dot{x}_0 \dot{z}_0 \\
c_{z,h2} &= \frac{3}{2} \frac{1}{n_0 R_0} x_0 \dot{z}_0 - \frac{1}{2} \frac{1}{n_0 R_0} z_0 \dot{x}_0 + \frac{1}{n_0^2 R_0} \dot{y}_0 \dot{z}_0
\end{aligned} \tag{11}$$

$$\begin{aligned}
\underbrace{x_c}_{2\text{nd Order}} &= \underbrace{x_e}_{1\text{st Order}} + \underbrace{\delta(x_e)1 + \delta(\dot{x}_e)\tau + \delta(\ddot{x}_e)\tau^2}_{\text{Distortions}} \\
\underbrace{y_c}_{2\text{nd Order}} &= \underbrace{y_e + \dot{y}_e\tau}_{1\text{st Order}} + \underbrace{\delta(y_e)1 + \delta(\dot{y}_e)\tau}_{\text{Distortions}} \\
\underbrace{z_c}_{2\text{nd Order}} &= \underbrace{0}_{1\text{st Order}} + \underbrace{\delta(z_e)1}_{\text{Distortions}}
\end{aligned} \tag{12}$$

The distortions can be interpreted as additional position, velocity, and acceleration sources. These distortions improve the characterization of the deputy motion physics including curved in-the-plane departure tracks and unbalanced out-of-plane harmonics [31,32]. Note if all second order initial condition terms are set to zero, all distortions become zero and the second order ROE collapse to the first order ROE.

The y axis amplitude $2a_e$ is constant in first order theory (Eq. (3)) and also in second order theory for the first harmonic term (Eq. (10)), but is statically altered. The linear initial condition terms $x_0, \dot{x}_0, \dot{y}_0$ appearing in coefficients $b_{y,h1}$ and $c_{y,h1}$ (Eq. (11)) after being squared precisely form the first order $4a_e^2$ expression. Other second order initial condition terms in $b_{y,h1}$ and $c_{y,h1}$ represent distortion on the first order ROE $2a_e$. In a similar way, the linear terms z_0, \dot{z}_0 in coefficients $b_{z,h1}$ and $c_{z,h1}$ (Eq. (11)) reproduce the first order z axis amplitude b_e (Eq. (3)) and the remaining initial condition terms cause a static distortion. Now consider a comparison of y axis harmonic angles. Both first order angle α and second order angle $\theta_{y,h1}$ have the same frequency term $n_0\tau$, so the only difference for α and $\theta_{y,h1}$ originates with phase angles $\alpha_0 = \alpha(0)$ and $\phi_{y,h1}$. The linear initial condition terms $x_0, \dot{x}_0, \dot{y}_0$ appearing in coefficients $b_{y,h1}$ and $c_{y,h1}$ (Eq. (11)) exactly match the terms of the arctangent argument ratio appearing in α_0 . All other second order initial condition terms in $b_{y,h1}$ and $c_{y,h1}$ represent distortion on the phase angle of the first order ROE α . Similarly, the linear terms z_0, \dot{z}_0 in coefficients $b_{z,h1}$ and $c_{z,h1}$ (Eq. (11)) reproduce the first order z axis phase angle $\beta_0 = \beta(0)$ (Eq. (3)) and the remaining initial condition terms cause a static distortion. A summary of these amplitude and phase distortions on the first order ROE is given in Eq. (13) where the new terms are not explicitly written out but have obvious definitions from the given data.

$$\begin{aligned}
\underbrace{a_{y,h1}^2}_{2\text{nd Order}} &= \underbrace{4a_e^2}_{1\text{st Order}} + \underbrace{\delta(4a_e^2)}_{\text{Distortions}}, \quad \underbrace{\tan(\phi_{y,h1})}_{2\text{nd Order}} = \underbrace{\tan(\alpha_0)}_{1\text{st Order}} + \underbrace{\tan\{\delta(\alpha_0')\}}_{\text{Distortions}} / [1 + \underbrace{\tan\{\delta(\alpha_0'')\}}_{\text{Distortions}}] \\
\underbrace{a_{z,h1}^2}_{2\text{nd Order}} &= \underbrace{b_e^2}_{1\text{st Order}} + \underbrace{\delta(b_e^2)}_{\text{Distortions}}, \quad \underbrace{\tan(\phi_{z,h1})}_{2\text{nd Order}} = \underbrace{\tan(\beta_0)}_{1\text{st Order}} + \underbrace{\tan\{\delta(\beta_0')\}}_{\text{Distortions}} / [1 + \underbrace{\tan\{\delta(\beta_0'')\}}_{\text{Distortions}}]
\end{aligned} \tag{13}$$

The distortions can be interpreted as additional amplitude and phase sources. These distortions also improve the characterization of the deputy motion physics including travel distances and travel sequencing in both in-plane and out-plane axes [31,32]. Note if all second order initial condition terms are set to zero, all distortions become zero and the second order ROE collapse to the first order ROE.

Other comparisons can be made between the first order and second order ROE, and their impact on the motion characteristics. Under first order theory, the in-plane harmonic motion

maintains a fixed $y \times x = 2 \times 1$ amplitude behavior, regardless of the initial conditions. To analyze the corresponding behavior for second order theory, compare the expressions for amplitudes $a_{x,h1}$ and $a_{y,h1}$, or $b_{x,h1}$, $c_{x,h1}$ and $b_{y,h1}$, $c_{y,h1}$. For every initial condition term in $b_{x,h1}$, there is a corresponding term of twice the value but with opposite sign appearing in $c_{y,h1}$ with two exceptions: 1) the \dot{x}_0^2 terms have the same sign and no doubling, and 2) $c_{y,h1}$ contains the extra term $y_0 \dot{x}_0$. Further, although two terms (\dot{x}_0 , $z_0 \dot{z}_0$) in $c_{x,h1}$ also appear in $b_{y,h1}$ with a factor of 2 and consistent sign, other terms are not scale and sign consistent. In general under second order theory, the in-plane motion does not strictly follow a 2-to-1 relationship, although an approximate 2-to-1 behavior is likely due to the many matching terms. An interesting observation noted in Ref. [31] is that two of the secular-harmonic coefficients have equal magnitudes and signs, or $b_{x,sh1} = c_{y,sh1}$, while another pair of the secular-harmonic coefficients have equal magnitudes but opposite signs, or $b_{y,sh1} = -c_{x,sh1}$.

Distortions on the first order ROE noted previously originate with the center point polynomials and first harmonic ellipses, and can be interpreted as parametric distortions where Eqs. (12)-(13) explicitly describe the distortion structure and how it affects the relative motion. Other distortions exist and originate with the first secular-harmonic and second harmonic ellipses. These effects can be interpreted as coordinate distortions since they are kept as separate terms in the expanded form of second order ROE. If the coordinate distortions are combined and labeled as δx , δy , δz , then the overall comparison of second order and first order ROE expressions would be of the form

$$\begin{aligned} x(t) &= x_c\{\tau, x_e, \delta(x_e), \delta(\dot{x}_e), \delta(\ddot{x}_e)\} + a_{x,h1}\{\tilde{a}_e, \delta(\tilde{a}_e^2)\}\cos[n_0\tau + \phi_{x,h1}\{\tilde{\alpha}_0, \delta(\tilde{\alpha}_0'), \delta(\tilde{\alpha}_0'')\}] + \delta x\{x_{sh1}(\tau), x_{h2}(\tau)\} \\ y(t) &= y_c\{\tau, y_e, \delta(y_e), \delta(\dot{y}_e)\} + a_{y,h1}\{a_e, \delta(4a_e^2)\}\sin[n_0\tau + \phi_{y,h1}\{\alpha_0, \delta(\alpha_0'), \delta(\alpha_0'')\}] + \delta y\{y_{sh1}(\tau), y_{h2}(\tau)\} \\ z(t) &= z_c\{0, \delta(z_e)\} + a_{z,h1}\{b_e, \delta(b_e^2)\}\sin[n_0\tau + \phi_{z,h1}\{\beta_0, \delta(\beta_0'), \delta(\beta_0'')\}] + \delta z\{z_{sh1}(\tau), z_{h2}(\tau)\} \end{aligned} \quad (14)$$

The overscript symbol "~" appearing in Eq. (14) distinguishes two different parameter sets based on different trigonometric forms used for $x(t)$ in the first order Eq. (3) and second order Eq. (10) expressions. The Eq. (14) expressions could be useful in performing error analysis on guidance, navigation, and control algorithms that employ first order dynamics, or exposing critical error sources when propagating the natural relative motion using first order dynamics.

Eq. (10) indicates overall deputy relative orbital motion consists of superpositioning (linear combining) three in-the-plane and three out-of-plane ellipses and polynomial center point curves. Each elliptic motion component is governed by a set of three-dimensional parametric Lissajous functions and underlying geometry characterized by the corresponding six relative orbital elements and associated auxiliary circles (see Section 4), giving $3 \times 6 = 18$ ROE for the elliptic motion. Movement of the ellipse centers are characterized by three additional ROE, yielding $18 + 3 = 21$ ROE in totality using the expanded formulation. In this formulation, two of the ellipse sets correspond to fixed Lissajous curves and the other ellipse set corresponds to variable amplitude Lissajous curves. Component motions can be thought of as natural modes that combine to form overall motion. This perspective was considered in Ref. [31].

To further explore component motions and the underlying geometry described by second order ROE, a three-dimensional numeric example is offered. Deputy initial position is along the LVLH x axis ("above" the chief) with initial velocity components in all three x , y , and z directions. Circular chief orbital parameters and deputy relative initial conditions are specified in Eq. (15), and Fig. 13 shows the corresponding relative trajectory, a corkscrew motion

representative of close proximity encounters, for approximately 2.5 orbits where T denotes chief orbital period. The deputy satellite is drifting significantly away from and behind the chief satellite while simultaneously oscillating about the reference orbit plane. After two orbits, deputy position is approximately -800 km along-track and -40 km radial with ± 20 km cross-track amplitudes during the motion. Two trajectories are shown in Fig. 13: the "exact" trajectory generated by nonlinear simulation (NLS) based on Runge-Kutta 4th order numerical integration and the approximate QV trajectory from Eq. (9). The overlay plot implies orbit propagation error due to differences between two-body exact and approximate QV motion models will be minimal for the temporal horizon shown. Simulation parameters include Earth gravitation constant $\mu = 398,600 \text{ km}^3/\text{s}^2$ and integration time step $\Delta t = (2\pi/n_o)/3600$ with rad/s units for n_o .

$$\begin{array}{ll} \text{Chief:} & \text{Deputy: } t_0 = 0 \text{ s} \\ \bar{R}_o = 7100 \text{ km} & x_0 = 0.2 \text{ km}, y_0 = 0 \text{ km}, z_0 = 0 \text{ km} \\ n_o = 0.001055 \text{ rad/s} & \dot{x}_0 = 0.002 \text{ km/s}, \dot{y}_0 = 0.02 \text{ km/s}, \dot{z}_0 = 0.02 \text{ km/s} \end{array} \quad (15)$$

The relative trajectory for 8 orbits (8T) is shown in Fig. 14 and is used to investigate the motion geometry and second order ROE based on the expanded formulation. Four specific times $t_1 = 1/8T$, $t_2 = 1/4T$, $t_3 = 1T$, $t_4 = 2T$ are highlighted along the trajectory and used in the discussion. Fig. 15 shows the four component trajectories: secular center point polynomial motion (c), first harmonic elliptic motion (h1), first secular-harmonic elliptic motion (sh1), and second harmonic elliptic motion (h2). Each curve shows the start and stop positions, and Tab. 1 lists the corresponding initial and final values for the twenty-one ROE. Note each three-dimensional elliptic curve can be projected to the xy and xz planes (shown in Fig. 15) with corresponding auxiliary circles and deputy shadow satellites (not shown in Fig. 15) to visualize and quantify the motion geometry. For example, the four start points in Fig. 15 can be graphically superimposed to form the overall start point in Fig. 14, or mathematically for $x(t_0)$

Table 1. ROE Initial and Final Values - Expanded Formulation

Units	km	km	km	deg	deg	deg
Initial Val.						
ROE	x_c	y_c	z_c			
Center Pt.	3.8899e+01	-3.8059e+00	7.5881e-03			
ROE	$a_{x,h1}, a_{x,sh1}, a_{x,h2}$	$a_{y,h1}, a_{y,sh1}, a_{y,h2}$	$a_{z,h1}, a_{z,sh1}, a_{z,h2}$	$\theta_{x,h1}, \theta_{x,sh1}, \theta_{x,h2}$	$\theta_{y,h1}, \theta_{y,sh1}, \theta_{y,h2}$	$\theta_{z,h1}, \theta_{z,sh1}, \theta_{z,h2}$
1st Har.	3.8864e+01	7.7727e+01	1.9004e+01	-1.7715e+02	2.8028e+00	-3.0503e-02
1st Sec.-Har.	0	0	0	-8.7182e+01	-8.7182e+01	-9.0000e+01
2nd Har.	1.1725e-01	3.9762e-02	5.1450e-02	5.0288e+00	7.4257e+00	2.8179e+00
Final Val.						
ROE	x_c	y_c	z_c			
Center Pt.	-5.6236e+02	-2.9417e+03	7.5881e-03			
ROE	$a_{x,h1}, a_{x,sh1}, a_{x,h2}$	$a_{y,h1}, a_{y,sh1}, a_{y,h2}$	$a_{z,h1}, a_{z,sh1}, a_{z,h2}$	$\theta_{x,h1}, \theta_{x,sh1}, \theta_{x,h2}$	$\theta_{y,h1}, \theta_{y,sh1}, \theta_{y,h2}$	$\theta_{z,h1}, \theta_{z,sh1}, \theta_{z,h2}$
1st Har.	3.8864e+01	7.7727e+01	1.9004e+01	2.7028e+03	2.8828e+03	2.8800e+03
1st Sec.-Har.	1.5844e+01	1.5844e+01	7.7894e+00	2.7928e+03	2.7928e+03	2.7900e+03
2nd Har.	1.1725e-01	3.9762e-02	5.1450e-02	5.7650e+03	5.7674e+03	5.7628e+03

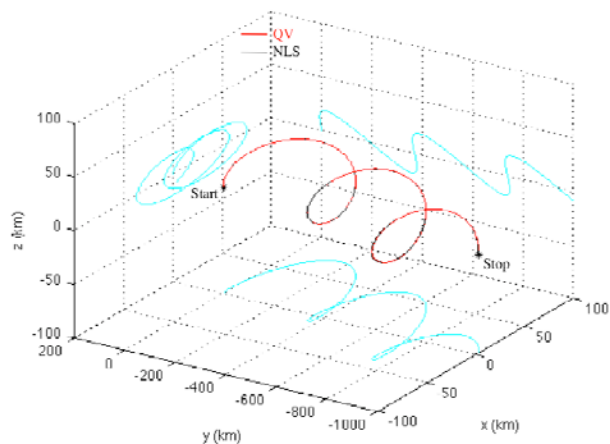


Figure 13. QV vs. NLS for 2.5T

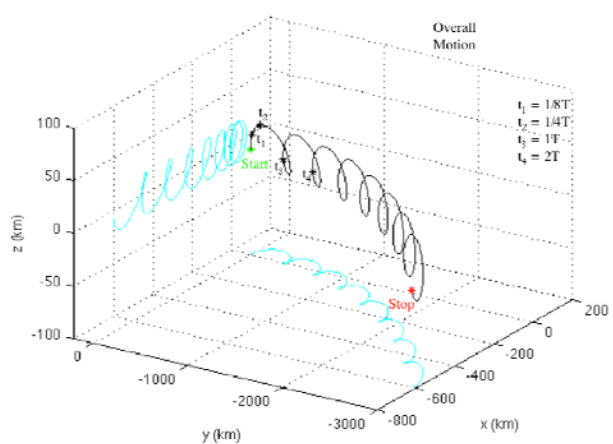


Figure 14. QV for 8T - Expanded Formulation

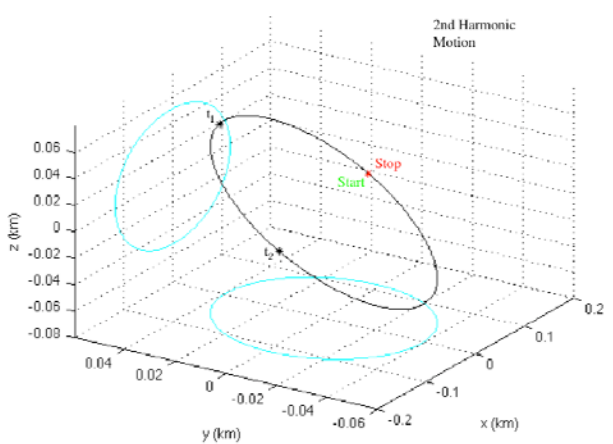
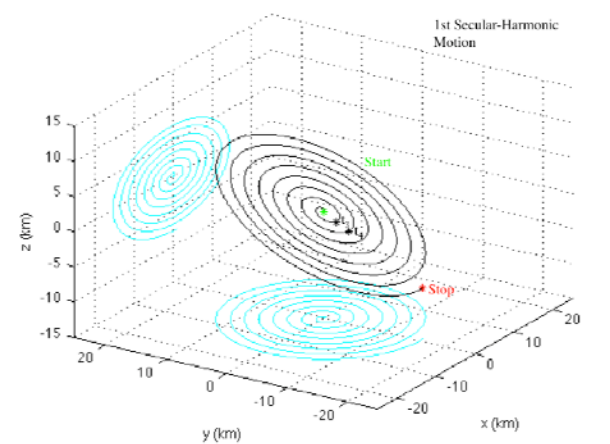
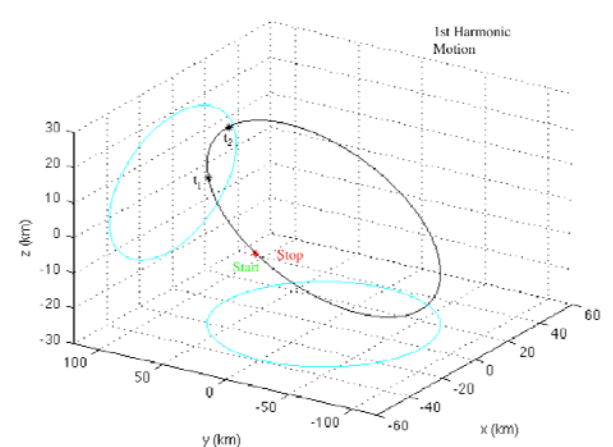
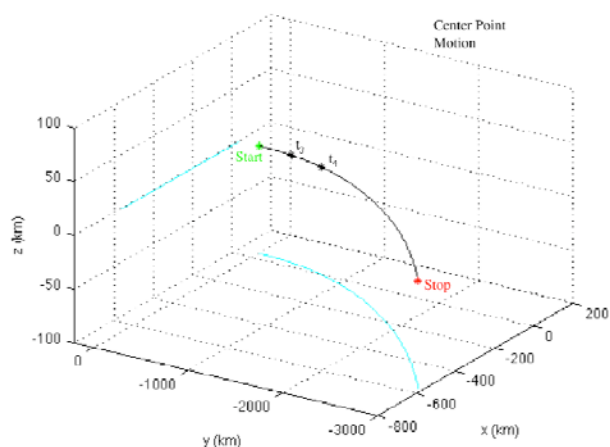


Figure 15. Component Motions - Expanded Formulation

$$\begin{aligned}
x(t_0) &= x_c(t_0) + x_{h1}(t_0) + x_{sh1}(t_0) + x_{h2}(t_0) \\
x_0 &= b_{x,s0} + a_{x,h1}\cos\{\theta_{x,h1}(t_0)\} + a_{x,sh1}(t_0)\cos\{\theta_{x,sh1}(t_0)\} + a_{x,h2}\cos\{\theta_{x,h2}(t_0)\} \\
0.2 \text{ km} &= 38.899 + 38.864\cos\{-177.15^\circ\} + 0\cos\{-87.182^\circ\} + 0.11725\cos\{5.0288^\circ\} \text{ km} \quad (16) \\
0.2 \text{ km} &= 38.899 + -38.8159 + 0 + 0.11680 \text{ km} \\
0.2 \text{ km} &= 0.1999 \text{ km} \sqrt{(0.1 \text{ m Truncation Error})}
\end{aligned}$$

Although a similar process can be carried out for $y(t_0)$, $z(t_0)$, or more generally for $x(t)$, $y(t)$, $z(t)$ at any specific time t , emphasis is now directed to higher level geometric characteristics.

Several observations are made from Fig. 15. The center point curve consists of quadratic propagation along the x axis and linear propagation along the y axis, while the whole curve is offset above the $z = 0$ km plane by a small constant amount ($z_c = 7.6$ m, see Tab. 1), causing the center point curve to lie in a plane parallel to the chief orbital plane. The first harmonic curve consists of a closed fixed Lissajous ellipse lying in a plane skewed to the chief orbital plane. The first secular-harmonic curve consists of an open variable amplitude Lissajous elliptical spiral, also lying in a skewed plane. Finally, the second harmonic curve also corresponds to a closed fixed Lissajous ellipse lying in a skewed plane. Note in Fig. 15 the center point x,y amplitudes are at least an order of magnitude larger than for the first harmonic amplitudes, in turn, the first harmonic x,y,z amplitudes are approximately one magnitude order larger than the first secular-harmonic amplitudes, and in turn again, the second harmonic amplitudes are much smaller than the first secular-harmonic amplitudes. In other words, the in-plane center point components determine to a large extent the overall nature of the deputy motion, and the first harmonic component introduces a three-dimensional perturbing oscillation about the parabolic path. Likewise, the first secular-harmonic components behave like a three-dimensional expanding oscillation perturbation about the first harmonic path, and all of the above is perturbed by a higher frequency oscillation originating from the second harmonic component.

When viewed from above the $z = 0$ km plane, the first harmonic motion is in an opposite direction to the first secular-harmonic and second harmonic motions (clockwise for $h1$, counter-clockwise for $sh1$, $h2$). Careful examination of the sequencing of indexed points t_1, t_2 for the $h1$ and $h2$ ellipses in Fig. 15 illustrates the opposing motions. Such peculiar behavior is a trait exhibited by Lissajous curves under certain parameter conditions. When the x,y or x,z angular ROE become sufficiently out-of-phase, the direction of motion along the Lissajous path can reverse ($\theta_{x,h1} = -177$ deg vs. $\theta_{y,h1} = 2.8$ deg or $\theta_{z,h1} = -0.031$ deg, see Tab. 1). The variable phase Lissajous curve example in Fig. 5 for the $0 \leq \tau \leq 4(2\pi)$ case exhibited similar behavior when the time dependent phase reached a critical value. Also, for every increment of first harmonic (and first secular-harmonic) angular motion occurring over a unit of time, approximately "two" increments of second harmonic angular motion simultaneously occur. Careful examination of the spacing of indexed points t_1, t_2 for the $h1$ and $h2$ ellipses in Fig. 15 illustrates the differing increments. This behavior is a consequence of the $n_0\tau$ vs. $2n_0\tau$ frequencies. Opposing travel directions and differing travel rates in the various elliptic motion components leads to quadrant dependent perturbations that push the deputy satellite outside of, or pull the deputy satellite inside of, the fundamental harmonic elliptical path. Fig. 16 shows the elliptical component motions overlaid. Note the required $sh1$ and $h2$ scalings ($\times 2.5$ for $sh1$ at $t = 8T$, $\times 250$ for $h2$) required to make the corresponding curves equally visible to the $h1$ curve. The side-view perspective shows that each plane containing the Lissajous ellipses have different relative "ascending longitudes" and "inclinations", further enriching the geometry underlying the overall deputy motion.

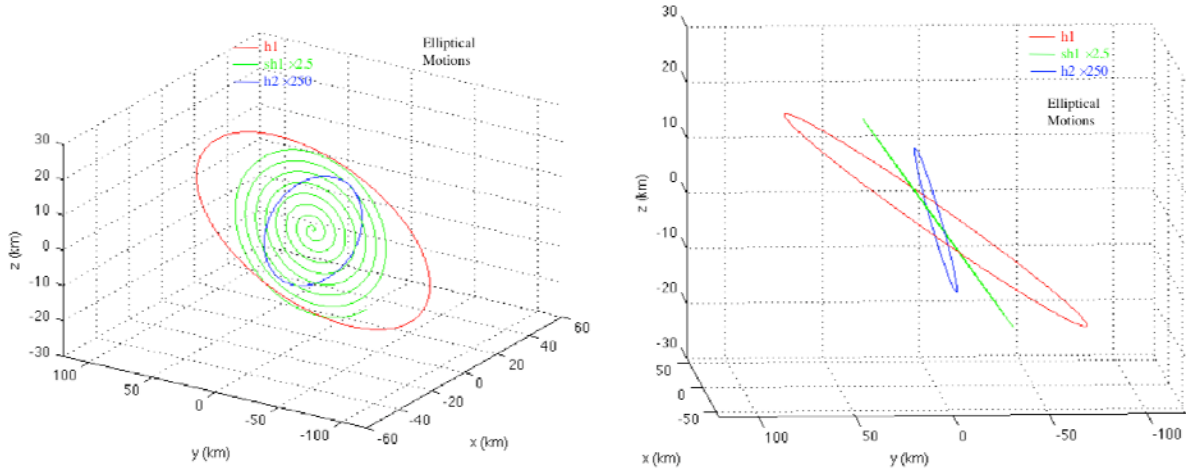


Figure 16. Overlaid Elliptic Component Motions - Expanded Formulation

Fig. 17 shows the twenty-one second order ROE time evolutions for the example. Note the radial and cross-track center point ROE are scaled ($\times 2.5$ for x_c , $\times 25000$ for z_c) to make the corresponding response curves equally visible to the along-track curve (y_c). The quadratic and linear drifts and constant offset behaviors in the center point coordinates are clearly noticeable. Observe how the first harmonic and second harmonic ROE amplitudes are constant (see Tab. 1 for numeric correlation), but the first secular-harmonic ROE amplitudes are linearly increasing from the initial values (see Tab. 1). For the h1 component, note the amplitude ratio $a_{y,h1}/a_{x,h1} = 1.99997$ is not precisely equal to 2 but is practically 2 as discussed in the analysis of coefficients $b_{x,h1}$, $c_{x,h1}$ and $b_{y,h1}$, $c_{y,h1}$. For the sh1 component, the ratio of amplitude rate of change is $d(a_{y,sh1})/dt/d(a_{x,sh1})/dt = 1$, and for the h2 component, the amplitude ratio is $a_{y,h2}/a_{x,h2} = 0.339$. The sh1 amplitude rate ratio equaling 1 is a consequence of the noted conditions $b_{y,sh1} = -c_{x,sh1}$ and $b_{x,sh1} = c_{y,sh1}$ discussed previously. In all elliptical motions, the ROE angles are linearly increasing from their initial values (see Tab. 1). In Fig. 17, the x,y ROE angles for the sh1 component are precisely equal for all times or initially $\theta_{x,sh1} = -87.182 \text{ deg} = \theta_{y,sh1}$ (see Tab. 1), again as a consequence of conditions $b_{y,sh1} = -c_{x,sh1}$ and $b_{x,sh1} = c_{y,sh1}$. Fig. 17 gives the impression that $\theta_{z,sh1}$ for sh1 is also equal to this value, however, $\theta_{z,sh1}$ is slightly different due to the initial phase offset ($\theta_{z,sh1} = -90.000 \text{ deg}$, see Tab. 1). For the h2 component, all three ROE angles appear equal but differ slightly due to the small dissimilar initial phases (see Tab. 1). These small phase differences for sh1 and h2 correlate to the counter-clockwise or direct movement around the respective ellipses. In contrast, the h1 angular ROE $\theta_{x,h1}$ evolution in Fig. 17 is approximately 180 deg behind the $\theta_{y,h1}$ and $\theta_{z,h1}$ responses, causing the clockwise or retrograde movement around the first harmonic ellipse noted previously. This example has demonstrated how the expanded formulation of second order relative orbital elements characterize the underlying geometry of the deputy satellite relative motion. This characterization may be useful for formulating strategy for predictive propagation, maneuvering planning, rendezvous-intercept, or determination-estimation.

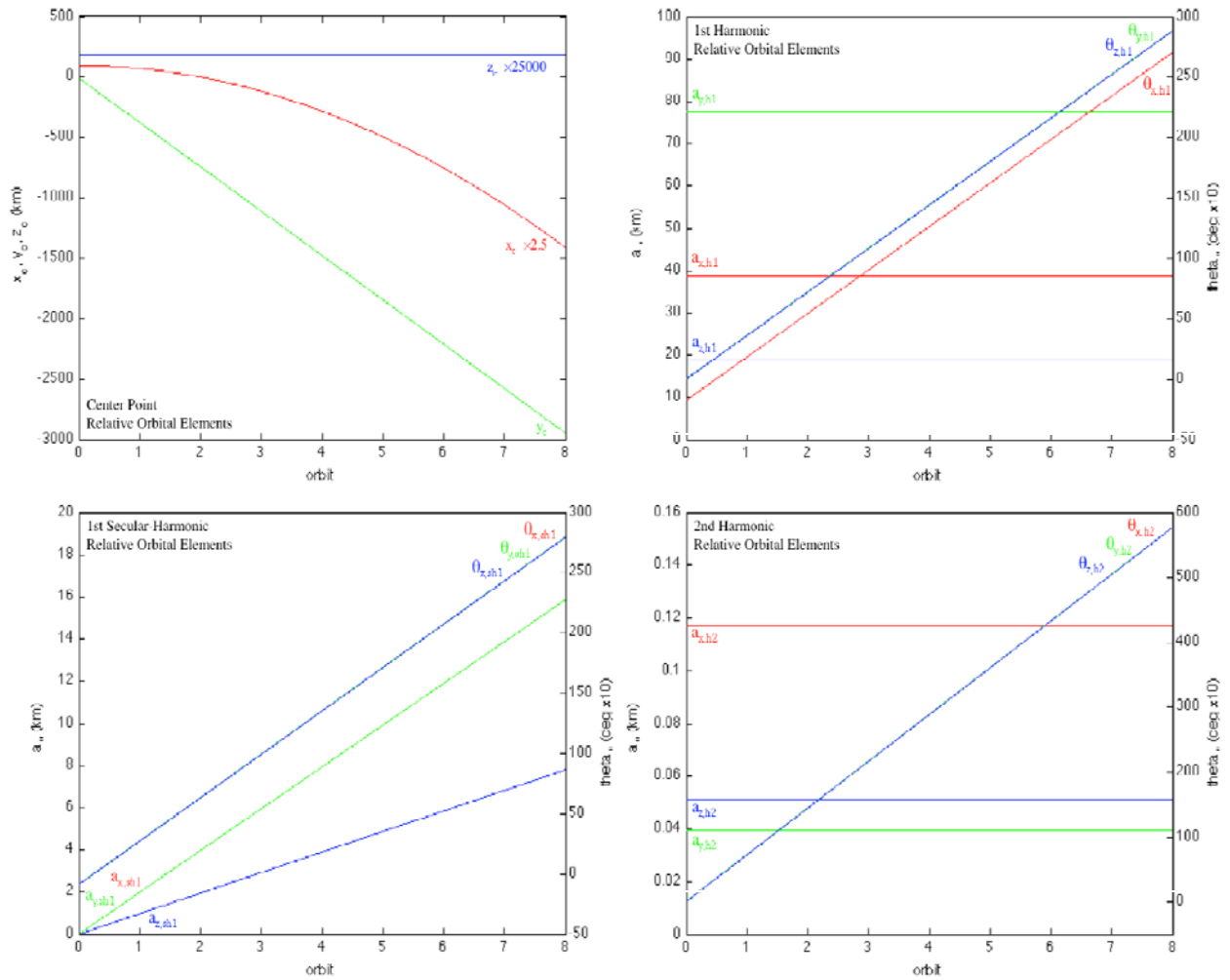


Figure 17. Second Order Relative Orbital Element Responses - Expanded Formulation

4.2 SECOND ORDER RELATIVE ORBITAL ELEMENTS - COMPACTED FORM

An alternate formulation of second order ROE is possible by expressing the nonlinear closed-form QV relative trajectory expressions for $x(t)$, $y(t)$, and $z(t)$ in a different manner. By using trigonometric identities to replace second harmonics with powers of first harmonics, grouping of terms in Eq. (9) can be accomplished on the individual expansion functions: 1, $n_o\tau$, $(n_o\tau)^2$, $\cos(n_o\tau)$, $\sin(n_o\tau)$, five functions rather than nine in the expanded formulation. Expressions in Eq. (9) can be converted to the form in Eq. (17), where Eqs. (18) and (11) provide lower level coefficient definitions. Eq. (17) indicates trajectory expressions contain one set of three-dimensional parametric Lissajous functions for the effective first harmonic $n_o\tau$ indicated by subscript "hle", in addition to a set of polynomial functions of $n_o\tau$ indicated by subscript "c". The Lissajous functions produce one elliptical space curve and correspondingly one set of xy and xz planar ellipses, and the polynomial functions produce a secular quadratic space curve. Following Sections 3-4, a set of nine ROE are defined directly from the compacted solution form in Eq. (17) and include: $\{x_c, y_c, z_c\}$ and $\{a_{x,hle}, a_{y,hle}, a_{z,hle}, \theta_{x,hle}, \theta_{y,hle}, \theta_{z,hle}\}$. Elements $\{x_c, y_c, z_c\}$ represent the in-plane and out-plane center point coordinates for the two-dimensional ellipses. Elements $\{a_{x,hle}, a_{y,hle}, a_{z,hle}, \theta_{x,hle}, \theta_{y,hle}, \theta_{z,hle}\}$ characterize the size-shape of, and angular position along, the two-dimensional ellipses corresponding to effective harmonic $n_o\tau$. Recall each ellipse will have two associated auxiliary circles that are explicitly described by the elements, which in turn implicitly describe the actual geometry of the motion along the ellipse in a meaningful way. In this formulation, all three amplitudes and all three phases are time dependent and correspond to a variable Lissajous curve. The two different formulations, expanded formulation in the previous section and the compacted formulation in this section, provide a clear trade-off regarding complexity: number of relative orbital elements vs. time dependent amplitudes-phases.

$$\begin{aligned} x(t) &= x_c(\tau) + x_{hle}(\tau) \\ y(t) &= y_c(\tau) + y_{hle}(\tau) \\ z(t) &= z_c + z_{hle}(\tau) \end{aligned} \tag{17}$$

where

$$\begin{aligned} x_c(\tau) &= b_{x,s0}(1) + b_{x,s1}(n_o\tau) + b_{x,s2}(n_o\tau)^2, & x_{hle}(\tau) &= a_{x,hle}(\tau)\cos\{\theta_{x,hle}(\tau)\} \\ y_c(\tau) &= b_{y,s0}(1) + b_{y,s1}(n_o\tau), & y_{hle}(\tau) &= a_{y,hle}(\tau)\sin\{\theta_{y,hle}(\tau)\} \\ z_c &= b_{z,s0}(1), & z_{hle}(\tau) &= a_{z,hle}(\tau)\sin\{\theta_{z,hle}(\tau)\} \end{aligned}$$

$$\begin{aligned} \theta_{x,hle}(\tau) &= n_o\tau - \phi_{x,hle}(\tau), & a_{x,hle}^2(\tau) &= b_{x,hle}^2(\tau) + c_{x,hle}^2(\tau), & \tan\{\phi_{x,hle}(\tau)\} &= c_{x,hle}(\tau) / b_{x,hle}(\tau) \\ \theta_{y,hle}(\tau) &= n_o\tau + \phi_{y,hle}(\tau), & a_{y,hle}^2(\tau) &= b_{y,hle}^2(\tau) + c_{y,hle}^2(\tau), & \tan\{\phi_{y,hle}(\tau)\} &= b_{y,hle}(\tau) / c_{y,hle}(\tau) \\ \theta_{z,hle}(\tau) &= n_o\tau + \phi_{z,hle}(\tau), & a_{z,hle}^2(\tau) &= b_{z,hle}^2(\tau) + c_{z,hle}^2(\tau), & \tan\{\phi_{z,hle}(\tau)\} &= b_{z,hle}(\tau) / c_{z,hle}(\tau) \end{aligned}$$

$$\begin{aligned}
b_{x,h1e}(\tau) &= b_{x,h1}(1) + b_{x,sh1}(n_o\tau) + b_{x,h1c}C_{n_o\tau} + b_{x,h1s}S_{n_o\tau} \\
c_{x,h1e}(\tau) &= c_{x,h1}(1) + c_{x,sh1}(n_o\tau) + c_{x,h1c}C_{n_o\tau} + c_{x,h1s}S_{n_o\tau} \\
b_{y,h1e}(\tau) &= b_{y,h1}(1) + b_{y,sh1}(n_o\tau) + b_{y,h1c}C_{n_o\tau} + b_{y,h1s}S_{n_o\tau} \\
c_{y,h1e}(\tau) &= c_{y,h1}(1) + c_{y,sh1}(n_o\tau) + c_{y,h1c}C_{n_o\tau} + c_{y,h1s}S_{n_o\tau} \\
b_{z,h1e}(\tau) &= b_{z,h1}(1) + b_{z,sh1}(n_o\tau) + b_{z,h1c}C_{n_o\tau} + b_{z,h1s}S_{n_o\tau} \\
c_{z,h1e}(\tau) &= c_{z,h1}(1) + c_{z,sh1}(n_o\tau) + c_{z,h1c}C_{n_o\tau} + c_{z,h1s}S_{n_o\tau} \\
\end{aligned} \tag{18}$$

$$\begin{aligned}
b_{x,h1c} &= \frac{9}{2} \frac{1}{R_o} x_0^2 - \frac{1}{4} \frac{1}{R_o} z_0^2 - \frac{1}{2} \frac{1}{n_o^2 R_o} \dot{x}_0^2 + 2 \frac{1}{n_o^2 R_o} \dot{y}_0^2 + \frac{1}{4} \frac{1}{n_o^2 R_o} \dot{z}_0^2 + 6 \frac{1}{n_o R_o} x_0 \dot{y}_0 \\
c_{x,h1c} &= -3 \frac{1}{n_o R_o} x_0 \dot{x}_0 - \frac{1}{2} \frac{1}{n_o R_o} z_0 \dot{z}_0 - 2 \frac{1}{n_o^2 R_o} \dot{x}_0 \dot{y}_0 \\
b_{x,h1s} &= -3 \frac{1}{n_o R_o} x_0 \dot{x}_0 - \frac{1}{2} \frac{1}{n_o R_o} z_0 \dot{z}_0 - 2 \frac{1}{n_o^2 R_o} \dot{x}_0 \dot{y}_0 \\
c_{x,h1s} &= -\frac{9}{2} \frac{1}{R_o} x_0^2 + \frac{1}{4} \frac{1}{R_o} z_0^2 + \frac{1}{2} \frac{1}{n_o^2 R_o} \dot{x}_0^2 - 2 \frac{1}{n_o^2 R_o} \dot{y}_0^2 - \frac{1}{4} \frac{1}{n_o^2 R_o} \dot{z}_0^2 - 6 \frac{1}{n_o R_o} x_0 \dot{y}_0 \\
b_{y,h1c} &= \frac{3}{2} \frac{1}{n_o R_o} x_0 \dot{x}_0 - \frac{1}{2} \frac{1}{n_o R_o} z_0 \dot{z}_0 + \frac{1}{n_o^2 R_o} \dot{x}_0 \dot{y}_0 \\
c_{y,h1c} &= \frac{9}{4} \frac{1}{R_o} x_0^2 + \frac{1}{4} \frac{1}{R_o} z_0^2 - \frac{1}{4} \frac{1}{n_o^2 R_o} \dot{x}_0^2 + \frac{1}{n_o^2 R_o} \dot{y}_0^2 - \frac{1}{4} \frac{1}{n_o^2 R_o} \dot{z}_0^2 + 3 \frac{1}{n_o R_o} x_0 \dot{y}_0 \\
b_{y,h1s} &= \frac{9}{4} \frac{1}{R_o} x_0^2 + \frac{1}{4} \frac{1}{R_o} z_0^2 - \frac{1}{4} \frac{1}{n_o^2 R_o} \dot{x}_0^2 + \frac{1}{n_o^2 R_o} \dot{y}_0^2 - \frac{1}{4} \frac{1}{n_o^2 R_o} \dot{z}_0^2 + 3 \frac{1}{n_o R_o} x_0 \dot{y}_0 \\
c_{y,h1s} &= -\frac{3}{2} \frac{1}{n_o R_o} x_0 \dot{x}_0 + \frac{1}{2} \frac{1}{n_o R_o} z_0 \dot{z}_0 - \frac{1}{n_o^2 R_o} \dot{x}_0 \dot{y}_0 \\
b_{z,h1c} &= \frac{3}{2} \frac{1}{R_o} x_0 z_0 + \frac{1}{n_o R_o} z_0 \dot{y}_0 + \frac{1}{2} \frac{1}{n_o^2 R_o} \dot{x}_0 \dot{z}_0 \\
c_{z,h1c} &= \frac{3}{2} \frac{1}{n_o R_o} x_0 \dot{z}_0 - \frac{1}{2} \frac{1}{n_o R_o} z_0 \dot{x}_0 + \frac{1}{n_o^2 R_o} \dot{y}_0 \dot{z}_0 \\
b_{z,h1s} &= \frac{3}{2} \frac{1}{n_o R_o} x_0 \dot{z}_0 - \frac{1}{2} \frac{1}{n_o R_o} z_0 \dot{x}_0 + \frac{1}{n_o^2 R_o} \dot{y}_0 \dot{z}_0 \\
c_{z,h1s} &= -\frac{3}{2} \frac{1}{R_o} x_0 z_0 - \frac{1}{n_o R_o} z_0 \dot{y}_0 - \frac{1}{2} \frac{1}{n_o^2 R_o} \dot{x}_0 \dot{z}_0
\end{aligned}$$

A comparison of second order and first order ROE expressions is considered next. Expressions for center point coordinates x_c , y_c , z_c are identical for both the compacted and expanded formulations (see Eqs. (17) vs. (10)), where coordinate x_c is time dependent and involves secular terms of powers 0,1,2, coordinate y_c is time dependent and involves secular terms of powers 0,1, and coordinate z_c is a constant. Further, the lower level secular polynomial coefficients with subscripts "s0", "s1", "s2" remain unchanged from the Eq. (11) definitions and are functions of the initial positions and velocities. Therefore, Eq. (12) describing distortions on the first order center point coordinate ROE also applies here. With the secular-harmonic terms and higher frequency terms absorbed into the fundamental harmonic terms, the compacted formulation provides a cleaner comparison between the first order and second order amplitude

and angle ROE. The y axis amplitude $2a_e$ is constant in first order theory (Eq. (3)) but the corresponding amplitude $a_{y,h1e}(\tau)$ for the first harmonic effective term is time dependent (Eq. (17)). Linear initial condition terms $x_0, \dot{x}_0, \dot{y}_0$ appearing in coefficients $b_{y,h1}$ and $c_{y,h1}$ within $b_{y,h1e}(\tau)$ and $c_{y,h1e}(\tau)$ (Eqs. (11) and (18)) form the first order $4a_e^2$ expression after being squared. All other second order initial condition terms within $b_{y,h1e}(\tau)$ and $c_{y,h1e}(\tau)$ originating from coefficients $b_{y,h1}$, $b_{y,sh1}$, $b_{y,h1c}$, $b_{y,h1s}$ and $c_{y,h1}$, $c_{y,sh1}$, $c_{y,h1c}$, $c_{y,h1s}$ augment the y axis amplitude statically and dynamically. The dynamic distortion involves a linearly increasing term and harmonic oscillating terms. In a similar way, the linear terms z_0, \dot{z}_0 in coefficients $b_{z,h1}$ and $c_{z,h1}$ within $b_{z,h1e}(\tau)$ and $c_{z,h1e}(\tau)$ (Eqs. (11) and (18)) generate the first order z axis amplitude b_e (Eq. (3)). All remaining second order initial condition terms within $b_{z,h1e}(\tau)$ and $c_{z,h1e}(\tau)$ coming from $b_{z,h1}$, $b_{z,sh1}$, $b_{z,h1c}$, $b_{z,h1s}$ and $c_{z,h1}$, $c_{z,sh1}$, $c_{z,h1c}$, $c_{z,h1s}$ modulate the z axis amplitude. The modulation again involves a static effect, a secular effect, and a harmonic effect. Therefore, relations between first order a_e , b_e and second order $a_{y,h1e}(\tau)$, $a_{z,h1e}(\tau)$ are similar to Eq. (13) but with different implied function definitions for the distortions. Moving on to the angular coordinate comparison, the only difference between the first order and second order ROE lies in the phase angles. For the y axis, the comparison is between first order phase angle α_0 and second order phase angle $\phi_{y,h1e}(\tau)$. Linear initial condition terms $x_0, \dot{x}_0, \dot{y}_0$ that generate α_0 (see Eq. (3)) can be found within coefficients $b_{y,h1e}(\tau)$ and $c_{y,h1e}(\tau)$ that contribute to $\phi_{y,h1e}(\tau)$ (Eqs. (17) and (18)). All other second order initial condition terms within $\phi_{y,h1e}(\tau)$ are static offset or time dependent distortions to α_0 . Similar conclusions can be drawn for β_0 , $\phi_{z,h1e}(\tau)$ and z_0, \dot{z}_0 . Relationships between first order α_0 , β_0 and second order $\phi_{y,h1e}(\tau)$, $\phi_{z,h1e}(\tau)$ are similar to Eq. (13) but with different implied function definitions for the distortions. In summary, Eq. (19) describes the parametric distortions for the compacted formulation of second order ROE. Note the absence of direct coordinate distortions (like in Eq. (14)) since all extra terms have been folded into the effective first harmonic term. As before, if all second order initial condition terms are set to zero, then all distortions become zero in Eq. (19), and the second order ROE reduce to the first order ROE. Eq. (19) again could be useful in specific applications concerning the control and dynamics of relative satellite motion.

Several interesting observations regarding effective first harmonic coefficient relationships are made here. First, previously noted relations (Section 5) between the in-plane x and y axis coefficients are also true here: $2b_{x,h1} \approx -c_{y,h1}$, $b_{y,h1} \approx 2c_{x,h1}$ and $b_{x,sh1} = c_{y,sh1}$, $b_{y,sh1} = -c_{x,sh1}$. Second, many additional harmonic terms within $b_{x,h1e}(\tau)$ and $c_{x,h1e}(\tau)$, $b_{y,h1e}(\tau)$ and $c_{y,h1e}(\tau)$, and within $b_{z,h1e}(\tau)$ and $c_{z,h1e}(\tau)$, are equivalent. These additional relations are summarized as $b_{x,h1c} = -c_{x,h1s}$, $b_{x,h1s} = c_{x,h1c}$, $b_{y,h1c} = -c_{y,h1s}$, $b_{y,h1s} = c_{y,h1c}$, $b_{z,h1c} = -c_{z,h1s}$, $b_{z,h1s} = c_{z,h1c}$. Only approximate conclusions can be drawn from these relations. The y-to-x amplitude behavior will initiate with an approximate 2-to-1 relation, the secular amplitude growth between the y and x axes will follow an approximate 1-to-1 relation, and although the harmonic oscillation amplitudes associated with a given axis are balanced between the cosine and sine terms, the y-to-x harmonic amplitude relation does not necessarily follow an approximate 2-to-1 or 1-to-1 rule. Eq. (17) indicates the overall deputy relative orbital motion consists of the direct sum of the in-plane and out-plane ellipses and polynomial center point curves. The elliptical motion is characterized by the six relative orbital elements and the associated auxiliary circles from the variable Lissajous functions, and movement of the ellipse centers are characterized by three additional ROE, yielding $6+3 = 9$ ROE in totality using the compacted formulation. These component motions can also be interpreted as natural modes that combine and form the overall motion.

$$\begin{aligned}
x(t) &= x_c\{\tau, x_e, \delta(x_e), \delta(\dot{x}_e), \delta(\ddot{x}_e)\} + a_{x,h1e}\{\tilde{a}_e, \delta(\tilde{a}_e^2)\} \cos[n_0\tau - \phi_{x,h1e}\{\tilde{\alpha}_0, \delta(\tilde{\alpha}_0'), \delta(\tilde{\alpha}_0'')\}] \\
y(t) &= y_c\{\tau, y_e, \dot{y}_e, \delta(y_e), \delta(\dot{y}_e)\} + a_{y,h1e}\{a_e, \delta(4a_e^2)\} \sin[n_0\tau + \phi_{y,h1e}\{\alpha_0, \delta(\alpha_0'), \delta(\alpha_0'')\}] \\
z(t) &= z_c\{0, \delta(z_e)\} + a_{z,h1e}\{b_e, \delta(b_e^2)\} \sin[n_0\tau + \phi_{z,h1e}\{\beta_0, \delta(\beta_0'), \delta(\beta_0'')\}]
\end{aligned} \quad (19)$$

$$\begin{aligned}
\underbrace{x_c}_{2nd \text{ Order}} &= \underbrace{x_e}_{1st \text{ Order}} + \underbrace{\delta(x_e)1 + \delta(\dot{x}_e)\tau + \delta(\ddot{x}_e)\tau^2}_{\text{Distortions}} \\
\underbrace{y_c}_{2nd \text{ Order}} &= \underbrace{y_e + \dot{y}_e\tau}_{1st \text{ Order}} + \underbrace{\delta(y_e)1 + \delta(\dot{y}_e)\tau}_{\text{Distortions}} \\
\underbrace{z_c}_{2nd \text{ Order}} &= \underbrace{0}_{1st \text{ Order}} + \underbrace{\delta(z_e)1}_{\text{Distortions}}
\end{aligned}$$

$$\begin{aligned}
\underbrace{a_{y,h1e}^2}_{2nd \text{ Order}} &= \underbrace{4a_e^2}_{1st \text{ Order}} + \underbrace{\delta(4a_e^2)}_{\text{Distortions}}, \quad \underbrace{\tan(\phi_{y,h1e})}_{2nd \text{ Order}} = \underbrace{[\tan(\alpha_0) + \tan\{\delta(\alpha_0')\}]}_{1st \text{ Order}} / \underbrace{[1 + \tan\{\delta(\alpha_0'')\}]}_{\text{Distortions}} \\
\underbrace{a_{z,h1e}^2}_{2nd \text{ Order}} &= \underbrace{b_e^2}_{1st \text{ Order}} + \underbrace{\delta(b_e^2)}_{\text{Distortions}}, \quad \underbrace{\tan(\phi_{z,h1e})}_{2nd \text{ Order}} = \underbrace{[\tan(\beta_0) + \tan\{\delta(\beta_0')\}]}_{1st \text{ Order}} / \underbrace{[1 + \tan\{\delta(\beta_0'')\}]}_{\text{Distortions}}
\end{aligned}$$

The previous numeric example in Eq. (15) is revisited here to further explore the component motions and underlying geometry described by the alternate second order ROE. The relative trajectory for $0 \leq t \leq 8T$ is shown in Fig. 18 and is used to examine the motion geometry and second order ROE based on the compacted formulation. Two specific times $t_5 = (1+3/8)T$, $t_6 = (3+3/8)T$ are highlighted along the trajectory and used in the discussion. Fig. 19 shows the two component trajectories: secular center point polynomial motion (c), and effective first harmonic elliptic motion (h1e). Each curve shows the start and stop positions, and Tab. 2 lists the corresponding initial and final values for the nine ROE. Note the three-dimensional elliptic curve can be projected to the xy and xz planes (shown in Fig. 19) with corresponding auxiliary circles and deputy shadow satellites (not shown in Fig. 19) to visualize and quantify the motion geometry. For example, the two start points in Fig. 19 can be graphically superimposed to form the overall start point in Fig. 18, or mathematically for $y(t_0)$

$$\begin{aligned}
y(t_0) &= y_c(t_0) + y_{h1e}(t_0) \\
y_0 &= b_{y,s0} + a_{y,h1e}(t_0)\sin\{\theta_{y,h1e}(t_0)\} \\
0 \text{ km} &= -3.8059 + 77.767\sin\{2.8052^\circ\} \quad \text{km} \\
0 \text{ km} &= -3.8059 + 3.8059 \quad \text{km} \\
0 \text{ km} &= 0 \text{ km} \quad \checkmark
\end{aligned} \quad (20)$$

Although a similar process can be carried out for $x(t_0)$, $z(t_0)$, or more generally for $x(t)$, $y(t)$, $z(t)$ at any specific time t , emphasis is now directed to higher level geometric characteristics.

Table 2. ROE Initial and Final Values - Compacted Formulation

Units	km	km	km	deg	deg	deg
Initial Val.						
ROE	x_c	y_c	z_c			
Center Pt.	3.8899e+01	-3.8059e+00	7.5881e-03			
ROE	$a_{x,h1e}$	$a_{y,h1e}$	$a_{z,h1e}$	$\theta_{x,h1e}$	$\theta_{y,h1e}$	$\theta_{z,h1e}$
1st Har. Eff.	3.8747e+01	7.7767e+01	1.9055e+01	-1.7716e+02	2.8052e+00	-2.2816e-02
Final Val.						
ROE	x_c	y_c	z_c			
Center Pt.	-5.6236e+02	-2.9417e+03	7.5881e-03			
ROE	$a_{x,h1e}$	$a_{y,h1e}$	$a_{z,h1e}$	$\theta_{x,h1e}$	$\theta_{y,h1e}$	$\theta_{z,h1e}$
1st Har. Eff.	4.1867e+01	7.9368e+01	2.0589e+01	2.7251e+03	2.8713e+03	2.8577e+03

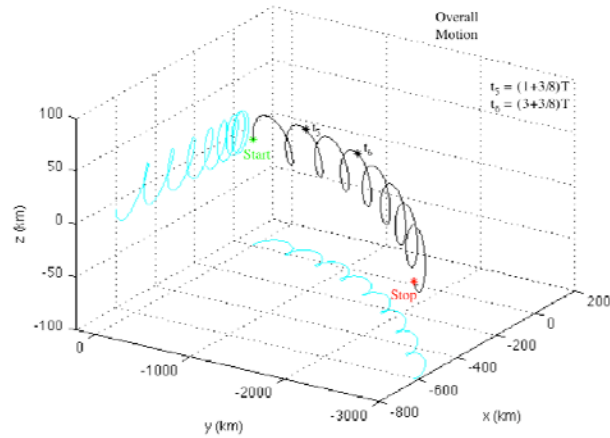


Figure 18. QV for 8T - Compacted Formulation

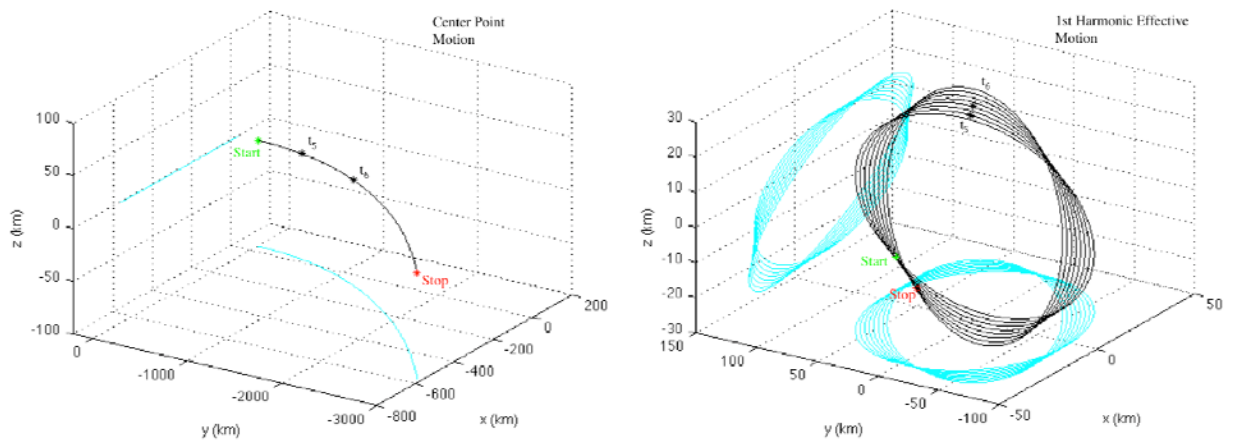


Figure 19. Component Motions - Compacted Formulation

Several observations are made from Fig. 19. The center point curve again lies in a plane slightly above the chief orbital plane ($z_c = 7.6$ m, see Tab. 2) and consists of quadratic propagation along the x axis and linear propagation along the y axis. The first harmonic effective curve consists of an open variable Lissajous ellipse. This space curve is three-dimensional and does not lie in any fixed plane. Note in Fig. 19 the center point x,y amplitudes are at least an order of magnitude larger than for the first harmonic effective amplitudes. In other words, the in-plane center point components determine to a large extent the overall nature of the deputy motion, and the first harmonic effective component introduces a three-dimensional perturbing oscillation about the parabolic path. The direction of first harmonic effective motion opposes the counter-clockwise buildup of angles $\theta_{x,h1e}$ and $\theta_{y,h1e}$, or angles $\theta_{x,h1e}$ and $\theta_{z,h1e}$, in the xy and xz planes. Careful examination of the sequencing of indexed points t_5 and t_6 from the start point in Fig. 19 illustrates the retrograde motion. The large phase angle difference noted in Tab. 2 between the x and y,z axes causes the retrograde behavior ($\theta_{x,h1e} = -177$ deg vs. $\theta_{y,h1e} = 2.8$ deg and $\theta_{z,h1e} = -0.023$ deg). Note the similarity of the first harmonic effective component motion in Fig. 19 with the variable amplitude-phase Lissajous space curve example in Section 4 for the $\theta_a = +30$ and -100 deg azimuth views in Fig. 12. In particular, the three-dimensional curve of Fig. 19 exhibits signatures of the conchiglie pasta or seashell shape and multi-coil spring shape. Also, the xz projected curve in Fig. 19 is highly similar to the example Lissajous planar curve with variable amplitude and phase in Fig. 7 for $0 \leq \tau \leq 8(2\pi)$. Although not visible in Fig. 19, the elliptical curve also experiences small oscillations along the entire length.

Fig. 20 shows the nine second order ROE time evolutions for the example. Note the radial and cross-track center point ROE are again scaled ($\times 2.5$ for x_c , $\times 25000$ for z_c) to make the corresponding response curves equally visible to the along-track curve (y_c). The quadratic and linear drifts and constant offset behaviors in the center point coordinates are clearly noticeable. The time dependent nature of the elliptical motion amplitudes is seen in Fig. 20, although over 8 orbits the amplitudes only change by several kilometers. With a tighter axis view, the secular growth and harmonic oscillation in the ROE amplitudes is visible where the y axis oscillation amplitude is much smaller than the x and z axis behavior. Further, the y axis secular growth lags the corresponding behavior in the x and z axes by a small amount. The y-to-x amplitude ratio at the initial time is $a_{y,h1e}/a_{x,h1e} = 2.007$ and after 8 orbits the ratio is $a_{y,h1e}/a_{x,h1e} = 1.896$. Although the precise 2-to-1 amplitude nature is not present in the second order motion, the actual amplitude relation is not far from the first order behavior, as predicted during the examination of coefficients $b_{x,h1e}(\tau)$, $c_{x,h1e}(\tau)$ and $b_{y,h1e}(\tau)$, $c_{y,h1e}(\tau)$. The z-to-x amplitude ratios at the initial and final times are $a_{z,h1e}/a_{x,h1e} = 0.492$ and 0.492 even though the ratio varies by a small amount over time. In the elliptical motion, the ROE angles are linearly increasing from their initial values (see Tab. 2). Fig. 20 gives the impression that angles $\theta_{y,h1e}$ and $\theta_{z,h1e}$ are equal, however these angles are slightly different due to the initial phase offset ($\theta_{y,h1e} = 2.8$ deg vs. $\theta_{z,h1e} = -0.023$ deg, see Tab. 2). In contrast, the angular ROE $\theta_{x,h1e}$ evolution in Fig. 20 is again approximately 180 deg behind the $\theta_{y,h1e}$ and $\theta_{z,h1e}$ responses, causing the clockwise or retrograde movement around the elliptical space curve noted previously. By plotting only the phase angles and removing the out-of-phase trait in the x axis, the time dependent nature of the phase angles in each axis of elliptical motion can be observed (see Fig. 20). This example has demonstrated how the compacted formulation of second order relative orbital elements characterize the underlying geometry of the deputy satellite relative motion.

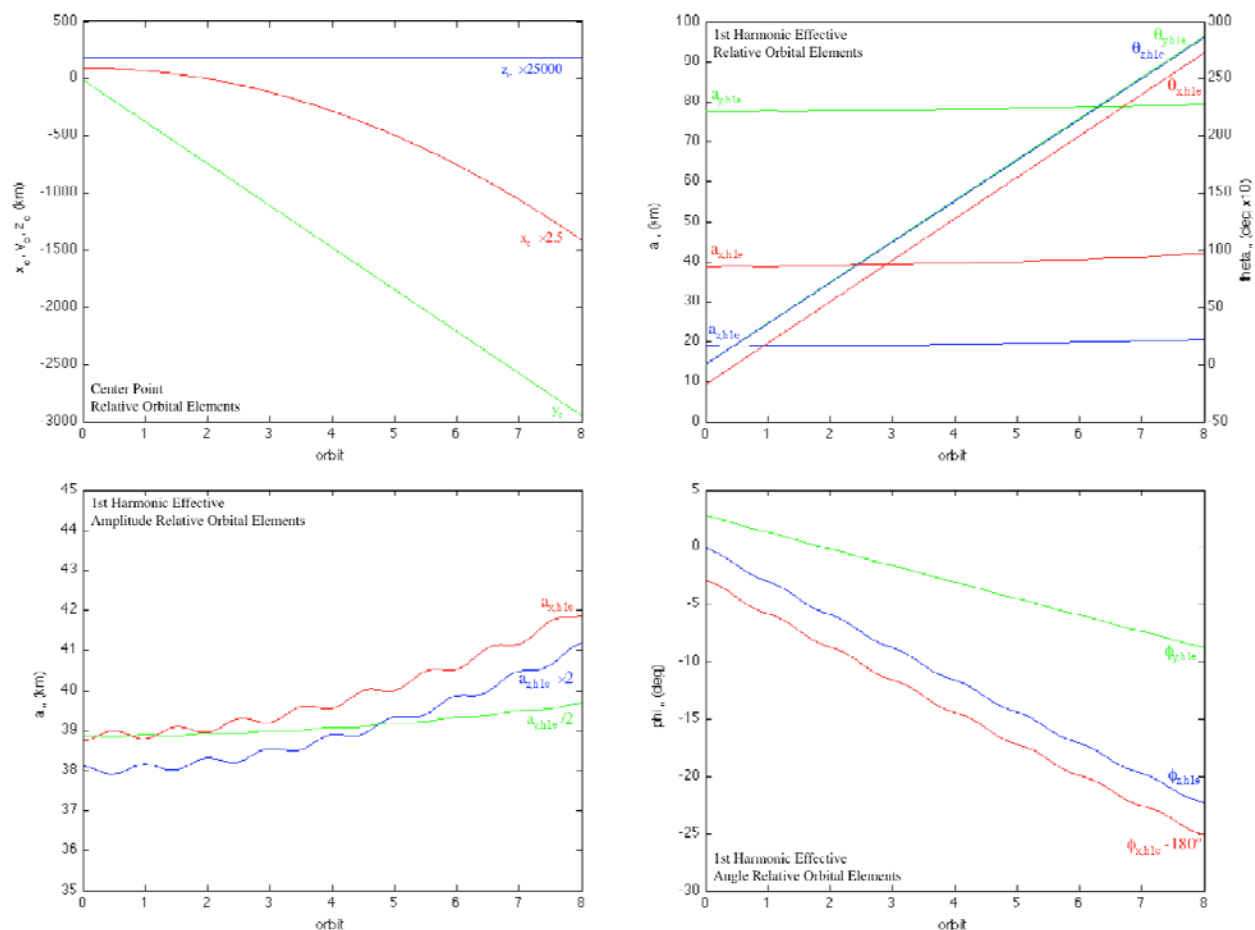


Figure 20. Second Order Relative Orbital Element Responses - Compacted Formulation

4.3 LISSAJOUS CURVES - REVISITED

Before considering second order conditions for periodic relative motion, conditions for fixed and variable closed Lissajous curves are examined. These topics are closely related to periodicity based on second order ROE. Note the following analysis emphasizes whole period return points and does not address rational sub-period or super-period self-intersection points. First, consider the case of variable frequency but constant amplitude-phase, or

$$\begin{aligned} x(t) &= a_x \cos\{\omega_x(\tau)\tau - \phi_x\} \\ y(t) &= a_y \sin\{\omega_y(\tau)\tau + \phi_y\} \end{aligned} \quad (21)$$

Parametric conditions are sought for the situation where coordinate values x, y simultaneously return to previous values after repeat time T_r indicated in Eq. (22). Note T_r represents a change in time, i.e., $T_r = \Delta t$ or $\Delta \tau$.

$$\begin{aligned} x(t+T_r) &= x(t) \\ y(t+T_r) &= y(t) \end{aligned} \quad (22)$$

The equivalent angular conditions from Eq. (22) after canceling out equal phase terms are

$$\begin{aligned} \underbrace{\omega_x(\tau+T_r)(\tau+T_r) - \omega_x(\tau)\tau}_{n_x f_x(\tau, T_r)} &= (2\pi n) n_x \\ \underbrace{\omega_y(\tau+T_r)(\tau+T_r) - \omega_y(\tau)\tau}_{n_y f_y(\tau, T_r)} &= (2\pi n) n_y \end{aligned} \quad (23)$$

where n represents a common integer number of whole function revolutions over time T_r while n_x and n_y denote revolution proportionality integers between the x and y axes. For a specific τ , Eq. (23) represents *two* conditions that the *one* variable T_r must simultaneously satisfy for repeating x, y . The closed curve requirement means the ratio of the x and y axis frequency function differences *evaluated at two specific times* separated by the repeat time must be rational,

$$\frac{n_x}{n_y} = \frac{\omega_x(\tau+T_r)(\tau+T_r) - \omega_x(\tau)\tau}{\omega_y(\tau+T_r)(\tau+T_r) - \omega_y(\tau)\tau} \quad (24)$$

otherwise the curve is open. With general time τ , Eqs. (23)-(24) greatly restrict the class of time dependent frequency functions that are capable of producing a closed curve. One class of *sufficient but not necessary* frequency functions for repeating x, y are rationally proportional $\omega_x(\tau)$ and $\omega_y(\tau)$, or $\omega_x(\tau)$ and $\omega_y(\tau)$ are obtained from whole number scaling of a base function $\omega(\tau)$ as indicated below.

$$\begin{aligned} \omega_x(\tau) &= n_x \omega(\tau) \\ \omega_y(\tau) &= n_y \omega(\tau) \end{aligned} \quad (25)$$

In this case, the two conditions in Eq. (23) reduce to the single condition

$$\underbrace{\omega(\tau+T_r)(\tau+T_r) - \omega(\tau)\tau}_{f(\tau, T_r)} = 2\pi n \quad (26)$$

where existence of repeat time T_r is problem dependent. Substitution of Eq. (25) into Eq. (24) confirms the evaluated frequency function rationality.

$$\frac{\omega_x(\tau+T_r)(\tau+T_r) - \omega_x(\tau)\tau}{\omega_y(\tau+T_r)(\tau+T_r) - \omega_y(\tau)\tau} = \frac{n_x\{\omega(\tau+T_r)(\tau+T_r) - \omega(\tau)\tau\}}{n_y\{\omega(\tau+T_r)(\tau+T_r) - \omega(\tau)\tau\}} = \frac{n_x}{n_y} \quad (27)$$

For a specific example, consider m^{th} degree polynomial frequency functions in Eq. (28).

$$\begin{aligned} \omega_x(\tau) &= \sum_{i=0}^m \omega_{x_i} \tau^i \\ \omega_y(\tau) &= \sum_{i=0}^m \omega_{y_i} \tau^i \quad \text{where} \quad \begin{aligned} \omega_{x_i} &= n_x \omega_i \\ \omega_{y_i} &= n_y \omega_i \end{aligned} \\ \omega(\tau) &= \sum_{i=0}^m \omega_i \tau^i \end{aligned} \quad (28)$$

With these specific functions, Eq. (26) becomes

$$[\sum_{i=0}^m \omega_i(\tau+T_r)^i](\tau+T_r) - [\sum_{i=0}^m \omega_i \tau^i]\tau = 2\pi n \quad (29)$$

For a second degree polynomial ($m = 2$) parameterized at zero time ($\tau = 0$), Fig. 21 shows a plot of function $f(\tau, T_r)$ for a specific set of coefficient values. The solution for the first ($n = 1$) and second ($n = 2$) repeat times are $T_{r1} = 4.8816$ and $T_{r2} = 7.5997$. Note how the repeat time increments are decreasing for each repeat cycle. Corresponding Lissajous curve and individual $x(t)$ and $y(t)$ responses are also shown in Fig. 21. Note the variable frequency Lissajous curve is closed as repeat times were found, but travel rate at a given point along the curve is non-uniform, specifically the travel rate at the given point on each subsequent pass is increasing, even though the curve takes the same spatial path in each cycle. Also note in this example individual $x(t)$ and $y(t)$ signals are not periodic. The Lissajous curve is spatial periodic but not temporal periodic. These observations underscore the meaning that Eq. (26) is a repeat condition; not a periodic condition. As a final point for this example, Fig. 22 shows results for the case when $\omega_x(\tau)$ does not satisfy Eq. (25), specifically, $\omega_{x1} = 0.025 \neq 0.02 = n_x \omega_1$. Fig. 22 shows how this small parameter perturbation leads to distinct functions $f_x(\tau, T_r)$ and $f_y(\tau, T_r)$ which cross the 2π and 4π lines at different points causing repeat time non-existence. Further, the small perturbation produces an open Lissajous curve which never returns to pass through the start point $(x(0), y(0)) = (1, 0.8660) = (1, 3^{1/2}/2)$.

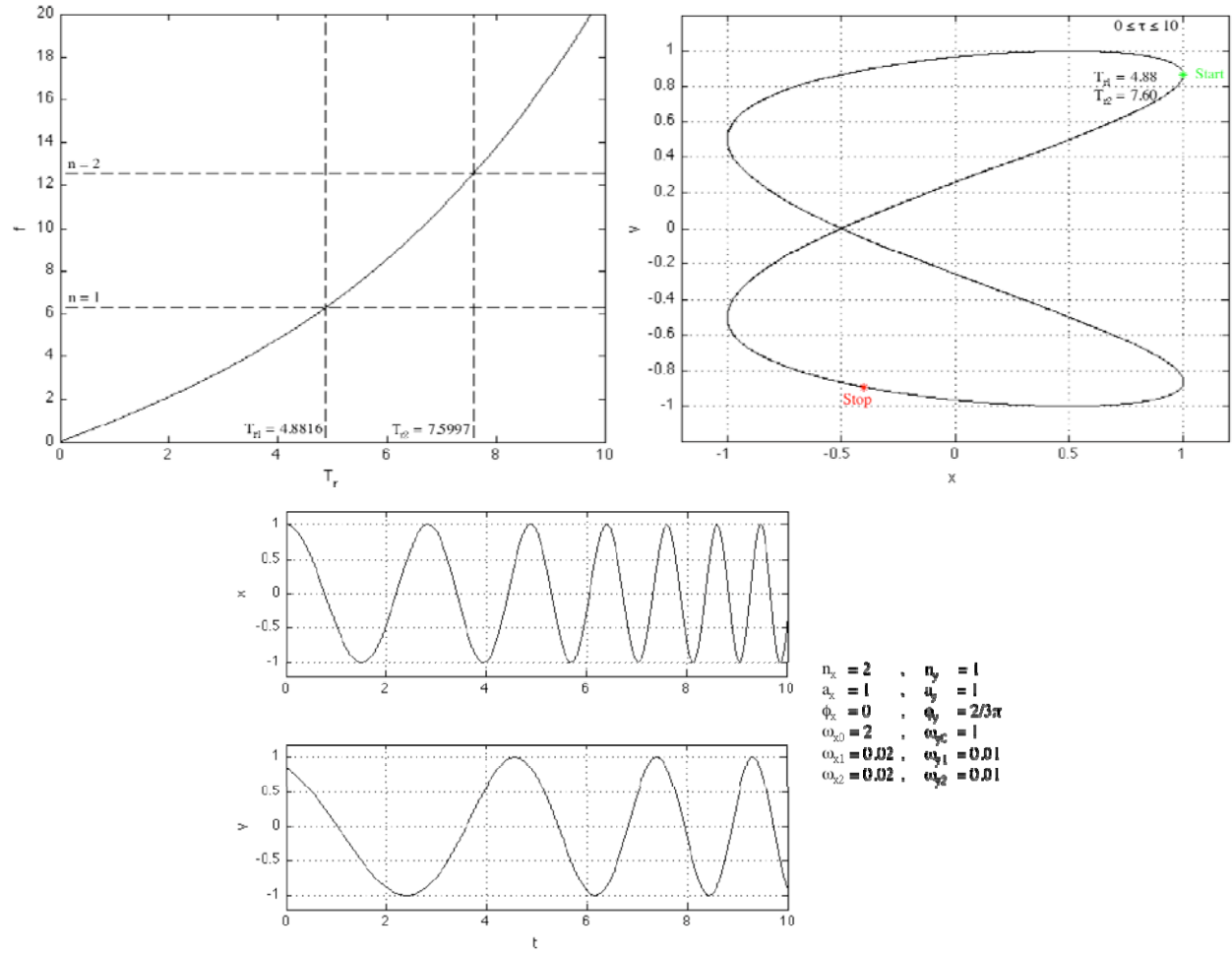


Figure 21. Variable Polynomial Frequency Repeating Lissajous Curve

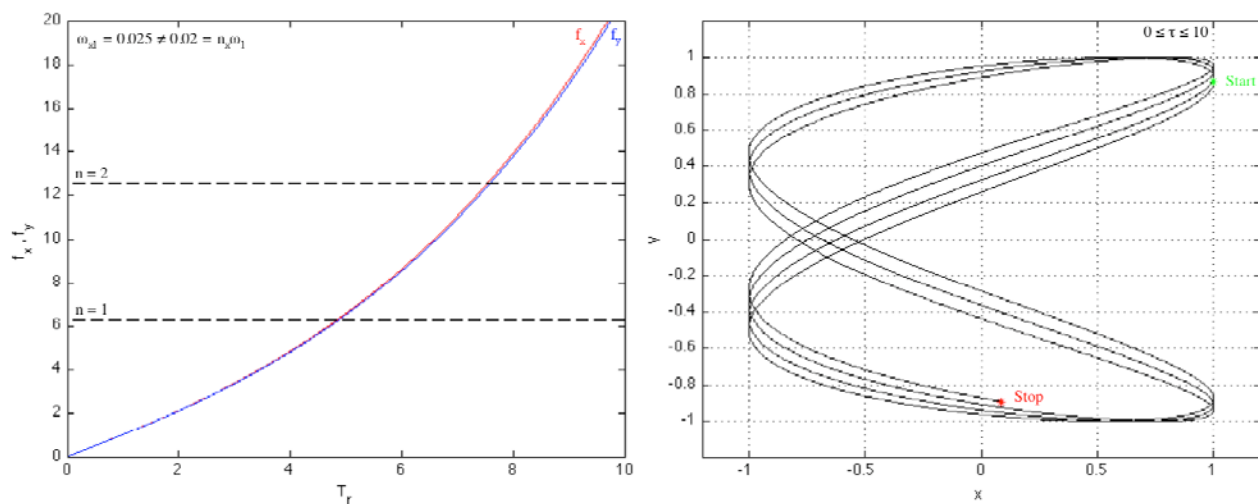


Figure 22. Variable Polynomial Frequency Non-Repeating Lissajous Curve

As another example, consider sinusoid frequency functions in Eq. (30).

$$\begin{aligned}\omega_x(\tau) &= \omega_{x0} + \sum_{i=1}^m \omega_{x_i} \sin(i\lambda\tau) \\ \omega_y(\tau) &= \omega_{y0} + \sum_{i=1}^m \omega_{y_i} \sin(i\lambda\tau) \quad \text{where} \quad \begin{aligned} \omega_{x_i} &= n_x \omega_i \\ \omega_{y_i} &= n_y \omega_i \end{aligned} \\ \omega(\tau) &= \omega_0 + \sum_{i=1}^m \omega_i \sin(i\lambda\tau)\end{aligned}\tag{30}$$

Under these specific functions, Eq. (26) simplifies to

$$[\omega_0 + \sum_{i=1}^m \omega_i \sin\{i\lambda(\tau+T_r)\}](\tau+T_r) - [\omega_0 + \sum_{i=1}^m \omega_i \sin\{i\lambda\tau\}]\tau = 2\pi n\tag{31}$$

For a single harmonic ($m = 1$), Fig. 23 shows function $f(\tau, T_r)$ for a specific set of coefficient values and the zero time parameterization ($\tau = 0$), resulting in the first and second repeat times $T_{r1} = 6.2832 = 2\pi$ and $T_{r2} = 12.5664 = 4\pi$. Note how the repeat time increments are constant for each repeat cycle. Corresponding Lissajous curve and individual $x(t)$ and $y(t)$ responses are also shown in Fig. 23. Individual $x(t)$ and $y(t)$ signals are still non-periodic but they do simultaneously repeat their values at times $\tau = 0, T_{r1}, T_{r2}, \dots$. Also note the variable frequency Lissajous curve is again closed and the instantaneous travel rate at a given point along the curve is still non-uniform, but the average travel rate for one cycle is constant. The Lissajous curve is both spatial and temporal periodic. To demonstrate that rationally proportional frequency functions (see Eq. (25)) are not necessary for a closed Lissajous curve, consider the results presented in Fig. 24 occurring from a small perturbation where $\omega_x(\tau)$ does not satisfy Eq. (25), specifically, $\omega_{x1} = 0.25 \neq 0.2 = n_x \omega_1$. Fig. 24 shows how this parametric change causes functions $f_x(\tau, T_r)$ and $f_y(\tau, T_r)$ to become distinct, yet still cross the 2π and 4π lines at uniformly spaced identical points facilitating repeat time existence. This feature gives rise to interesting behavior exhibited by the Lissajous curve shown in Fig. 24. The Lissajous curve passes through the repeat point $(x(0), y(0)) = (1, 0.8660) = (1, 3^{1/2}/2)$ every $\Delta\tau = 2\pi$ units of time but never takes the same spatial path in each cycle. Although the Lissajous curve has remained temporal periodic and closed under the parameter change, the curve is not spatial periodic. In other words, the fundamental requirement for a repeat point is rationality of frequency function differences *evaluated at two specific times; not all times*.

Second, consider the case of variable phase but constant amplitude-frequency, or

$$\begin{aligned}x(t) &= a_x \cos\{\omega_x \tau - \phi_x(\tau)\} \\ y(t) &= a_y \sin\{\omega_y \tau + \phi_y(\tau)\}\end{aligned}\tag{32}$$

Parametric conditions are again sought where Eq. (22) is satisfied: x, y coordinate values return to previous values after repeat time T_r . Angular conditions from Eq. (22) after canceling out equal frequency terms are

$$\begin{aligned}\omega_x T_r - \phi_x(\tau+T_r) + \phi_x(\tau) &= (2\pi n) n_x \\ \omega_y T_r + \phi_y(\tau+T_r) - \phi_y(\tau) &= (2\pi n) n_y\end{aligned}\tag{33}$$

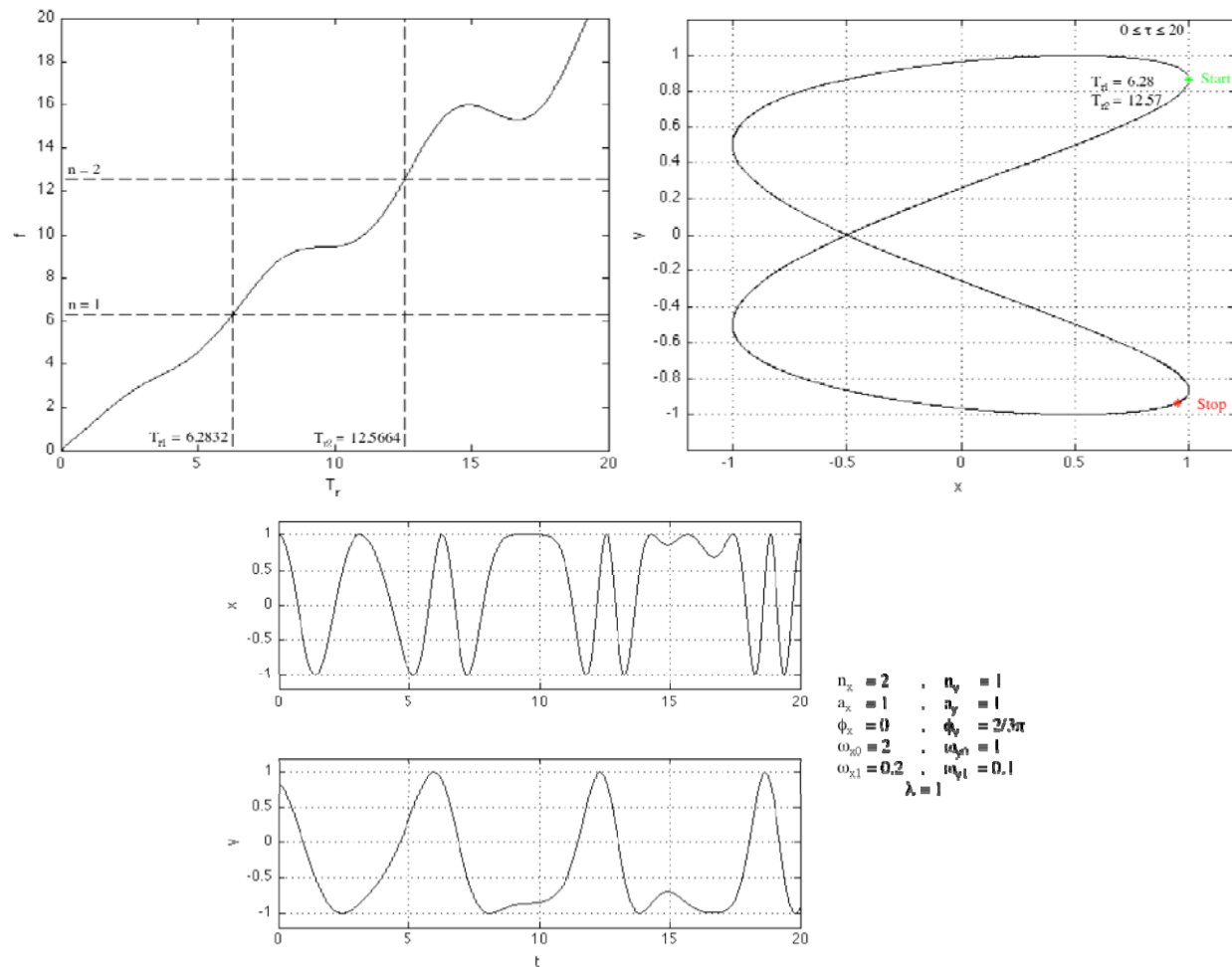


Figure 23. Variable Sinusoid Frequency Repeating Lissajous Curve

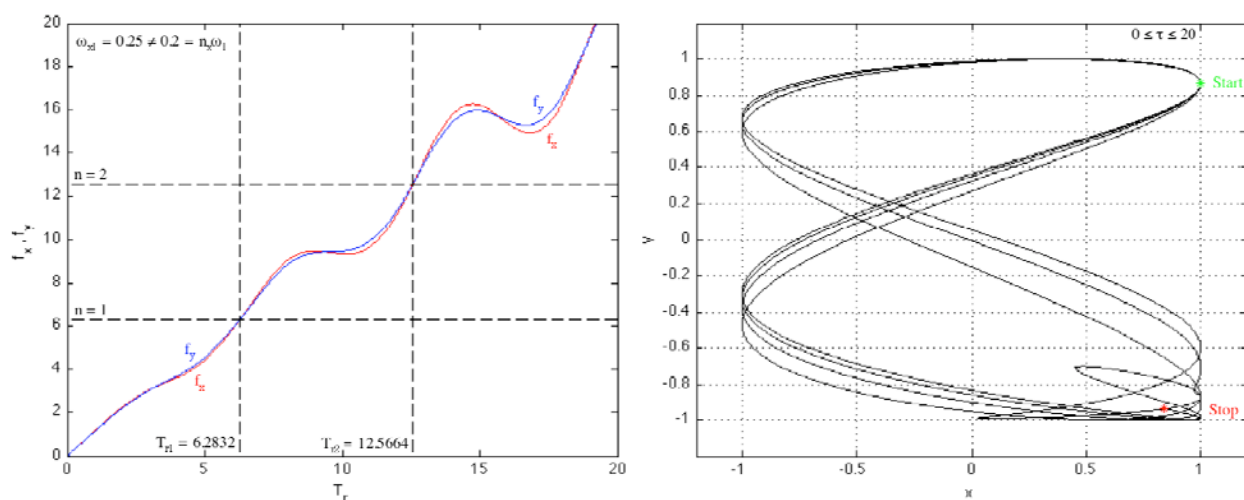


Figure 24. Variable Sinusoid Frequency Spatial Non-Repeating Lissajous Curve

Repeat time T_r must again satisfy both conditions for repeating x,y values. Also, the closed curve requirement again means the phase function difference ratio evaluated across the repeat time must be rational,

$$\frac{n_x}{n_y} = \frac{\omega_x T_r - \phi_x(\tau + T_r) + \phi_x(\tau)}{\omega_y T_r + \phi_y(\tau + T_r) - \phi_y(\tau)} \quad (34)$$

otherwise the curve is open. The variable phase repeat conditions here in Eqs. (33)-(34) have similarities to the variable frequency repeat conditions in Eqs. (23)-(24), but subtle differences are present. Eqs. (33)-(34) strongly restrict the class of time dependent phase functions that are capable of producing a closed curve, specifically, $\phi_x(\tau)$ and $\phi_y(\tau)$ must be rationally proportional and *out-of-phase* to one another. Also note the constant frequencies ω_x , ω_y are still present in Eqs. (33)-(34) and must also share the same integer proportionality for satisfying the closed curve requirement. This *frequency-phase coupling* was not present in Eqs. (23)-(24) where constant phase angles ϕ_x , ϕ_y canceled out from the expressions. A class of sufficient time dependent phase functions and constant frequencies that satisfy rationality using base terms $\phi(\tau)$ and ω are

$$\begin{aligned} \phi_x(\tau) &= -n_x \phi(\tau) & \text{and} & & \omega_x &= n_x \omega \\ \phi_y(\tau) &= +n_y \phi(\tau) & & & \omega_y &= n_y \omega \end{aligned} \quad (35)$$

In this case, the two conditions in Eq. (33) reduce to the single condition

$$\omega T_r + \phi(\tau + T_r) - \phi(\tau) = 2\pi n \quad (36)$$

where existence of repeat time T_r is again problem dependent. Substitution of Eq. (35) into Eq. (34) confirms the evaluated phase function rationality.

$$\frac{\omega_x T_r - \phi_x(\tau + T_r) + \phi_x(\tau)}{\omega_y T_r + \phi_y(\tau + T_r) - \phi_y(\tau)} = \frac{n_x \{\omega T_r + \phi(\tau + T_r) - \phi(\tau)\}}{n_y \{\omega T_r + \phi(\tau + T_r) - \phi(\tau)\}} = \frac{n_x}{n_y} \quad (37)$$

Examples of specific phase functions are not considered here due to the similarities between the variable phase and variable frequency conditions for closed Lissajous curves.

Third, consider the case of variable amplitude but constant frequency-phase, or

$$\begin{aligned} x(t) &= a_x(\tau) \cos\{\omega_x \tau - \phi_x\} \\ y(t) &= a_y(\tau) \sin\{\omega_y \tau + \phi_y\} \end{aligned} \quad (38)$$

This third case is fundamentally different from the first two cases in that the time dependent parameter lies outside the Lissajous cosine and sine function arguments. Applying the Eq. (22) repeat condition for this varying amplitude case yields

$$\begin{aligned} a_x(\tau + T_r) \cos\{\omega_x(\tau + T_r) - \phi_x\} &= a_x(\tau) \cos\{\omega_x \tau - \phi_x\} \\ a_y(\tau + T_r) \sin\{\omega_y(\tau + T_r) + \phi_y\} &= a_y(\tau) \sin\{\omega_y \tau + \phi_y\} \end{aligned} \quad (39)$$

For a specific τ , Eq. (39) again represents *two necessary* conditions that a *single* value of T_r must

simultaneously satisfy. Requiring the amplitude and harmonic factors to repeat *independently*, and after canceling out equal frequency and phase terms, Eq. (39) leads to the *sufficient* conditions

$$\begin{array}{c} \underbrace{a_x(\tau+T_r) - a_x(\tau)}_{f_x(\tau, T_r)} = 0 \\ \underbrace{a_y(\tau+T_r) - a_y(\tau)}_{f_y(\tau, T_r)} = 0 \end{array} \quad \text{and} \quad \begin{array}{l} \omega_x T_r = (2\pi n)n_x \\ \omega_y T_r = (2\pi n)n_y \end{array} \quad (40)$$

Although Eq. (40) represents *four* separate conditions, this expansion helps to further develop the framework. Due to the simple nature of the angular conditions, frequencies ω_x , ω_y must be rationally proportional, or integer scalings of a base frequency ω .

$$\frac{\omega_x}{\omega_y} = \frac{n_x}{n_y}, \quad \begin{array}{l} \omega_x = n_x \omega \\ \omega_y = n_y \omega \end{array} \quad (41)$$

Consequently, repeat time T_r must be integer multiples of $2\pi/\omega$, or

$$T_r = \frac{2\pi}{\omega} n \quad (42)$$

The remaining amplitude conditions, with the known repeat time from Eq. (42), become

$$\begin{array}{l} a_x(\tau+T_r) - a_x(\tau) = 0 \\ a_y(\tau+T_r) - a_y(\tau) = 0 \end{array} \quad \text{where} \quad T_r = \frac{2\pi}{\omega} n \quad (43)$$

Note the harmonic factors have *constrained* the amplitude repeat behavior to be *synchronized* to the harmonic frequencies with constant repeat time increments. Unlike the harmonic factors in Eq. (39) which are fundamentally driven by the same periodic behavior, the amplitude factors in general do not have any underlying basis, and their conditions in Eq. (43) cannot be further manipulated without considering specific amplitude functions.

Consider m^{th} degree polynomial amplitude functions in Eq. (44) as an example.

$$\begin{array}{l} a_x(\tau) = a_{x0} + a_{xk} \prod_{i=1}^m (\tau - r_{xi}) \\ a_y(\tau) = a_{y0} + a_{yk} \prod_{i=1}^m (\tau - r_{yi}) \end{array} \quad (44)$$

In most situations, these amplitude functions would never repeat, leading to an open Lissajous curve. Exceptions to this behavior do exist over a finite time span, or indefinitely if piecewise polynomials are employed. Consider third degree piecewise polynomial amplitude functions that have roots at three consecutive repeat times indicated by n , $n+1$, $n+2$ where the applicable time span is $T_{rn} \leq \tau \leq T_{rn+2}$.

$$\begin{aligned} a_x(\tau) &= a_{x_0} + a_{x_k}(\tau - T_{r_n})(\tau - T_{r_{n+1}})(\tau - T_{r_{n+2}}) \\ a_y(\tau) &= a_{y_0} + a_{y_k}(\tau - T_{r_n})(\tau - T_{r_{n+1}})(\tau - T_{r_{n+2}}) \end{aligned} \quad (45)$$

Periodic amplitude functions are easily constructed from a sequence of these polynomials. Two-piece amplitude functions for $a_x(\tau)$ and $a_y(\tau)$ starting at the reference repeat time (T_{r0}, T_{r1}, T_{r2} and T_{r2}, T_{r3}, T_{r4}) are utilized in this example. Fig. 25 shows a plot of amplitude difference functions $f_x(\tau, T_r)$ and $f_y(\tau, T_r)$ (which are equal here) parameterized at zero time ($\tau = 0$) for a specific set of coefficient values. Fig. 25 confirms the *a priori* repeat times (see Eq. (43)) whereby amplitude functions cross the zero axis at integer multiples of $2\pi/\omega$ ($T_{r1} = 2\pi$, $T_{r2} = 4\pi$, $T_{r3} = 6\pi$ where $\omega = 1$). Corresponding Lissajous curve and individual $x(t)$ and $y(t)$ responses are also shown in Fig. 25 for approximately 3.2 revolutions. Note the variable amplitude Lissajous curve is closed as repeat times exist. The curve passes through the repeat point $(x(0), y(0)) = (1, 0.8660) = (1, 3^{1/2}/2)$ every $\Delta\tau = 2\pi$ units of time but alternates between two paths on every cycle due to the polynomial amplitude frequency ($2\pi/(T_{r2}-T_{r0}) = 2\pi/4\pi = 1/2$) being one-half of the base harmonic frequency ($\omega = 1$). Travel rate at a given point is uniform (fixed frequencies), as can be seen from the periodic $x(t)$ and $y(t)$ signals in Fig. 25. The Lissajous curve is both spatial and temporal periodic. As a final point for this example, Fig. 26 shows results for the case when $a_x(\tau)$ and $a_y(\tau)$ are perturbed from the repeating piecewise polynomial structure in Eq. (45). Specifically, when $\tau \geq T_{r2}$, additive exponential amplitude perturbations are activated, as described below where $a_{x\delta} = 0.005$, $a_{y\delta} = 0.004$, $\lambda = 0.5$.

$$\begin{aligned} a_x(\tau) &= a_{x_0} + a_{x_k}(\tau - T_{r_2})(\tau - T_{r_3})(\tau - T_{r_4}) + a_{x\delta}(e^{\lambda(\tau - T_{r_2})} - 1) \\ a_y(\tau) &= a_{y_0} + a_{y_k}(\tau - T_{r_2})(\tau - T_{r_3})(\tau - T_{r_4}) + a_{y\delta}(e^{\lambda(\tau - T_{r_2})} - 1) \end{aligned} \quad (46)$$

Amplitudes $a_x(\tau)$ and $a_y(\tau)$ do not satisfy Eq. (43) for $\tau \geq T_{r2}$. Fig. 26 shows how this exponential perturbation leads to distinct functions $f_x(\tau, T_r)$ and $f_y(\tau, T_r)$ after τ exceeds T_{r2} eliminating existence of T_{r3} (zero crossing removed). After passing through the repeat point at the end of the second cycle, the perturbation produces an open Lissajous curve which never returns through this point. The Lissajous curve has become non-periodic in space and time.

As a second example of variable amplitude, consider sinusoid amplitude functions in Eq. (47).

$$\begin{aligned} a_x(\tau) &= a_{x_0} + \sum_{i=1}^m a_{x_i} \sin(i\lambda\tau) \\ a_y(\tau) &= a_{y_0} + \sum_{i=1}^m a_{y_i} \sin(i\lambda\tau) \end{aligned} \quad (47)$$

A single harmonic ($m = 1$) is utilized in this example. Fig. 27 shows a plot of amplitude difference functions $f_x(\tau, T_r)$ and $f_y(\tau, T_r)$ (which are equal here) parameterized at zero time ($\tau = 0$) for a specific set of coefficient values. Fig. 27 confirms the *a priori* repeat times (see Eq. (43)) whereby amplitude functions cross the zero axis at integer multiples of $2\pi/\omega$ ($T_{r1} = 2\pi$, $T_{r2} = 4\pi$, $T_{r3} = 6\pi$ where $\omega = 1$). Corresponding Lissajous curve and individual $x(t)$ and $y(t)$ responses are also shown in Fig. 27 for approximately 3.2 cycles. Note the variable amplitude Lissajous curve is closed as repeat times exist. The curve passes through repeat point $(x(0), y(0)) = (1, 0.8660) =$

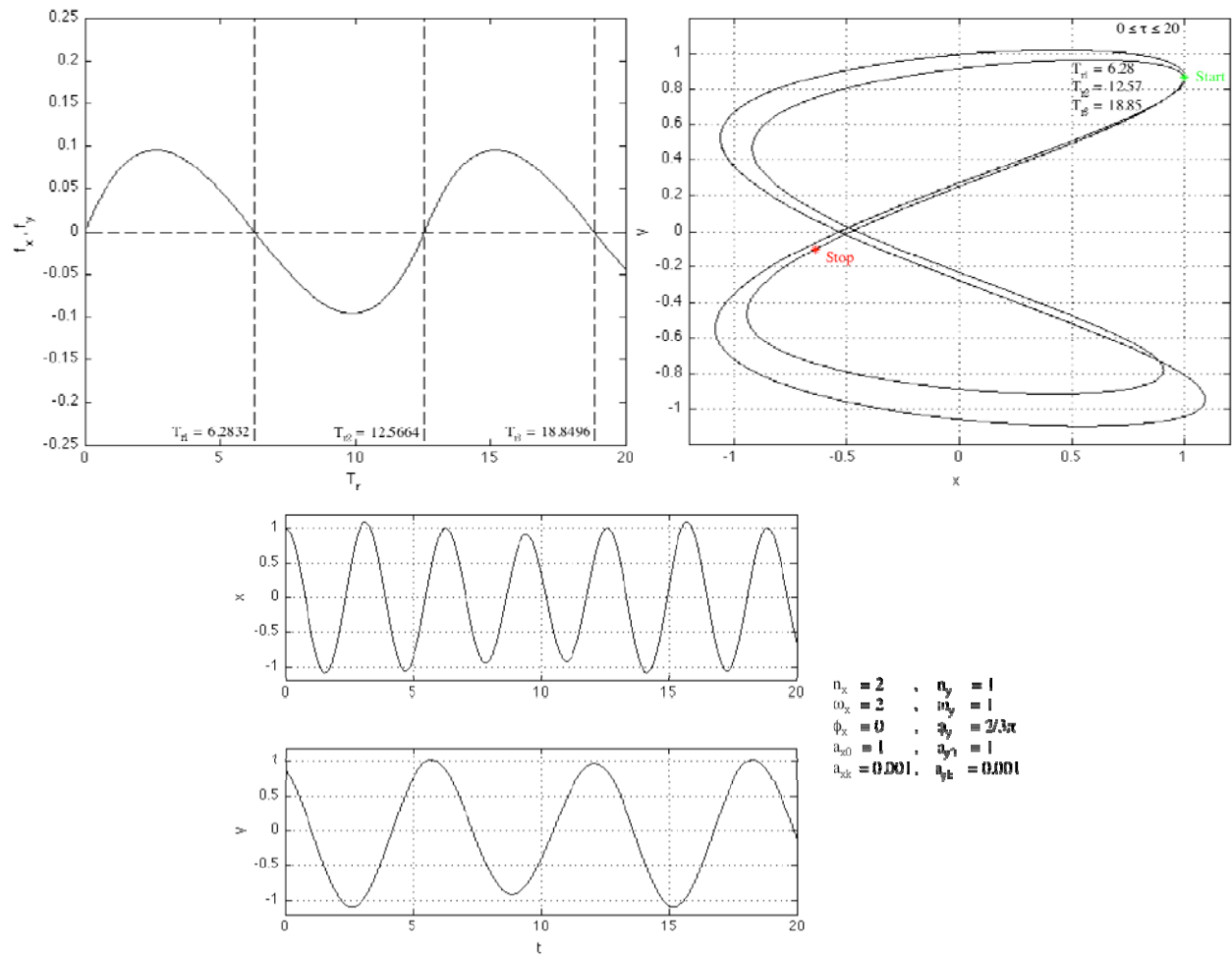


Figure 25. Variable Polynomial Amplitude Repeating Lissajous Curve

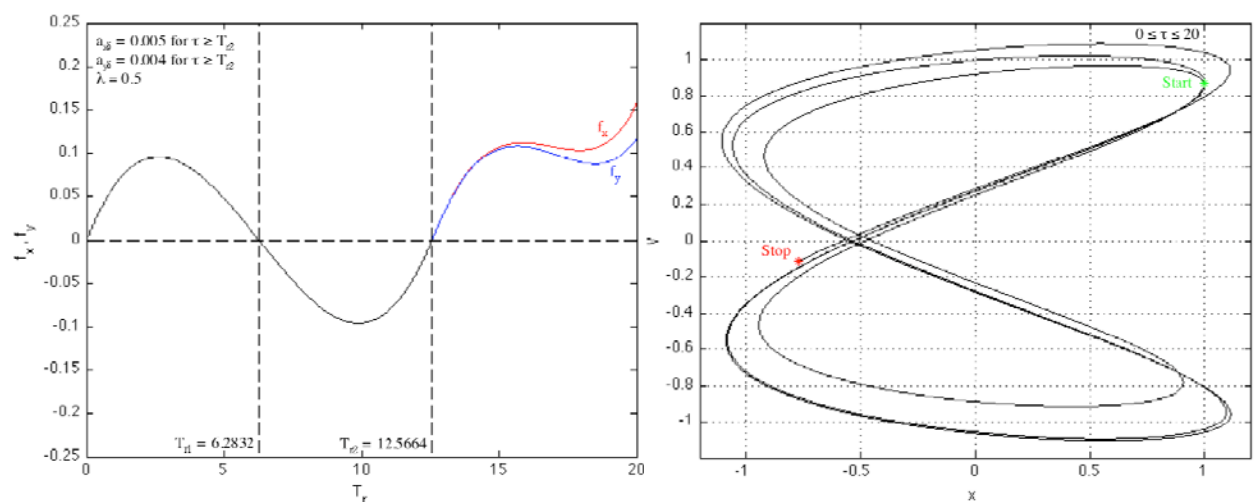


Figure 26. Variable Polynomial Amplitude Non-Repeating Lissajous Curve

($1, 3^{1/2}/2$) every $\Delta\tau = 2\pi$ units of time but again alternates between two paths on every cycle due to the sinusoid amplitude frequency ($\lambda = 1/2$) being one-half of the base harmonic frequency ($\omega = 1$). Travel rate at a given point is uniform (fixed frequencies), as can be seen from the periodic $x(t)$ and $y(t)$ signals in Fig. 27. The Lissajous curve is both spatial and temporal periodic. As a final point for this example, Fig. 28 shows results for the case when $a_x(\tau)$ and $a_y(\tau)$ are perturbed from the sinusoidal structure in Eq. (47). Specifically, when $\tau \geq T_{r2}$, multiplicative quadratic secular amplitude perturbations are activated, as described below where $a_{x\delta} = 0.05$, $a_{y\delta} = 0.04$.

$$\begin{aligned} a_x(\tau) &= a_{x0} + a_{x1} \sin(\lambda\tau) \{1 + a_{x\delta}(\tau - T_{r2})^2\} \\ a_y(\tau) &= a_{y0} + a_{y1} \sin(\lambda\tau) \{1 + a_{y\delta}(\tau - T_{r2})^2\} \end{aligned} \quad (48)$$

Even with perturbation, amplitudes $a_x(\tau)$ and $a_y(\tau)$ continue to satisfy Eq. (43) for $\tau \geq T_{r2}$. Fig. 28 shows how this secular perturbation leads to distinct functions $f_x(\tau, T_r)$ and $f_y(\tau, T_r)$ after τ exceeds T_{r2} but existence of T_{r3} remains (zero crossing retained). After passing through the repeat point at the end of the second revolution, the perturbation produces a spatially non-repeating but still closed Lissajous curve. On every revolution, the Lissajous curve follows a different path, but the curves all return to pass through the repeat point. The Lissajous curve has become spatial non-periodic but still temporal periodic.

This section has explored necessary and/or sufficient conditions for closed Lissajous curves with either varying frequency, varying phase, or varying amplitude, separately, for two dimensions. Extensions for simultaneous parametric variations, extensions to three dimensions, and allowance for multi-harmonic terms is straightforward but requires more effort. In the simpler case of constant parameters, conditions reduce to the fixed Lissajous curve conditions noted in Section 4. Fundamentally, the closed curve conditions describe repeating Lissajous curve points. Analysis has shown that a closed curve is not necessarily a periodic curve in the traditional sense of both time and space. By example, the closed condition was shown to expose temporal periodic curves, spatial periodic curves, and temporal-spatial periodic curves. Additional framework would be required to assess the hierarchy of periodic curve type, such as constant repeat time increments, applicability of a specific repeat time across spatially varying curve points, or curve continuity through derivative considerations.

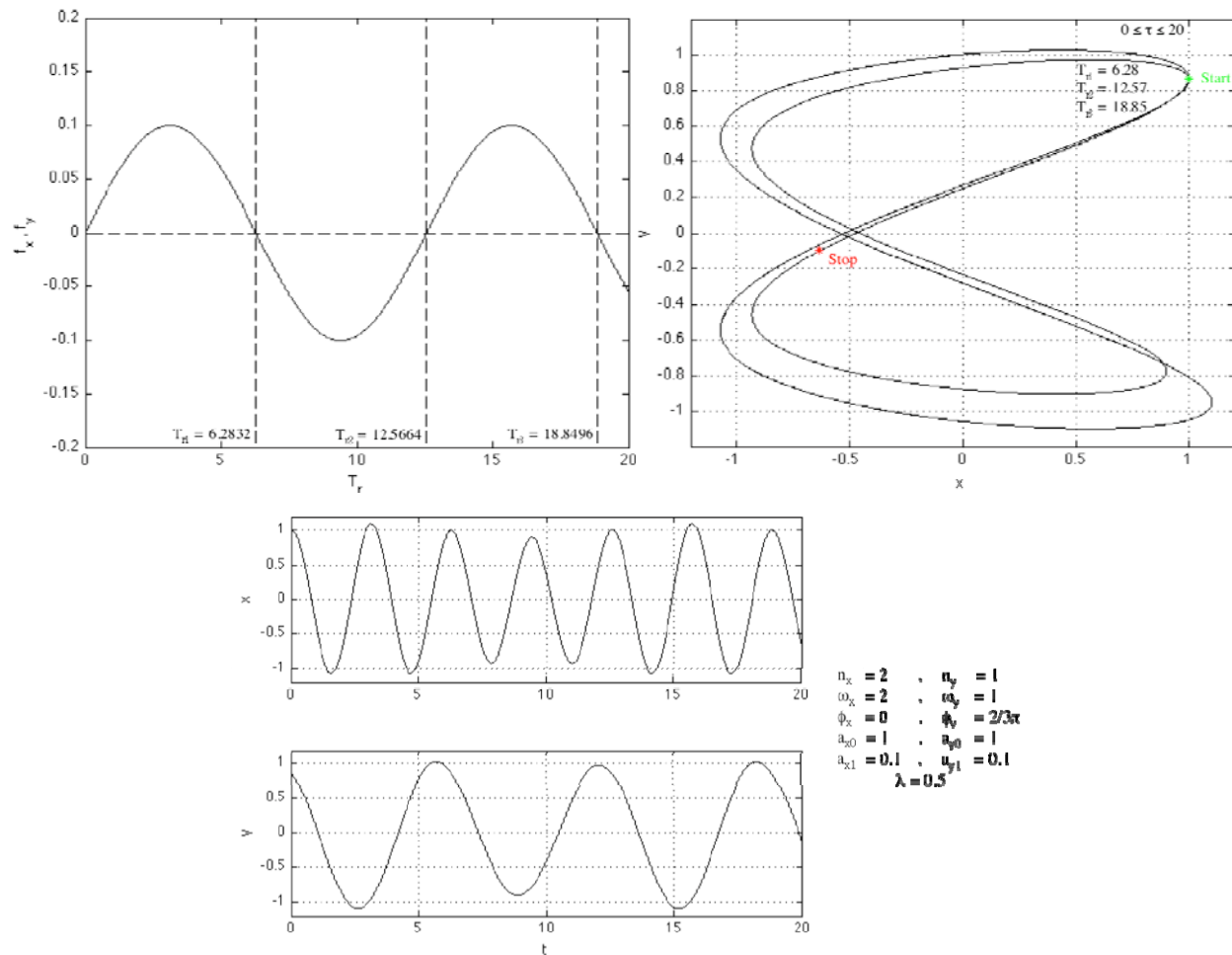


Figure 27. Variable Sinusoid Amplitude Repeating Lissajous Curve

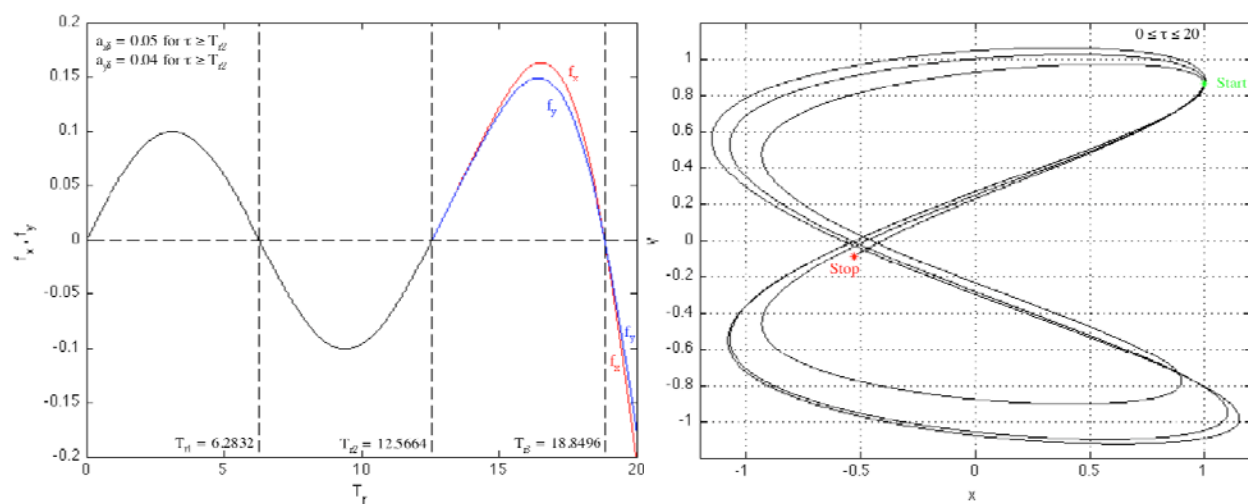


Figure 28. Variable Sinusoid Amplitude Spatial Non-Repeating Lissajous Curve

4.4 SECOND ORDER PERIODICITY

Return to the topic of periodicity based on second order ROE. For this development, the expanded formulation of second order ROE employing variable amplitude but fixed frequency and phase in Section 5 is chosen. Extra complexity that was not considered in Section 7, in the form of polynomial center point terms, multiple harmonics, and three-dimensional coordinates, is present in the second order ROE motion expressions. These features will be addressed in a systematic process. Parametric conditions for relative motion evolution where coordinate values x, y, z simultaneously return to previous values after repeat time T_r are developed from Eq. (49), which is an extension of Eq. (22) from Section 7. Note the meaning of parametric conditions here refers to deputy relative initial states which reside in a layer of the motion model below the amplitude-frequency-phase parameters.

$$\begin{aligned} x(t+T_r) &= x(t) \\ y(t+T_r) &= y(t) \\ z(t+T_r) &= z(t) \end{aligned} \quad (49)$$

Using the expanded structure of Eq. (10), these necessary conditions become

$$\begin{aligned} x_c(\tau+T_r) + x_{h1}(\tau+T_r) + x_{sh1}(\tau+T_r) + x_{h2}(\tau+T_r) &= x_c(\tau) + x_{h1}(\tau) + x_{sh1}(\tau) + x_{h2}(\tau) \\ y_c(\tau+T_r) + y_{h1}(\tau+T_r) + y_{sh1}(\tau+T_r) + y_{h2}(\tau+T_r) &= y_c(\tau) + y_{h1}(\tau) + y_{sh1}(\tau) + y_{h2}(\tau) \\ z_c(\tau+T_r) + z_{h1}(\tau+T_r) + z_{sh1}(\tau+T_r) + z_{h2}(\tau+T_r) &= z_c(\tau) + z_{h1}(\tau) + z_{sh1}(\tau) + z_{h2}(\tau) \end{aligned} \quad (50)$$

A set of sufficient conditions, that require secular polynomial center point coordinates (x_c, y_c, z_c), first harmonic coordinates (x_{h1}, y_{h1}, z_{h1}), secular first harmonic coordinates ($x_{sh1}, y_{sh1}, z_{sh1}$), and second harmonic coordinates (x_{h2}, y_{h2}, z_{h2}), to repeat separately, established from Eq. (50), is

$$\begin{aligned} x_c(\tau+T_r) &= x_c(\tau) , \quad x_{h1}(\tau+T_r) = x_{h1}(\tau) , \quad x_{sh1}(\tau+T_r) = x_{sh1}(\tau) , \quad x_{h2}(\tau+T_r) = x_{h2}(\tau) \\ y_c(\tau+T_r) &= y_c(\tau) , \quad y_{h1}(\tau+T_r) = y_{h1}(\tau) , \quad y_{sh1}(\tau+T_r) = y_{sh1}(\tau) , \quad y_{h2}(\tau+T_r) = y_{h2}(\tau) \\ z_c(\tau+T_r) &= z_c(\tau) , \quad z_{h1}(\tau+T_r) = z_{h1}(\tau) , \quad z_{sh1}(\tau+T_r) = z_{sh1}(\tau) , \quad z_{h2}(\tau+T_r) = z_{h2}(\tau) \end{aligned} \quad (51)$$

First, consider the center point conditions. Progressing to the ROE secular polynomial coefficient level, Eq. (51) requires

$$\begin{aligned} b_{x,s0}\{1\} + b_{x,s1}\{n_o(\tau+T_r)\} + b_{x,s2}\{[n_o(\tau+T_r)]^2\} &= b_{x,s0}\{1\} + b_{x,s1}\{n_o\tau\} + b_{x,s2}\{(n_o\tau)^2\} \\ b_{y,s0}\{1\} + b_{y,s1}\{n_o(\tau+T_r)\} &= b_{y,s0}\{1\} + b_{y,s1}\{n_o\tau\} \\ b_{z,s0}\{1\} &= b_{z,s0}\{1\} \end{aligned} \quad (52)$$

By taking each polynomial term separately, repeat conditions become

$$\begin{aligned}
b_{x,s0}\{1\} - b_{x,s0}\{1\} &= 0 \rightarrow 0=0 \\
&\rightarrow \text{No Condition on } b_{x,s0} \\
b_{x,s1}\{n_o(\tau+T_r)\} - b_{x,s1}\{n_o\tau\} &= 0 \rightarrow b_{x,s1}\{n_oT_r\} = 0 \\
&\rightarrow b_{x,s1} = 0 \text{ or } T_r = 0 \\
b_{x,s2}\{[n_o(\tau+T_r)]^2\} - b_{x,s2}\{(n_o\tau)^2\} &= 0 \rightarrow b_{x,s2}\{n_o^2(2\tau+T_r)T_r\} = 0 \\
&\rightarrow b_{x,s2} = 0 \text{ or } 2\tau+T_r = 0 \text{ or } T_r = 0 \quad (53) \\
b_{y,s0}\{1\} - b_{y,s0}\{1\} &= 0 \rightarrow 0=0 \\
&\rightarrow \text{No Condition on } b_{y,s0} \\
b_{y,s1}\{n_o(\tau+T_r)\} - b_{y,s1}\{n_o\tau\} &= 0 \rightarrow b_{y,s1}\{n_oT_r\} = 0 \\
&\rightarrow b_{y,s1} = 0 \text{ or } T_r = 0 \\
b_{z,s0}\{1\} - b_{z,s0}\{1\} &= 0 \rightarrow 0=0 \\
&\rightarrow \text{No Condition on } b_{z,s0}
\end{aligned}$$

Moving on to first and second harmonic terms, Eq. (51) imposes several conditions on the ROE coefficients.

$$\begin{aligned}
a_{x,h1}\cos\{n_o(\tau+T_r) - \phi_{x,h1}\} &= a_{x,h1}\cos\{n_o\tau - \phi_{x,h1}\} \\
a_{y,h1}\sin\{n_o(\tau+T_r) + \phi_{y,h1}\} &= a_{y,h1}\sin\{n_o\tau + \phi_{y,h1}\} \\
a_{z,h1}\sin\{n_o(\tau+T_r) + \phi_{z,h1}\} &= a_{z,h1}\sin\{n_o\tau + \phi_{z,h1}\} \\
\text{and} & \\
a_{x,h2}\cos\{2n_o(\tau+T_r) - \phi_{x,h2}\} &= a_{x,h2}\cos\{2n_o\tau - \phi_{x,h2}\} \\
a_{y,h2}\sin\{2n_o(\tau+T_r) + \phi_{y,h2}\} &= a_{y,h2}\sin\{2n_o\tau + \phi_{y,h2}\} \\
a_{z,h2}\sin\{2n_o(\tau+T_r) + \phi_{z,h2}\} &= a_{z,h2}\sin\{2n_o\tau + \phi_{z,h2}\}
\end{aligned} \quad (54)$$

Note these conditions are the extension of Eq. (39) in Section 7. Treating amplitude and harmonic factors separately leads to repeat conditions

$$\begin{aligned}
a_{i,h1} - a_{i,h1} &= 0 \rightarrow 0=0 \quad \text{where } i = x,y,z \\
&\rightarrow \text{No Condition on } a_{i,h1} \\
&\rightarrow \text{No Condition on } b_{i,h1}, c_{i,h1} \\
n_o(\tau+T_r) - n_o\tau &= (2\pi n)1 \rightarrow n_oT_r = 2\pi n \\
\text{and} & \\
a_{i,h2} - a_{i,h2} &= 0 \rightarrow 0=0 \quad \text{where } i = x,y,z \\
&\rightarrow \text{No Condition on } a_{i,h2} \\
&\rightarrow \text{No Condition on } b_{i,h2}, c_{i,h2} \\
2n_o(\tau+T_r) - 2n_o\tau &= (2\pi n)2 \rightarrow n_oT_r = 2\pi n
\end{aligned} \quad (55)$$

In Eq. (55), n again represents a common integer number of whole revolutions over time T_r as in Eq. (40), and integers like n_x , n_y , n_z are not required here since deputy motion along the LVLH

axes oscillates at the common chief mean motion frequency n_o or double frequency $2n_o$. Finally, consider the secular first harmonic terms. Repeat conditions on the ROE coefficients from Eq. (51) require

$$\begin{aligned} a_{x,sh1}(\tau+T_r)\cos\{n_o(\tau+T_r) - \phi_{x,sh1}\} &= a_{x,sh1}(\tau)\cos\{n_o\tau - \phi_{x,sh1}\} \\ a_{y,sh1}(\tau+T_r)\sin\{n_o(\tau+T_r) + \phi_{y,sh1}\} &= a_{y,sh1}(\tau)\sin\{n_o\tau + \phi_{y,sh1}\} \\ a_{z,sh1}(\tau+T_r)\sin\{n_o(\tau+T_r) + \phi_{z,sh1}\} &= a_{z,sh1}(\tau)\sin\{n_o\tau + \phi_{z,sh1}\} \end{aligned} \quad (56)$$

Again taking the amplitude and harmonic factors separately gives

$$\begin{aligned} a_{i,sh1}(\tau+T_r) - a_{i,sh1}(\tau) &= 0 \quad \rightarrow \quad \{b_{i,sh1}^2 + c_{i,sh1}^2\}^{1/2}(n_o T_r) = 0 \quad \text{where } i = x,y,z \\ &\rightarrow \quad b_{i,sh1} = 0, c_{i,sh1} = 0 \quad \text{or } T_r = 0 \\ n_o(\tau+T_r) - n_o\tau &= (2\pi n)l \quad \rightarrow \quad n_o T_r = 2\pi n \end{aligned} \quad (57)$$

Three possible cases for repeating x,y,z coordinates exist and are summarized below.

$$\begin{aligned} \text{Trivial Case: } (T_r, n) &= (0, 0) \\ \text{Specific Case: } T_r &= \frac{2\pi}{n_o} n, \quad \tau = -\frac{1}{2} T_r \\ &b_{x,s1} = 0, \quad b_{y,s1} = 0 \\ &b_{i,sh1} = 0, \quad c_{i,sh1} = 0 \quad \text{where } i = x,y,z \\ \text{General Case: } T_r &= \frac{2\pi}{n_o} n \\ &b_{x,s2} = 0 \\ &b_{x,s1} = 0, \quad b_{y,s1} = 0 \\ &b_{i,sh1} = 0, \quad c_{i,sh1} = 0 \quad \text{where } i = x,y,z \end{aligned} \quad (58)$$

The trivial case is not useful. Although the specific case describes a correct physical motion where the combined parabolic center point travel and oscillatory harmonic travel generate a single repeat of x,y,z coordinates (non-periodic) associated with a specific time τ , this case has limited utility and is not of interest here. The general case, which allows for an infinite number of repeat cycles and no restriction on time, is the case of interest for constructing initial condition relations that result in deputy periodic motion, both spatial and temporal, under second order accuracy. Nine separate conditions are part of the general case listed in Eq. (58) in terms of ROE coefficients, which could have been alternatively derived from the second order compacted formulation (Section 6), or the original QV motion expressions (Eq. (9)). Only seven of these conditions are potentially independent (see Eq. (11)), which after simplification, are identified below in terms of deputy initial conditions.

$$\begin{aligned}
b_{x,s2}: & (2n_o x_0 + \dot{y}_0)^2 = 0 \\
b_{x,s1}: & (2n_o x_0 + \dot{y}_0)(n_o y_0 - 2\dot{x}_0) = 0 \\
b_{y,s1}: & 2n_o \bar{R}_o(2n_o x_0 + \dot{y}_0) + n_o^2(11x_0^2 + 2y_0^2 + z_0^2) \\
& + (\dot{x}_0^2 + 4\dot{y}_0^2 + \dot{z}_0^2) + 2n_o(7x_0\dot{y}_0 - y_0\dot{x}_0) = 0 \\
c_{x,sh1} \text{ or } b_{y,sh1}: & (2n_o x_0 + \dot{y}_0)(3n_o x_0 + 2\dot{y}_0) = 0 \\
c_{y,sh1} \text{ or } b_{x,sh1}: & (2n_o x_0 + \dot{y}_0)\dot{x}_0 = 0 \\
b_{z,sh1}: & (2n_o x_0 + \dot{y}_0)\dot{z}_0 = 0 \\
c_{z,sh1}: & (2n_o x_0 + \dot{y}_0)z_0 = 0
\end{aligned} \tag{59}$$

Note six of the seven equations have been factored, with one factor being the linear CW drift condition term which appears in all six factored equations, as well as in the seventh unfactored equation. The $b_{x,s2} = 0$ condition in Eq. (59) requires

$$\dot{y}_0 = -2n_o x_0 \tag{60}$$

in all second order periodic solutions. Thus, from the seven conditions in Eq. (59), only two of these conditions are ultimately independent, which after simplification, are identified below.

$$\begin{aligned}
b_{x,s2}, \dots: & 2n_o x_0 + \dot{y}_0 = 0 \\
b_{y,s1}: & n_o^2(11x_0^2 + 2y_0^2 + z_0^2) + (\dot{x}_0^2 + 4\dot{y}_0^2 + \dot{z}_0^2) + 2n_o(7x_0\dot{y}_0 - y_0\dot{x}_0) = 0
\end{aligned} \tag{61}$$

In the CW first order solution, only one condition exists between x_0, \dot{y}_0 for a periodic orbit, which is the first condition in Eq. (61). Note how the QV second order solution requires an extra condition for periodicity involving all six deputy initial conditions in Eq. (61). One way that the $b_{y,s1} = 0$ condition constrains the possible periodic motion is that deputy cross-track or z axis motion cannot evolve independently as in a first order model, where the deputy can oscillate in cross-track with zero radial (x) and zero along-track (y) displacement (assuming collision with the chief at the origin is somehow avoided). In the second order framework, if $x_0, y_0, \dot{x}_0, \dot{y}_0$ are all zero, the second condition from Eq. (61) requires z_0 and \dot{z}_0 to equal zero with no other physical possibility. Another way that the $b_{y,s1} = 0$ condition constrains the possible periodic motion is that some combinations of in-plane initial states are not allowed. Note a combination of non-zero initial conditions where $7x_0\dot{y}_0 = y_0\dot{x}_0$ can never lead to a second order accurate periodic orbit as the $b_{y,s1} = 0$ condition would become inconsistent. Even though an extra constraint on the initial conditions exists in second order accuracy, an infinite number of periodic motions is still possible since Eq. (61) represents two requirements in six initial conditions.

Several simple analytical solutions for the initial conditions are possible. Consider eliminating \dot{y}_0 in the second condition in Eq. (61) in terms of x_0 using Eq. (60). The resulting single periodic condition in five variables, written in two different ways, is noted below.

$$\begin{aligned}
& n_o^2(x_0^2 - 2y_0^2) + (2n_o y_0 - \dot{x}_0)\dot{x}_0 - (n_o^2 z_0^2 + \dot{z}_0^2) = 0 \\
& \text{or} \\
& (n_o^2 x_0^2 - \dot{x}_0^2) + 2n_o(\dot{x}_0 - n_o y_0)y_0 - (n_o^2 z_0^2 + \dot{z}_0^2) = 0
\end{aligned} \tag{62}$$

Treating x_0 as a specified independent variable, if y_0 is chosen according to $2y_0^2 = x_0^2$, and \dot{x}_0 is chosen according to $\dot{x}_0 = 2n_0 y_0$, along with \dot{y}_0 satisfying Eq. (60), then z_0 and \dot{z}_0 must be zero and an in-plane periodic orbit will ensue. Likewise, if \dot{x}_0 is chosen according to $\dot{x}_0^2 = n_0^2 x_0^2$ and y_0 is chosen according to $n_0 y_0 = \dot{x}_0$, then another in-plane periodic orbit is created. Further, suppose x_0, y_0, z_0 are specified and \dot{x}_0 is chosen according to $\dot{x}_0 = 2n_0 y_0$, along with \dot{y}_0 satisfying Eq. (60), then Eq. (62) provides a condition for computing a corresponding \dot{z}_0 that produces a three-dimensional out-of-plane periodic motion to second order accuracy. Ultimately, any specification of four initial conditions from the five member set $x_0, y_0, z_0, \dot{x}_0, \dot{z}_0$ with the fifth member computed from Eq. (62), that results in a consistent and physically realizable initial relative ephemeris, leads to periodic motion. Conditions in Eq. (61) could be useful for initializing numerical shooting methods or differential correction methods to establish exact three-dimensional periodic orbits under two-body circular reference assumptions.

5.0 CONCLUSIONS

An analytical framework has been developed for the concept of second order relative orbital elements, extending ideas that first originated by reformulating the first order Clohessy-Wiltshire Cartesian relative motion solution in a more geometrically meaningful characterization. The framework is built around the second order Quadratic Volterra relative motion solution, and is thus limited by two-body circular reference conditions and a bounded separation between deputy and chief satellites. The new relative orbital elements are defined in such a way that geometric insight to the relative orbit size, shape, orientation, and satellite location along the orbit in three-dimensional settings is preserved. The new element set is based on amplitude and angular quantities related to the concept of an instantaneous ellipse. Through the use of auxiliary circles, a given element set can be used to geometrically characterize the satellite orbit. Second order motion produces varying amplitude and phase behavior, and the new relative orbital element variables are well-suited for describing this complex behavior. The new framework is highly related to the concept of variable Lissajous space curves, which was utilized to develop the new element variables. New relations were developed to describe and quantify how first order relative orbital elements are distorted by second order gravitational effects, that may be useful in dynamical guidance and estimation error analysis. Finally, new conditions for periodic orbits to second order accuracy were developed from the new element set and repeating Lissajous curve conditions. These second order conditions were shown to be more restrictive on initial condition sets that produce periodic motion, when compared to corresponding first order conditions.

6.0 RECOMMENDATIONS

Several follow-on research and development efforts to the work presented in this report should be pursued. First, a software package that utilizes computer generated three-dimensional color visualizations to facilitate the practical use of the second order relative orbital elements and the geometrical information they depict should be developed. A tool such as this could enhance flight control operations, space situational awareness, and rapid comprehension and adaptation of complex multi-satellite formations. Second, the analytical framework and underlying numerical calculations of second order relative orbital elements should be applied to maneuver planning and execution strategies. Orbital maneuver strategy based on the new motion description could be exploited to provide more efficient, more accurate, and more transparent guidance and control functions involving multiple close-proximity cooperative satellites. Third, the new perspective on necessary conditions for periodic relative orbits should be further examined and potentially utilized in orbital flight control procedures addressing the objectives of maneuvering to and from, and maintaining, periodic relative orbits in an optimal fashion. Increased knowledge from this subject area should also be considered for initialization of numerical search algorithms attempting to achieve high precision conditions for achieving periodic relative orbits.

REFERENCES

- [1] Junkins, J. L., "Adventures on the Interface of Dynamics and Control," *Journal of Guidance, Control, and Dynamics*, Vol. 20, No. 6, pp. 1058-1071, November-December 1997.
- [2] Junkins, J. L. and Singla, P., "How Nonlinear Is It?, A Tutorial on Nonlinearity of Orbit and Attitude Dynamics," *Journal of the Astronautical Sciences*, Vol. 52, No. 1-2, pp. 7-60, 2004.
- [3] Hintz, G. R., "Survey of Orbit Element Sets," *Journal of Guidance, Control, and Dynamics*, Vol. 31, No. 3, pp. 785-790, May-June 2008.
- [4] Bate, R. R., Mueller, D. D., and White, J. E., **Fundamentals of Astrodynamics**, Dover, New York, New York, 1971.
- [5] Battin, R. H., **An Introduction to the Mathematics and Methods of Astrodynamics**, American Institute of Aeronautics and Astronautics, Reston, Virginia, 1987.
- [6] Vallado, D. A., **Fundamentals of Astrodynamics and Applications**, Microcosm, Hawthorne, California, 2001.
- [7] Carter, T. E., "State Transition Matrices for Terminal Rendezvous Studies: Brief Survey and New Example," *Journal of Guidance, Control, and Dynamics*, Vol. 21, No. 1, pp. 148-155, January-February 1998.
- [8] Clohessy, W. H. and Wiltshire, R. S., "Terminal Guidance System for Satellite Rendezvous," *Proceedings of the IAS Summer Meeting*, IAS-1959-93, Los Angeles, California, June 1959.
- [9] Clohessy, W. H. and Wiltshire, R. S., "Terminal Guidance System for Satellite Rendezvous," *Journal of the Aerospace Sciences*, Vol. 27, No. 9, pp. 653-658, September 1960.
- [10] Steffan, K. F., "Satellite Rendezvous Terminal Guidance System," *ARS Journal*, Vol. 31, No. 11, pp. 1516-1521, Nov 1961.
- [11] Stern, R. G., "Interplanetary Midcourse Guidance Analysis," Experimental Astronomy Laboratory, Report TE-5, Massachusetts Institute of Technology, Cambridge, Massachusetts, 1963.
- [12] Hill, G. W., "Researches in the Lunar Theory," *American Journal of Mathematics*, Vol. 1, No. 1, pp. 5-26, March 1978.
- [13] Karlgaard, C. D. and Lutze, F. H., "Second-Order Relative Motion Equations," *Journal of Guidance, Control, and Dynamics*, Vol. 26, No. 1, pp. 41-49, Jan-Feb 2003.

- [14] Berreen, T. F. and Crisp, J. D. C., "An Exact and a New First-Order Solution for the Relative Trajectories of a Probe Ejected from a Space Station," *Celestial Mechanics*, Vol. 13, No. 1, pp. 75–88, Feb 1976.
- [15] Geller, D. K. and Lovell, T. A., "Relative Orbital Motion and Angles-Only Relative State Observability in Cylindrical Coordinates," AAS-2014-211, *Proceedings of the AAS-AIAA Space Flight Mechanics Meeting*, Santa Fe, New Mexico, Advances in the Astronautical Sciences, Vol. 152, pp. 133-148, Jan 2014.
- [16] Lancaster, E. R., "Relative Motion of Two Particles in Elliptic Orbits," *AIAA Journal*, Vol. 8, No. 10, pp. 1878-1879, Oct 1970.
- [17] Eades, J. B. and Drewry, J. W., "Relative Motion of Near Orbiting Satellites," *Celestial Mechanics*, Vol. 7, No. 1, pp. 3-30, Jan 1973.
- [18] Garrison, J. L., Gardner, T. G., and Axelrad, P., "Relative Motion in Highly Elliptical Orbits," AAS-1995-194, *Proceedings of the AAS-AIAA Space Flight Mechanics Meeting*, Albuquerque, New Mexico, Advances in the Astronautical Sciences, Vol. 89, pp. 1359-1376, Feb 1995.
- [19] Gurfil, P. and Kasdin, N. J., "Nonlinear Modeling of Spacecraft Relative Motion in the Configuration Space," *Journal of Guidance, Control, and Dynamics*, Vol. 27, No. 1, pp. 154-157, Jan-Feb 2004.
- [20] Condurache, D. and Martinusi, V., "Relative Spacecraft Motion in a Central Force Field," *Journal of Guidance, Control, and Dynamics*, Vol. 30, No. 3, pp. 873-876, May-June 2007.
- [21] Schaub, H., "Relative Orbit Geometry Through Classical Orbit Element Differences," *Journal of Guidance, Control, and Dynamics*, Vol. 27, No. 5, pp. 839-848, Sept-Oct 2004.
- [22] Gim, D. W. and Alfrend, K. T., "State Transition Matrix of Relative Motion for the Perturbed Noncircular Reference Orbit," *Journal of Guidance, Control, and Dynamics*, Vol. 26, No. 6, pp. 956-971, Nov-Dec 2003.
- [23] Gim, D. W. and Alfrend, K. T., "Satellite Relative Motion Using Differential Equinoctial Elements," *Celestial Mechanics and Dynamical Astronomy*, Vol. 92, No. 4, pp. 295-336, Aug 2005.
- [24] Deprit, A. and Rom, A., "The Main Problem of Artificial Satellite Theory for Small and Moderate Eccentricities," *Celestial Mechanics*, Vol. 2, No. 2, pp. 166-206, Jun 1970.
- [25] D'Amico, S. and Montenbruck, O., "Proximity Operations of Formation-Flying Spacecraft Using an Eccentricity/Inclination Vector Separation," *Journal of Guidance, Control, and Dynamics*, Vol. 29, No. 3, pp. 554-563, May-June 2006.

- [26] Condurache, D. and Martinusi, V., "Quaternionic Exact Solution to the Relative Orbital Motion Problem," *Journal of Guidance, Control, and Dynamics*, Vol. 33, No. 4, pp. 1035-1047, July-Aug 2010.
- [27] Lovell, T. A., Tragesser, S. G., and Tollefson, M. V., "A Practical Guidance Methodology for Relative Motion of LEO Spacecraft Based on the Clohessy-Wiltshire Equations," AAS-2004-252, *Proceedings of the AAS-AIAA Spaceflight Mechanics Meeting*, Maui, Hawaii, Advances in the Astronautical Sciences, Vol. 119, pp. 2355-2369, Feb 2004.
- [28] Lovell, T. A. and Tragesser, S. G., "Guidance for Relative Motion of Low Earth Orbit Spacecraft Based on Relative Orbit Elements," AIAA-2004-4988, *Proceedings of the AIAA-AAS Astrodynamics Specialist Conference*, Providence, Rhode Island, August, 2004.
- [29] Lovell, T. A. and Spencer, D. A., "Relative Orbital Elements Formulation Based upon the Clohessy-Wiltshire Equations," *Journal of the Astronautical Sciences*, Vol. 61, No. 4, pp. 341-366, Dec 2014.
- [30] Spencer, D. A. and Lovell, T. A., "Maneuver Design Using Relative Orbital Elements," *Journal of the Astronautical Sciences*, Vol. 62, No. 4, pp. 315-350, Dec 2015.
- [31] Benhacine, L., Harris, A., Lovell, T. A., and Sinclair, A. J., "A Geometric Approach to Second-Order, Circular-Reference Spacecraft Relative Motion," AAS-2016-013, *Proceedings of the AAS Guidance and Control Conference*, Breckenridge, Colorado, Advances in the Astronautical Sciences, Vol. 157, pp. 29-42, Feb 2016.
- [32] Stringer, M. T., Newman, B., Lovell, T. A., and Omran, A., "Second Order Nonlinear Initial Value Solution for Relative Motion Using Volterra Theory," AAS-2013-469, *Proceedings of the AAS-AIAA Space Flight Mechanics Meeting*, Lihue, Hawaii, Advances in the Astronautical Sciences, Vol. 148, pp. 2133-2149, Feb 2013.
- [33] Seggern, D. V., **Practical Handbook of Curve Design and Generation**, CRC Press, Boca Raton, Florida, 1994.
- [34] Resnick, R. and Halliday, D., **Physics, Part 1**, John Wiley and Sons, New York, New York, 1977.
- [35] Cundy, H. M. and Rollett, A. P., **Mathematical Models**, Oxford University Press, Oxford, England, 1961.
- [36] Whitaker, R. J., "Types of Two-Dimensional Pendulums and Their Uses in Education," *Science & Education*, Vol. 13, No. 4, pp. 401-415, July 2004.
- [37] Ashton, A., **Harmonograph: A Visual Guide to the Mathematics of Music**, Walker Publishing, New York, New York, 2003.

- [38] McKenna, D., "From Lissajous to Pas de Deux to Tattoo: The Graphic Life of a Beautiful Loop," *Proceedings of the 2011 Bridges Conference on Mathematics, Music, Art, Architecture, Culture*, Coimbra, Portugal, July, pp. 295-302, 2011.
- [39] Hoste, J. and Zirbel, L., "Lissajous Knots and Knots with Lissajous Projections," arXiv:math/0605632 [math.GT], Geometric Topology, arXiv Scientific Advisory Board, Cornell University Library, Ithaca, New York, May 2006.
- [40] Bogle, M. G. V., Hearst, J. E., Jones, V. F. R., and Stoilov, L., "Lissajous Knots," *Journal of Knot Theory and Its Ramifications*, Vol. 3, No. 2, pp. 121-140, June 1994.
- [41] Crowell, R. H. and Fox, R. H., **Introduction to Knot Theory**, Dover Publications, Mineola, New York, 1963.
- [42] Ghazy, M. A. and Newman, B., "Analytic Theory for High-Inclination Orbits in the Restricted Three-Body Problem," *Journal of Guidance, Control, and Dynamics*, Vol. 33, No. 2, pp. 565-583, Mar-April 2010.
- [43] Howell, K. C. and Pernicka, H. J., "Numerical Determination of Lissajous Trajectories in the Restricted Three-Body Problem," *Celestial Mechanics*, Vol. 41, No. 1, pp. 107-124, Mar 1987.
- [44] Szebehely, V. G., **Theory of Orbits - The Restricted Problem of Three Bodies**, Academic Press, New York, New York, 1967.
- [45] Hildebrand, F. B., **Advanced Calculus for Applications**, Prentice-Hall, Englewood Cliffs, New Jersey, 1976.

LIST OF SYMBOLS, ABBREVIATIONS, AND ACRONYMS

CW	Clohessy-Wiltshire
ECI	Earth-Centered Inertial
LVLH	Local-Vertical Local-Horizontal
NLS	Nonlinear Simulation
OED	Orbital Element Differences
QV	Quadratic Volterra
ROE	Relative Orbital Elements

DISTRIBUTION LIST

DTIC/OCP 8725 John J. Kingman Rd, Suite 0944 Ft Belvoir, VA 22060-6218	1 cy
AFRL/RVIL Kirtland AFB, NM 87117-5776	1 cy
Official Record Copy AFRL/RVSV/Thomas A. Lovell	1 cy

This page intentionally left blank